Particle-Hole Symmetric Localization Problems in One and Two Dimensions

Olexei I. Motrunich

(defended: June 29, 2001)

A DISSERTATION
PRESENTED TO THE FACULTY
OF PRINCETON UNIVERSITY
IN CANDIDACY FOR THE DEGREE
OF DOCTOR OF PHILOSOPHY

RECOMMENDED FOR ACCEPTANCE
BY THE DEPARTMENT OF PHYSICS

NOVEMBER 2001

Abstract

Particle-hole symmetric localization problems are studied in low dimensions with the emphasis on understanding the origin of the observed singularities in the low-energy density of states. Pure imaginary random hopping and bipartite random hopping problems are considered.

In quasi-1D geometry, such systems generically exhibit localized behavior, and are also found to have power-law density of states with nonuniversal dynamical exponents. Griffiths-like mechanism is identified that generates the singularly many low-energy states. Distinct localized phases are separated by delocalized critical points, and at these points the density of states has strong Dyson singularity near the band center.

Similar mechanism is argued to be operative in all particle-hole symmetric localized phases in any dimension. Higher-dimensional systems can also exhibit true metallic or critical delocalized phases, and one such system—the 2D bipartite random hopping problem—is studied in great detail. General such system is known to exhibit critical behavior and a density of states that diverges stronger than any integrable power-law. Crucial to understanding the origin of this behavior is a particular model—the random vector potential model—which is critical and has a power-law density of states with a continuously varying dynamical exponent. This model is shown to undergo a dynamical transition from a weak-disorder regime to a strong-disorder regime, with the dynamical exponent changing its behavior, and in the strong-disorder regime the low-energy states are identified with local extrema of the defining two-dimensional Gaussian surface. This dynamical transition is a counterpart of the static transition known to occur in this system, thus completing the available physical picture of the random vector potential model. In the general case, this "surface fluctuation" mechanism, combined with a well-known RG treatment of a vortex glass problem, leads to a proposal of the asymptotic behavior of the density of states $\rho(E) \sim E^{-1} e^{-|\ln E|^{2/3}}$ different from previous predictions. Analytical and numerical arguments are given in support of this picture.

Acknowledgments

I want to use this opportunity to thank the people who contributed most to my Condensed Matter Physics times at Princeton. First and foremost, I am indebted to my adviser David Huse for his patient guidance and constant encouragement and support during my years here. Getting involved in the work on random quantum Ising model (Ref. [1]) defined my calling in the beautiful physics of random systems. I am also thankful to Kedar Damle for initiation and fruitful collaboration on the projects reported in Refs. [2, 3, 4].

Chapter 2 is based on one such paper Ref. [4] written together with Kedar Damle and David Huse, while Chapter 3 describes our continuing work.

Finally, I enjoyed and profited from the company of my Condensed Matter Theory classmates Akakii Melikidze and Ashvin Vishwanath.

Contents

Chapter 1

Introduction

1.1 The focus of the thesis

This thesis studies effects of rare fluctuations in two special classes of single-particle localization problems—random hopping on a bipartite lattice and pure imaginary random hopping problems. These are defined as follows: Consider a tight-binding Hamiltonian on some d-dimensional lattice

$$\hat{H} = \sum_{i,j} t_{ij} |i\rangle\langle j| \ , \tag{1.1}$$

with random couplings $t_{ij} = t_{ji}^*$.

1) *Bipartite random hopping problem* (BPRH) is obtained if the lattice can be decomposed into two sublattices A and B such that t_{ij} is nonzero only when i and j belong to different sublattices, say $i \in A$ and $j \in B$.

2) *Pure imaginary random hopping problem* (ImRH) is obtained if all the amplitudes t_{ij} are pure imaginary, $t_{ij}^* = -t_{ij}$, with no further restrictions on the lattice.

To put these definitions in perspective, recall that the usual Anderson localization problems have the general form Eq. (1.1) with both the on-site and intersite terms present; typically, the disorder is introduced via random on-site energies $\epsilon_i \equiv t_{ii}$, while the intersite hopping amplitudes are taken to be regular, say, $t_{ij} \equiv t$ for nearest neighbors $\langle ij \rangle$. On the other hand, the BPRH and ImRH models have no such on-site (diagonal) terms, $t_{ii} \equiv 0$, and the randomness is in the intersite (off-diagonal) hopping terms. However, it is not just the off-diagonal character of the two models that makes them special. Indeed, a sufficiently general (not pure imaginary) random hopping (RH) problem on a nonbipartite lattice (e.g., RH on a triangular lattice) belongs to one of the usual Anderson localization classes, even when all the on-site energies are zero—this is because randomness in the hopping amplitudes generates (in some effective RG sense) such effective random on-site energies, transforming the system into the usual Anderson localization problem.

What makes the BPRH and ImRH problems special (and similar to each other in many respects) is the *particle-hole symmetry* present in the two models. More precisely, in both models, every eigenstate with energy E has a partner with energy $-E$ [in the BPRH problem the partner to the eigenstate $\vec{\Psi} = \{\vec{\psi}_A, \vec{\psi}_B\}$ is the eigenstate $\{\vec{\psi}_A, -\vec{\psi}_B\}$, while in the ImRH problem the partner to the eigenstate $\vec{\Psi}$ is the eigenstate $\vec{\Psi}^*$]. The center of the band $E = 0$ is then a special point in the spectrum, and the physics at this special energy is "protected" from becoming the usual Anderson localization type by the particle-hole symmetry, which prohibits the appearance of the on-site energies in any effective description.

What is the physical motivation for studying such special localization problems? Plateau transitions of the integer quantum Hall effect represent an outstanding challenge in the localization physics,[5, 6] and it is in this context that the two-dimensional (2D) bipartite hopping problem received most attention.[7, 8, 9] The bare schematics is presented in Fig. 1.1, which shows two consecutive Landau bands. Considering one such band, it is believed that only the states at the band center E_c are delocalized, while all the other states are localized. The transition between the plateaus of the integer quantum Hall effect, which occurs as the Fermi energy is tuned through E_c, is thus a delocalization transition between localized and delocalized states. At the transition, the localization length diverges as

$$\xi(E) \sim |E - E_c|^{-\nu}, \tag{1.2}$$

with $\nu \approx 2.3$. While there has been considerable effort to study such plateau transitions, the complete understanding is still missing, roughly because the plateau transition is believed to be controlled by a strong coupling fixed point that is very difficult to treat.

The bipartite hopping problems have a similar delocalization transition occurring at the band center $E = 0$, and are more tractable. However, unlike the quantum Hall systems, which have analytic density of states (DOS) at the transitions, the sublattice problems are found to have singular DOS near the band center. This unusual feature makes the sublattice problems very interesting in their own right, even if somewhat exceptional.

Recently, the interest in the localization physics has been further stimulated by the availability of novel mesoscopic systems on one hand, and by the discovery

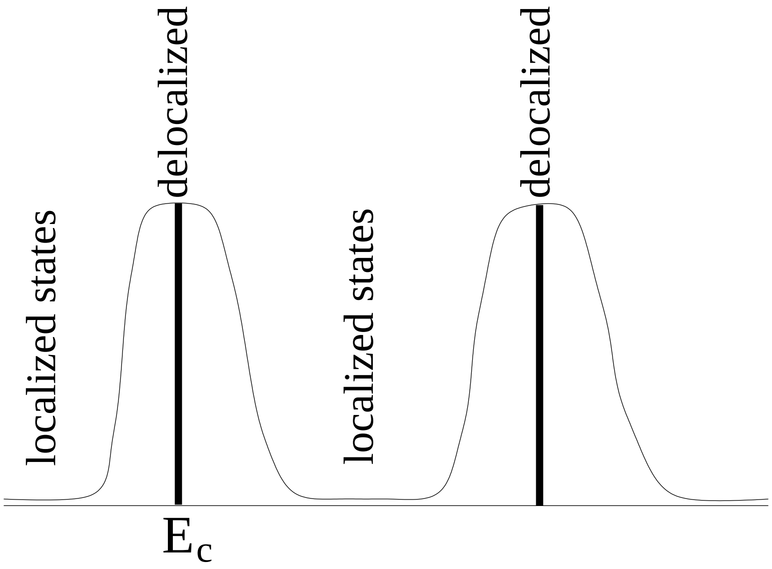

Figure 1.1: The density of states in two consecutive Landau bands.

of high-temperature superconductors on the other. It has been realized[10] that new classes of single-particle localization problems appear naturally when describing quasiparticles in disordered superconductors. While the electrical current in a superconductor is shunted by the superfluid, the thermal current is carried by the quasiparticles, and it is the localization physics of the quasiparticles (which can be fairly rich) that determines the heat transport properties of the superconductor. The ImRH problems appear naturally when studying the most random such quasiparticle systems with broken spin-rotation and time-reversal invariance (describing, for example, quasiparticle heat transport in a superconductor with magnetic impurities or with spin-orbit scattering). The bipartite hopping problems are closely related to such pure imaginary hopping problems; in fact, real BPRH problems represent one subclass of ImRH problems with bipartite hopping lattice, which occurs, e.g., for the quasiparticle system in a spin-polarized superconductor with time-reversal invariance. Also, in the Bogoliubov–de Gennes construction for the quasiparticles that leads to the ImRH formulation, the Fermi energy is fixed at $E = 0$, and this special point in the spectrum is very natural in this setting.

In the usual localization problems, the effects due to rare disorder fluctuations—large atypical regions, e.g., containing anomalously high concentration of impurities—are not particularly important, and are responsible only for weak (Lifshits) tails in the spectral density beyond the band edges.[11] However, in the two special localization problems considered here, the effects due to rare fluctuations are strong, producing, for example, nonuniversal power-law contributions to the density of states near the center of the band in the localized phases of the models. Such Griffiths-McCoy–like effects (subsequently referred to as simply Griffiths effects for brevity) are especially strong in the (quasi)one-dimensional systems, dominating much of the phase diagram, but also occur in higher dimensions. The study of such Griffiths effects is the main focus of this thesis.

The results of this study can be summarized as follows. Quasi-one-dimensional BPRH and ImRH problems (Chapter 2) exhibit two kinds of states with respect to their $E = 0$ localization properties—the localized band insulator phases (there can in turn be several distinct such phases) and the delocalized critical points separating the band insulators. In a localized phase, the density of states $\rho(E)$ is a power-law

$$\rho(E) \sim E^{-1+d/z} \ , \qquad (\textit{Griffiths}) \tag{1.3}$$

with a variable dynamical exponent z. As one approaches the delocalization transition, the dynamical exponent z diverges, and at the transition the density of states has the following form

$$\rho(E) \sim \frac{1}{E|\ln E|^3} \ , \qquad (\textit{Dyson singularity}). \tag{1.4}$$

In the localized phases, the density of states Eq. (1.3) diverges at the band center for $z > d$. The very many low-energy states that thus appear, especially near the transitions, originate from a peculiar "string mechanism", thereby a particular regular pattern that brings about the band insulator phase is broken along a string connecting two sites (see Fig. 3.1). In the simplest quasi-one-dimensional systems considered, such "strings" can also be viewed as droplets of the "opposite" localized phase embedded in the dominant background phase. In this respect, the mechanism is very similar to the conventional picture of Griffiths effects in disordered quantum systems (see below), and we dub such localized phases "Griffiths band insulators."

The same string mechanism is also operative in the localized phases of the BPRH and ImRH problems in higher dimensions—in particular, in 2D. In addition to the localized phases, the hopping problems can also have delocalized phases in $d \geq 2$.

Thus, in 2D, the general ImRH problem has a true metallic phase[12] (just as a disordered electronic system with spin-orbit scattering can be a metal in two dimensions), while the BPRH problem has a very unconventional critical delocalized "Gade" phase,[7] and it is this Gade phase that is the main focus of Chapter 3. The Gade critical state resembles the one-dimensional Dyson critical point in that the density of states is predicted to have a strong divergence

$$\rho(E) \sim \frac{1}{E} e^{-|\ln E|^x} , \qquad (\textit{modified Gade}) \tag{1.5}$$

with $x = 3/2$, which is stronger than any finite z divergence of Eq. (1.3). The presence of the strong divergence in this critical state has been known for some time. The physical picture how the low-energy states are generated by disorder is developed in Chapter 3. The mechanism is more subtle here. Roughly speaking, the low-energy states are produced near the local extrema of some two-dimensional random surface, and it is the extremal properties of the surface that determine the density of states. In this case, the relevant surface fluctuations are not truly rare fluctuations in the conventional sense of large regions locally in some opposite phase. Rather, they are the usual surface fluctuations of a two-dimensional Gaussian surface, with the additional wrinkle that the disorder strength of the random Gaussian surface itself depends on (renormalizes with) the length scale considered. This detailed analysis of the origin of states allows us to correct the original Gade's prediction $x = 2$ to the above $x = 3/2$ form. Also, it provides a very direct physical picture of the low-energy states not available from other approaches to this problem.

Having described the problems studied in this thesis, few words are in order on the organization of what follows. Each chapter constitutes a fairly self-contained part of the thesis. Chapter 2 considers quasi-one-dimensional BPRH and ImRH problems. Chapter 3 considers specifically two-dimensional bipartite hopping problems. Each chapter starts with its own introduction that describes in detail the particular setting to which the results of the chapter are relevant and reviews the previously known results. The main content then follows, and if some relevant but technical information is needed, it is given in the appendices to this chapter. Each chapter ends with a discussion of some remaining open questions.

To set the stage for the main themes of the thesis, in the rest of this Introduction, let us review the canonical examples of the rare fluctuation effects.

1.2 Rare fluctuations: Survey

The canonical examples of the rare fluctuation effects are the *Griffiths-McCoy singularities* in the classical and quantum statistical mechanics of disordered systems (discovered by Griffiths[13] and McCoy and Wu[14, 15, 16] in the 2D Ising model with general and with columnar-correlated randomness respectively), and the *Lifshits tails* in the spectrum of disordered electronic systems (studied in the context of heavily doped semiconductors[11, 17]). The common premise here is that because of randomness, there can and do occur with small but finite probability some anomalous situations that are disallowed in the corresponding pure system, and these occurrences then produce features that are absent in the pure system; this will be elaborated in more detail in the concrete examples below.

Griffiths effects show up most strongly in a disordered phase near the phase transition to an ordered phase, and originate from large rare regions that are locally in the wrong phase, with such rare occurrences actually producing singular contributions to the thermodynamic properties.

In the Lifshits tails situations, randomness in the system generates nonzero spectral density in the parts of the spectrum, which have no states in the pure system (e.g., randomness can fill-in the band gap or produce the spectral tail below the band edge of the pure system).

The systems considered in this thesis have the elements of both, with randomness enhancing the spectral density near the band center (filling the gap in the band insulator phases) and doing so very strongly in a manner similar to the strong Griffiths effects.

Griffiths effects in classical systems

Griffiths[13] studied the randomly diluted Ising ferromagnet and found that the magnetization is a nonanalytic function of the field H at $H = 0$ for a range of temperatures above the ordering temperature. In physical terms, Griffiths' argument can be summarized as follows: Consider ferromagnetic Ising model

$$E = -\sum_{\langle ij \rangle} J_{ij} S_i S_j + H \sum_i S_i \tag{1.6}$$

on a d-dimensional regular lattice with random nearest-neighbor exchanges J_{ij} taken from some distribution with finite support $[J_l, J_u]$, $0 < J_l < J_u < \infty$ (here and in the following, the particular model choices make the discussion most transparent, but do not affect the generality of the arguments and conclusions). The uniform magnetic field H is zero or small, and is included to probe the system's magnetization.

In $d \geq 2$, this system has a disordered (paramagnetic) phase at high temperatures (T) and an ordered (ferromagnetic) phase at low temperatures. The transition temperature T_c satisfies $T_c^{(0)}(J_l) < T_c < T_c^{(0)}(J_u)$, where $T_c^{(0)}(J)$ is the critical temperature of the corresponding pure model with all couplings equal to J. At T_c, the system exhibits thermodynamic singularities associated with the ordering transition, but the precursors of the transition appear already at $T_c^{(0)}(J_u)$, and the free energy of the system is nonanalytic in the whole Griffiths range $T_c < T < T_c^{(0)}(J_u)$. The nonanalytic contributions come from rare regions that are locally in the ferromagnetic phase at this temperature—droplets with effective $J_{\rm loc}$ (e.g., J_{ij} averaged over the droplet) such that $T < T_{c,{\rm loc}} \approx T_c^{(0)}(J_{\rm loc})$.

To see how the nonanalyticity appears, consider contributions from such regions to the average magnetization of the system in a small ordering field H. Probability that a given compact region of size L has local temperature $T_{c,{\rm loc}}$ is given roughly by the law of large numbers

$$\mathrm{P}_L(T_{c,{\rm loc}})\; dT_{c,{\rm loc}} \approx \sqrt{\frac{aL^d}{\pi T_c^2}}\; \exp\left[-a\left(\frac{T_{c,{\rm loc}}}{T_c}-1\right)^2 L^d\right]\; dT_{c,{\rm loc}}\;, \tag{1.7}$$

where a is some number of order one. In the following, we will ignore all pre-exponential factors (including powers of L), focusing on the dominant exponential term. The magnetization per spin of such a region in the applied field H at temperature T is roughly

$$m(H,T;L,T_{c,{\rm loc}}) \sim m^{(0)}(\tau_{\rm loc})\; \tanh\frac{m^{(0)}(\tau_{\rm loc})L^d H}{T}\;, \tag{1.8}$$

where $m^{(0)}(\tau) \sim (-\tau)^\beta$ is the magnetization density of the pure model at reduced temperature $\tau < 0$, and $\tau_{\rm loc} \equiv (T/T_{c,{\rm loc}} - 1)$. Important feature of this finite-size scaling form is that because of the disordering effects of the temperature, only sufficiently large droplets with $m^{(0)}(\tau_{\rm loc})L^d H \gtrsim T$ are ordered by the applied field. We can now estimate the contribution from such large rare droplets to the average magnetization of the system

$$m_{\rm sing}(H) \sim \exp\left[-a\left(\frac{T_{c,{\rm loc}}}{T_c}-1\right)^2 \frac{T}{m^{(0)}(\tau_{\rm loc})H}\right] \sim \exp\left[-c'\frac{T}{H}\right]\;; \tag{1.9}$$

in the last equation we optimized over $T_{c,{\rm loc}} > T$ obtaining some (minimal) numerical coefficient $c' = c'_{T-T_c}$. The nonanalytic contribution $m_{\rm sing}(H)$ to the magnetization is a very weak singularity—an essential singularity—since $m_{\rm sing}(H)$ and all its derivatives with respect to H vanish when $H \to 0$. The weakness of Griffiths effects can be traced back to the strong disordering action of the temperature in this classical system.

Griffiths effects in quantum systems

Such Griffiths effects are much more pronounced in disordered quantum systems. This is because a zero-temperature d-dimensional quantum system with any randomness is equivalent to a $d+1$-dimensional classical system with randomness that is perfectly correlated in the (additional) time direction, so a rare-fluctuation droplet in the quantum system is a rare-fluctuation slab of infinite extent in the time direction in the corresponding classical system.

Consider the ground state of the d-dimensional ferromagnetic quantum Ising model

$$\hat{H} = -\sum_{\langle ij \rangle} J_{ij} \hat{S}_i^z \hat{S}_j^z + \Gamma \sum_i \hat{S}_i^x + H \sum_i \hat{S}_i^z \ , \tag{1.10}$$

where $\hat{\mathbf{S}}_i$ are now quantum spin-$\frac{1}{2}$ operators; the classical part of the Hamiltonian (involving only $\hat{S}_i^z$) is the same as in Eq. (1.6), while the transverse field Γ introduces quantum fluctuations in the system. This model is equivalent to the classical Ising model in $d+1$ dimensions with randomness perfectly correlated along the time direction. The above analysis of the singular contribution to the magnetization from rare fluctuations can be now repeated in this classical language, if we replace Eq. (1.8) with the appropriate finite-size scaling form for the magnetization of the Ising slab infinite in one direction. For the purposes of illustration, however, we give the Griffiths effects argument directly in the quantum language.

Consider again the Griffiths disordered phase $\Gamma_c < \Gamma < \Gamma_c^{(0)}(J_u)$, and consider contributions to the magnetization from rare regions locally in the ordered phase with $\Gamma < \Gamma_{c,\rm loc} \approx \Gamma_c^{(0)}(J_{\rm loc})$. Probability of finding such a region of size L is again given by Eq. (1.7) with Γ's replacing T's, but now the (quantum) disordering effects are much weaker: We can view such a region as a large effective (super)spin, and to flip this superspin from an up-state to down-state, we need to flip all the L^d microscopic spins, which is a process of order L^d in perturbation theory in $\Gamma/\Gamma_{c,\rm loc}$ and happens with effective rate

$$\Gamma_{\rm eff} \sim \exp\left[-c(1-\Gamma/\Gamma_{c,\rm loc})L^d\right] \ . \tag{1.11}$$

The transition rate is written as Γ_{eff} since it is essentially the effective transverse field that acts to flip the large superspin. Equivalently, the degeneracy-lifting splitting in the space of the two spin-polarized states of the droplet occurs at order L^d in the perturbation theory and is roughly given by Γ_{eff}. Since it is only Γ_{eff} that counteracts the ordering of the droplet in the applied longitudinal field H, when $\Gamma_{\text{eff}} < H$ the region polarizes macroscopically in the z direction, and all such regions will produce a contribution to the average magnetization of the system

$$m_{\text{sing}}(H) \sim \exp\left[(\ln H) \times \frac{a\,(\Gamma_{c,\text{loc}}/\Gamma_c - 1)^2}{c(1 - \Gamma/\Gamma_{c,\text{loc}})}\right] \sim H^{1/z} \;, \tag{1.12}$$

where we optimized local $\Gamma_{c,\text{loc}} > \Gamma$ to obtain the most singular (smallest) exponent $1/z \equiv 1/z_{\Gamma-\Gamma_c}$. Unlike the classical case, the singularity in the quantum case is a power-law singularity. In particular, close enough to Γ_c, where $z > 1$, the susceptibility $\chi = \partial m/\partial H$ diverges at $H = 0$. This basic physical picture of the Griffiths effects can be formalized into a powerful real-space RG analysis, leading to a fairly complete description of both the disordered and ordered phases of the system, and also of the critical point separating the two.[18, 1, 2, 3]

Note in passing that such strong Griffiths effects occur in this system because the ordered phase breaks discrete symmetry, so that the characteristic time scale associated with an ordered droplet of size L—the correlation length in the corresponding slab in the imaginary time direction—scales with L as $\xi_\tau \sim \exp(cL^d)$. On the other hand, in a system with broken continuous symmetry such as quantum rotors of Ref. [19], ξ_τ scales as $\xi_\tau \sim L^d$ leading only to weak essential singularities at low energy scales.

Lifshits tails in the Anderson localization problems

Let us now turn to the rare-fluctuation effects in the Anderson localization problems. Consider Schrödinger equation

$$-\frac{\hbar^2}{2m}\triangle\psi + V(\mathbf{r})\psi = E\psi \tag{1.13}$$

for a particle in a random Gaussian potential $V(\mathbf{r})$ with zero mean and with second moments

$$\langle V(\mathbf{r})V(\mathbf{r}')\rangle = B(\mathbf{r} - \mathbf{r}') \;. \tag{1.14}$$

We write r_c for the correlation radius of the potential, i.e., $B(\mathbf{r}) \approx B(0)$ for $|\mathbf{r}| \lesssim r_c$ and $B(\mathbf{r})$ decreases quickly to zero for $|\mathbf{r}| \gtrsim r_c$; we also define v_0^2 from $v_0^2 r_c^d = \int d\mathbf{r}\; B(\mathbf{r})$.

The pure system with $V(\mathbf{r}) \equiv 0$ has no states with negative energy, and $E = 0$ is the edge of the spectrum. On the other hand, the system with randomness will have states with arbitrarily large (in absolute value) negative energies, since the potential $V(\mathbf{r})$ can attain such values with small but finite probability. Thus, there will be a nonzero (Lifshits) tail in the density of states $\rho(E)$ for $E < 0$ below the pure-system band edge, and we now discuss the functional form of this tail.

In the extreme limit $E \to -\infty$, an eigenstate with such E will be concentrated in a small region of size r_c where the potential happens to have very large negative value $V \approx E$. The density of states in this classical regime follows the probability distribution of the potential $V(\mathbf{r})$

$$\rho(E) \sim \exp\left[-\frac{E^2}{2B(0)}\right] , \qquad \text{for } |E| \gg \frac{\hbar^2}{mr_c^2} . \tag{1.15}$$

This holds as long as the kinetic energy cost of localizing the wave function in a region of size r_c (due to quantum zero-point motion) is small compared to $|E|$—therefore the name classical. Clearly, the behavior of $\rho(E)$ in this extreme regime depends on the tails of the distribution of the potential, and is thus nonuniversal.

Consider now the more interesting quantum regime $|E| \lesssim \hbar^2/(mr_c^2)$, so that the kinetic energy cannot be ignored. To find such a negative energy ($E < 0$) state, we look for a large region of size $R > r_c$ with sufficiently negative average potential $\overline{V}_R = R^{-d} \int d\mathbf{r}\, V(\mathbf{r})$ such that together with the kinetic energy cost $\sim\hbar^2/(mR^2)$ of localizing the wave function in this region we obtain the sought for

$$E = \overline{V}_R + \frac{\hbar^2}{mR^2} . \tag{1.16}$$

The probability of finding such a region is given by the law of large numbers

$$\text{Prob}[\overline{V}_R; R] \sim \exp\left[-\frac{\overline{V}_R^2 R^d}{v_0^2 r_c^d}\right] . \tag{1.17}$$

Optimizing this probability subject to constraint Eq. (1.16), we find that both the potential $-\overline{V}_R$ and the kinetic energy $\hbar^2/(mR^2)$ need to be of order $|E|$, with the resulting density of states

$$\rho(E) \sim \exp\left[-c|E|^{2-d/2}\right] , \tag{1.18}$$

having a fairly universal functional form in this regime (for $d < 4$).

Similar analysis can be also carried through in other situations, e.g., for randomly placed point impurities, even including screening of the impurity potential (see Refs. [11, 17]). Quite generally, all such treatments go under the name of optimal fluctuation methods. Note that the resulting Lifshits tails provide smooth and at the same time very weak filling of the "forbidden" parts of the spectrum; note also that the optimal wave functions are fairly smooth over the corresponding rare fluctuation regions. Particle-hole symmetric localization problems that we are about to consider are very different in these respects.

One-dimensional random hopping chain

To conclude this survey, consider the simplest particle-hole symmetric localization problem — the single-chain model

$$\hat{H} = \sum_j t_j \Big(|j\rangle\langle j+1| + |j+1\rangle\langle j| \Big) \ . \tag{1.19}$$

This example has been extensively studied in the past using a variety of techniques (see, e.g., Refs. [11, 20, 21]) and provides primary motivation and intuition for much of the work reported in this thesis.

When all the random hopping amplitudes are taken from the same distribution, the localization length diverges at the band center as $\xi_{\rm typ} \sim |\ln E|$, and the density of states exhibits the Dyson singularity Eq. (1.4). [Note here that the pure chain has a constant density of states near $E = 0$.] If we introduce enforced dimerization into the system making even couplings t_{2n} larger on average than odd couplings t_{2n+1}, the system is localized and the density of states is power-law vanishing or diverging Eq. (1.3), with a continuously varying dynamical exponent that goes to infinity for zero dimerization. [The pure dimerized system has a gap at the band center.] This singular filling in of the gap by disorder comes from rare large droplets that are locally in the opposite dimerized phase relative to the dominant background pattern: Indeed, the energy scale associated with the "free" (because of dimerization mismatch) boundary sites of such a droplet of size l is of order $\epsilon \sim e^{-cl}$, while the occurrence probability of this region is of order $p^l \sim \epsilon^{|\ln p|/c}$. At the Dyson critical point, such Griffiths generation of low-energy states is happening on all hierarchical scales.

A simple strong-randomness RG technique due to D. Fisher[18] formalizing the above observations reproduces all the known results and much more, giving direct information not available by any other means. The RG itself is described in the main text, and can be solved analytically for the $1D$ chain.[18] Not going into details, it also supplies a simple visual picture of the low-energy physics, which we briefly

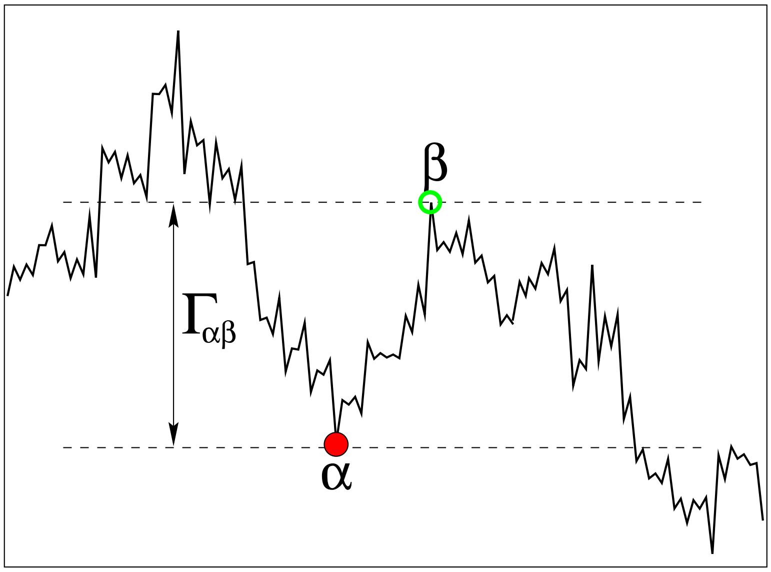

Figure 1.2: Pictorial representation of a given realization of random hopping amplitudes: "Random walker" steps up by $\ln(\Omega_0/t_{2n-1})$ from every odd site $2n-1$ and steps down by $\ln(\Omega_0/t_{2n})$ from every even site $2n$; Ω_0 is some microscopic energy scale. We indicated corresponding local minimum α and maximum β; there is a $\pm$ pair of low-energy states "living" on the two sites with the log-energy given by the height difference $\Gamma_{\alpha\beta}$

describe (this picture is an essential part of our arguments in Chapter 3 for the critical 2D models).

Consider "transferring" wave function at zero energy: $\psi_{2n+1} = -(t_{2n-1}/t_{2n})\psi_{2n-1} = \prod_{j=1}^{n}(-t_{2j-1}/t_{2j})\psi_1$. This is a true $E = 0$ eigenstate in an odd-length chain with open boundaries; in a general case, this ψ is only a "pseudo-eigenstate," but is still a useful zero-energy characterization of the system. The logarithm of the wave function performs a random walk shown in Fig. 1.2, which provides a particularly convenient visualization of a given disorder realization. Thus, the strong-randomness RG can be formulated entirely in terms of the properties of this random walk "surface," and associates the low-energy states and their log-energies with the local extrema and the corresponding surface height differences. More precisely, consider the situation in Fig. 1.2. "Probing" around the local minimum α, it is "seen" as a minimum until our "measuring" effective log-energy scale $\Gamma_E \equiv \ln(\Omega_0/E)$ becomes larger than $\Gamma_{\alpha\beta}$, and similarly for the local maximum β. Then, there is a pair of low-energy states "living" on the two sites α and β with the corresponding energies $\pm\epsilon_{\alpha\beta} = \pm\Omega_0 \exp(-\Gamma_{\alpha\beta})$. On the other hand, all the sites between α and β are associated with higher energy scales.

In such unbiased one-dimensional random walk $\upsilon(x)$, the extremal height difference associated with the "time" scale L (the length along the chain) is $\upsilon_{\max} - \upsilon_{\min} \sim \sqrt{L}$, and we immediately obtain the Dyson critical scaling $\Gamma_E \sim \sqrt{L_E}$ without actually doing any calculation!

Chapter 2

One-dimensional dirty superconductors without spin-rotation invariance

2.1 Introduction

Recently, there has been considerable theoretical activity concerning the effect of disorder on the quasiparticle spectrum in dirty superconductors with different pairing symmetries. [22, 23, 24, 25, 26, 12] The basic philosophy underlying most of these developments is to start with a weakly disordered problem and investigate the fate [in some renormalization group (RG) sense] of disorder at large length scales using field theoretic methods (see, however, Refs. [27, 28]). An analysis of this sort depends most crucially on the possible symmetries of the quasiparticle Hamiltonian, and it is the corresponding universal properties that have received most attention thus far. These include the leading effects of disorder on the conductivity and density of states in the delocalized regime, as well as the universal scaling properties of the localization transition.

Our focus here is quite different: We ask if Griffiths effects, whereby rare configurations of the disorder potential over large regions of space give rise to *nonuniversal* contributions that dominate some low-energy property, may be important in dirty superconductors. In particular, are there situations in which such Griffiths effects lead to a singular enhancement in the quasiparticle density of states near the Fermi energy? Unfortunately, this intriguing possibility has not attracted much attention in previous work.

Such issues are difficult to address within the weak-disorder framework mentioned above. Instead, we introduce an RG approach that is suitable for situations in which the effective value of disorder becomes large at low energies. Our basic result is simply stated: It is indeed possible for such Griffiths effects to dominate the low-energy properties, at least in one-dimensional models with either triplet pairing, or strong spin-orbit effects, or spin-flip scattering off frozen magnetic impurities. More specifically, we show that such models with broken spin rotation (SR) invariance *generically* lie in one of two distinct localized phases. These two phases are distinguished by a topological property (reflected in the presence or absence of zero-energy end states in a large but finite wire) that makes it impossible to go smoothly from one phase to the other. At the phase transition separating the two, the effective disorder grows without bound when viewed on ever-smaller energy scales, and the low-energy density of states behaves as $\rho(\epsilon) \sim 1/\epsilon|\ln^3\epsilon|$ (Dyson [29] singularity). The localized phases near this transition, on both sides, are *Griffiths phases* having a power-law singularity (with a nonuniversal exponent) in the low-energy density of states; these Griffiths phases are themselves characterized by strong (but not infinite) effective disorder in the limit of low energies. [We remark that a recent weak-disorder analysis, Refs. [30] and [31], of this problem has been carried out only at criticality. The results of these references for the thermal conductance and the density of states are consistent with the predictions of our RG approach at such a critical point—however, as we show here, the generic behavior of the system is localized rather than critical. [32]]

The detailed scaling properties of the low-energy strong-disorder critical point and the nearby Griffiths phases are, of course, specific to our one-dimensional (1D) examples. However, our RG approach is well suited for studying possible Griffiths effects in two or more dimensions as well, and some speculations along these lines are briefly discussed towards the end of this chapter.

2.2 Physical picture and motivation

Before plunging into the details of our analysis, it is useful to have a heuristic picture of the basic physics of our 1D problems. To this end, we consider a simple toy model for a disordered spinless (more physically, spin-polarized triplet) superconducting "wire" with a single transverse mode (channel) active. We model our system by a lattice Bogoliubov–de Gennes (BdG) Hamiltonian

$$\hat{H} = \sum_n (t c_n^\dagger c_{n+1} + \Delta c_n^\dagger c_{n+1}^\dagger + \mathrm{H.c.}) + \sum_n \epsilon_n c_n^\dagger c_n \ . \tag{2.1}$$

In this toy model, the nearest neighbor hopping amplitude t and the "p-wave" pairing amplitude Δ are real constants, while the impurity potential ϵ_n can take on values V_1 and V_2 with some probabilities p and $1-p$ respectively. Furthermore, we stipulate that $|V_1| < V_c$ and $|V_2| > V_c$, where $V_c \equiv 2|t|$.

The significance of the critical value V_c is readily seen by solving the pure problem with fixed $\epsilon_n = V$, i.e., with the chemical potential equal to $-V$. One easily finds that there is a gap in the quasiparticle excitation spectrum around the Fermi energy for both $|V| > V_c$ and $|V| < V_c$. However, at the critical point $|V| = V_c$, the system is gapless. Thus, there are two different gapped phases for our pure system (the phase with $|V| > V_c$ simply corresponds, in the absence of the pairing term, to a situation in which the Fermi level has gone below the bottom of the band or above the top of the band; thus, it is essentially a "band insulator"). For our purposes here, the important distinction between the two phases has to do with low-energy bound states at the ends of a long but finite wire of length L with free boundary conditions. In the "gapped superconductor" phase with $|V| < V_c$, such a wire has a single quasiparticle state below the gap with an excitation energy that is exponentially small in the length L; the corresponding wave function has weight only in the vicinity of the two ends of the chain (in the language of Ref. [33], in the $L \to \infty$ limit, we thus have two zero-energy Majorana fermions, one at each end of the chain) . In the other gapped phase, $|V| > V_c$, there is no such low-energy quasiparticle state. [34]

Now, imagine a disorder realization in which the potential has value V_1 throughout the region between, say, sites 0 and L, and value V_2 out to a distance L on either side of this central segment. The value of the potential is left unspecified in the rest of the system. The probability of this happening is $p^L(1-p)^{2L} = e^{-cL}$, with c appropriately defined. Now, the central region can be thought of, for large L, as a finite wire in the phase with $|V| < V_c$ surrounded by *vacuum* (this is reasonable since the long segments on either side can be roughly thought of as regions with no particle because the Fermi energy $-V_2$ has gone below the bottom of the band; effective couplings of the central region with the rest of the system, mediated through such isolating segments, are exponentially small in L). Such a situation will lead to a low-energy quasiparticle state with excitation energy $\epsilon_L \sim e^{-c'L}$, with some c' of order one. Since such low-energy states living on "domain walls" between large regions in "opposite" phases can happen anywhere along the entire length of our wire, such disorder configurations will give a non-zero contribution to the density of states in the thermodynamic limit. This contribution can be estimated as

$\rho_{\mathrm{Griff}}(\epsilon) = \int dL\, \delta(\epsilon - e^{-c'L})\, e^{-cL} \sim \epsilon^{-1+1/z}$, where we have introduced the dynamical exponent $z = c'/c$. This serves as a lower bound on the actual low-energy density of states in our disordered problem—thus, we *generically* have a power-law behavior (with a nonuniversal continuously varying exponent) of the density of low-energy excitations in our toy model. Although this model is admittedly crude, the picture of rare configurations of disorder over large regions of space leading to singular low-energy behavior is at the heart of the more precise strong-disorder RG analysis of Sec. 2.6.

We conclude this section with some comments on our choice of the toy model and, more generally, on the results obtained in this chapter. First, note that we completely ignored the self-consistency condition that, in principle, determines Δ in terms of the other parameters. [35, 36] This is not expected to matter; in fact, the precise choices made for various parameter values are not very important for our conclusion—nor is it important that our toy model has time reversal symmetry. As far as this model is concerned, the only important thing is the existence of two different gapped phases, with one of them supporting zero-energy end states. [Note that this is the main distinction of our models without SR invariance from the models with SR invariance: When the quasiparticle spin is a good quantum number, there are no such end states in any finite open chain, and we expect no Griffiths effects in this case—this will also become clear from our more detailed RG analysis.]

Another concern is that we are treating a one-dimensional superconductor with the BdG equations, which ignore quantum fluctuations of the condensate order parameter Δ. When the superconductor is in more than one dimension, Δ does have a nonvanishing static component at zero temperature, but in a strictly one-dimensional system, divergent quantum fluctuations mean that the superconducting state does not have true long range order or a gap. However, in highly anisotropic quasi-one-dimensional superconductors, T_c (and the gap) can, in principle, be large compared to the interchain hopping energy, and our approach should then apply in the range between these two energy scales (while no such regime appears to exist in quasi-one-dimensional superconductors known so far, *a priori*, there are no physical reasons that would prevent this from happening in some cases [37]). Another possible physical realization [25, 26] is that of a vortex in a three-dimensional gapped superconductor in the presence of frozen magnetic impurities or spin-orbit scattering. In such a situation, the effect of disorder on the quasiparticle states confined to the vortex core can be analyzed by a 1D BdG equation approach such as the one we employ.

Naturally, the choice of probability distributions for various quenched random variables will be different depending on the physical realization one is interested in (for instance, it is more natural to use a quenched random Δ with zero mean when considering the vortex problem). However, as will be clear from our later analysis, the precise form of the probability distribution for various bare couplings in the problem does not play an important role in determining the nature of the low-energy physics. Finally, note that the effects of the residual quasiparticle interactions are beyond the scope of our analysis.

2.3 Formalism, symmetry classes, our 1D models

It is useful to set up notation and review some basics [10, 12] before proceeding to our actual calculations. To this end, consider a general lattice BdG Hamiltonian

$$\hat{H}_{\rm SC} = \sum_{\alpha\beta} \left(h_{\alpha\beta} c_\alpha^\dagger c_\beta + \frac{1}{2}\Delta_{\alpha\beta} c_\alpha^\dagger c_\beta^\dagger + \frac{1}{2}\Delta_{\alpha\beta}^* c_\beta c_\alpha \right) , \tag{2.2}$$

where we use a composite label $\alpha = \{i, \mu\}$ for the site and spin indices of fermion orbitals. Hopping amplitudes, the effects of spin-orbit interaction on the hopping amplitudes, spin-flip scattering from frozen magnetic impurities, and random potential terms corresponding to nonmagnetic impurities are now all included in $h_{i\mu,j\nu}$, while pairing amplitudes are represented by $\Delta_{i\mu,j\nu}$. Hermiticity requires $h_{\beta\alpha} = h_{\alpha\beta}^*$, and we choose $\Delta_{\beta\alpha} = -\Delta_{\alpha\beta}$ consistent with the fermion anticommutation relations. Additional restrictions (to be reviewed below) arise when T invariance is a good symmetry (but we will not consider cases with SR invariance here).

The spectrum of quasiparticle excitations for $\hat{H}_{\rm SC}$ is specified by the spectrum of a (Hermitian) matrix

$$\mathcal{H} = \begin{pmatrix} h & \Delta \\ -\Delta^* & -h^* \end{pmatrix} \tag{2.3}$$

acting in an enlarged "particle-hole" Hilbert space. A particle/hole mixing unitary transformation $U_0 = \frac{1}{\sqrt{2}} \begin{pmatrix} 1 & -i \\ 1 & i \end{pmatrix} \otimes \mathbf{1}_{2N}$ (where N is the number of lattice sites), which acts independently on states corresponding to each α, transforms $\mathcal{H}$ into an antisymmetric *pure imaginary* form

$$\mathcal{H}_{\rm Im} = U_0^{-1} \mathcal{H} U_0 = \begin{pmatrix} i\,{\rm Im}(h+\Delta) & i\,{\rm Re}(-h+\Delta) \\ i\,{\rm Re}(h+\Delta) & i\,{\rm Im}(h-\Delta) \end{pmatrix} . \tag{2.4}$$

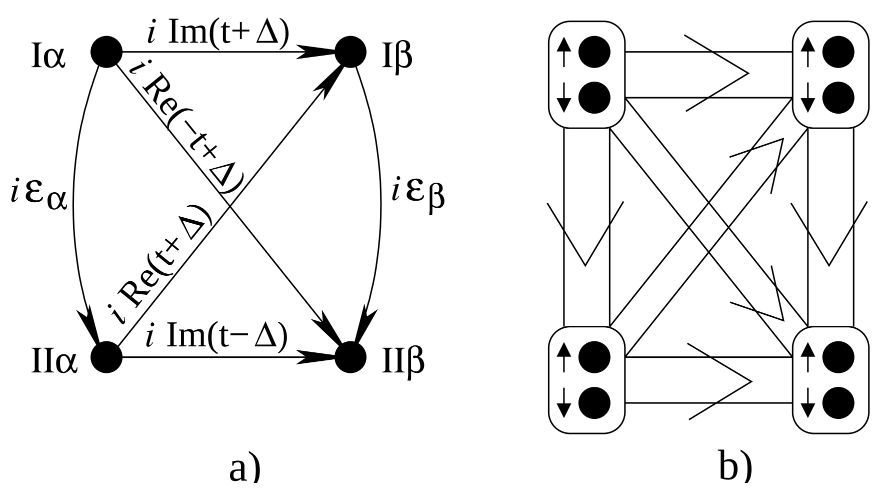

Figure 2.1: (a) General pure imaginary representation of hopping (t) and pairing (Δ) couplings between two fermion orbitals α and β. (b) In the T-invariant case, it is more convenient (see text) to work with block-sites and block-couplings shown here.

This representation is well suited for a discussion of heat transport properties of the quasiparticles. Indeed, the quasiparticle thermal conductivity is simply proportional to $k_B T \sigma$, where σ is the $T = 0$ conductivity of a (normal) system of noninteracting fermions described by the lattice Schrödinger equation corresponding to $\mathcal{H}_{\mathrm{Im}}$ (see Ref. [12] and references therein). (Note that $\mathcal{H}_{\mathrm{Im}}$ may also be obtained, as in Ref. [12], from the original $\hat{H}_{\mathrm{SC}}$ by writing everything in terms of Majorana fermions and then doubling the system, and we will therefore use a "copy index" K below to label the different blocks of $\mathcal{H}_{\mathrm{Im}}$.)

Most of our discussion will use this pure imaginary form. In the absence of both SR invariance and T invariance, the different matrix elements of $\mathcal{H}_{\mathrm{Im}}$ take on roughly independent imaginary values (apart from the requirements imposed by hermiticity). Thus, we have a general *pure imaginary* random hopping (ImRH) problem on a *doubled* lattice. Each original fermion orbital $\alpha = \{i, \mu\}$ is "represented" by two "copies" Iα and IIα; the energy of an orbital α is represented by an imaginary hopping amplitude between Iα and IIα, while hopping and pairing amplitudes between two orbitals α and β are represented by imaginary hopping amplitudes between the two pairs $\{\mathrm{I}\alpha, \mathrm{II}\alpha\}$ and $\{\mathrm{I}\beta, \mathrm{II}\beta\}$ [see Fig. 2.1(a)].

In the presence of T invariance, h and Δ satisfy $\boldsymbol{\sigma}_y h^* \boldsymbol{\sigma}_y = h$ and $\boldsymbol{\sigma}_y \Delta^* \boldsymbol{\sigma}_y = \Delta$, where $\boldsymbol{\sigma}_y = \sigma_y \otimes \mathbf{1}_N$ and σ_y acts on the spin degree of freedom at each site. The corresponding restrictions on $\mathcal{H}_{\mathrm{Im}}$ are best stated as follows: Group the different spin states on the same lattice site i and with the same copy index K into a block pair $\{Ki\uparrow, Ki\downarrow\}$. T invariance then implies that there are no internal couplings within such blocks. Moreover, the couplings between two blocks with the same copy index have a form

$$\hat{t}_{\text{block}} = \begin{pmatrix} i\,a & i\,b \\ i\,b & -i\,a \end{pmatrix} = ir \begin{pmatrix} \cos\theta & \sin\theta \\ \sin\theta & -\cos\theta \end{pmatrix} \tag{2.5}$$

with real a and b ($r = \sqrt{a^2+b^2}$), while the couplings between two blocks with different copy indices have a form $\begin{pmatrix} i\,c & -i\,d \\ i\,d & i\,c \end{pmatrix}$ with real c and d. Simply relabeling the spin states of copy II brings all block-couplings to the same form Eq. (2.5), and we will find it convenient to discuss the T-invariant case using this picture of block-sites connected by block-couplings [see Fig. 2.1(b) where each fat arrow represents the corresponding block coupling Eq. (2.5) with independent a and b, and different arrows are roughly independent of each other]. We also use another representation of $\mathcal{H}$ in the T-invariant case: This is obtained [10] by performing a particle-hole and spin-up-down mixing unitary transformation $U_\tau = \frac{1}{\sqrt{2}}(\mathbf{1}_2 \otimes \tau_z + \sigma_y \otimes \tau_x) \otimes \mathbf{1}_N$ (here, $\mathbf{1}_2$ and the Pauli matrix σ_y act on the spin label, while the Pauli matrices τ act on the particle-hole label):

$$\mathcal{H}_\tau = U_\tau^{-1} \mathcal{H} U_\tau = \begin{pmatrix} 0 & h\boldsymbol{\sigma}_y - \Delta \\ \boldsymbol{\sigma}_y h + \Delta^* & 0 \end{pmatrix}\,. \tag{2.6}$$

$\mathcal{H}_\tau$ thus has a *bipartite* complex hopping form, which will prove useful for our transfer matrix analysis (note however that strong correlations among matrix elements of $\mathcal{H}_\tau$ limit its usefulness in other contexts).

Finally, in the spinless case with no T invariance, we simply drop the spin label altogether and do not have any constraints on the bonds of the corresponding ImRH problem. Here and in the following, we use the designation ‘spinless’ to also refer to all situations in which the spin label of the electron can be dropped—such as spin-polarized triplet superconductors. Also, we do not consider specifically the spinless case with T invariance, but only mention the relevant results as we go along. This case is very special [12] and maps onto a class of bipartite hopping problems that have been studied both in one [38, 39] and two [7] dimensions. In one dimension, our RG approach yields results consistent with what is known from Refs. [38, 39] and can provide more details about the low-energy properties of any particular system in this universality class, while the two-dimensional bipartite hopping systems are considered in the next chapter.

Here, we consider specifically three one-dimensional systems: the spinless superconductor without T invariance, the spinful T-invariant superconductor, and the spinful superconductor without T invariance. In all three examples, the bulk of our discussion is for the case with a single transverse mode (channel) present. However, as will become clear from our analysis of the spinful superconductor without T invariance, our basic conclusions regarding the low-energy physics apply equally well for the multi-channel case of all three problems.

We model these systems by the appropriate BdG Hamiltonians with only nearest neighbor hopping and pairing amplitudes, in addition to same–lattice-site terms (the restriction to such nearest neighbor models is not at all crucial for any of our conclusions). The ImRH problem corresponding to the single-channel spinless case is a two-leg ladder with all couplings pure imaginary and roughly independent, but no other restrictions—in particular, couplings along the rungs of the ladder are allowed. Such "rung-couplings" [which we will sometimes refer to as "vertical" couplings—see Fig. 2.1(a)] correspond to any on-site terms in the original lattice BdG Hamiltonian; in the spinless case, these can only be random potential terms, but more generally, one can also have "s-wave" pairing amplitudes and spin-flip scattering potentials (the latter due to frozen magnetic impurities). For the single-channel spinful T-invariant case, the corresponding ImRH problem is an analogous two-leg ladder of block-sites with pure imaginary block-couplings that are roughly independent of one another—in other words, we have a four-leg ladder with this special block structure. Finally, the single-channel spinful case without T invariance is a pure-imaginary four-leg ladder with no other restrictions. These ladder problems are related to the bipartite random hopping (RH) ladder problems [38, 39] in which rung couplings are disallowed but the other hopping amplitudes do not have to be pure imaginary—as mentioned earlier, these are in the same universality class as spinless superconducting wires with T invariance. (The connection between this special class of models with sublattice symmetry and the more general systems that we study here is in fact surprisingly close, as will become apparent from our transfer matrix and RG analyses.)

Finally, it is worth emphasizing at this point that our focus in all these cases is on the low-energy physics: The systems mentioned above will all differ from each other at higher energy scales, particularly in the initial "diffusive" crossover regime that would be present in any weakly-disordered problem. However, at energies below this crossover scale, the effective value of disorder becomes large and all these systems can be described by a unified physical picture.

2.4 Strong-randomness RG approach

In order to go beyond the heuristic ideas of Sec. 2.2, we need a controlled approach that works in situations with strong Griffiths effects [such that z, defined by the low-energy behavior $\rho(\epsilon) \sim \epsilon^{-1+1/z}$ of the density of states, is large]. Such situations are expected to correspond to large values of effective disorder in the low-energy limit (in fact, a simple scaling argument indicates that the width of the distribution of the logarithms of the effective couplings is expected to be of order z in the low-energy limit). We are thus led to formulate a strong-disorder RG approach to this problem.

Consider the ImRH Hamiltonian $\mathcal{H}_{\rm Im} = \sum_{ij} t_{ij} |i\rangle\langle j|$ with $t_{ji} = t_{ij}^* = -t_{ij}$. The eigenstates of $\mathcal{H}_{\rm Im}$ occur in pairs with energies $\pm\epsilon$, and the strong-randomness RG proceeds by eliminating, at each step, such a pair of states with energies at the top and at the bottom of the band: One finds the largest (in absolute value) coupling in the system, say t_{12} connecting sites 1 and 2; this defines the bandwidth of the problem $2\Omega = 2\max\{|t_{ij}|\}$. If the distribution of the couplings is broad, the eigenfunctions of the two-site problem $\mathcal{H}_{\rm Im}[1,2]$ will be good approximations to the eigenstates with energies $\pm\Omega$, since the couplings t_{1j} and t_{2j} of the pair to the rest of the system will typically be much smaller. These couplings can then be treated perturbatively, and eliminating the high-energy states living on the sites 1 and 2 gives us the following effective couplings between the remaining sites:

$$\tilde{t}_{ij} = t_{ij} - t_{i1}(t_{12}^\dagger)^{-1} t_{2j} - t_{i2}(t_{21}^\dagger)^{-1} t_{1j} \ . \tag{2.7}$$

Clearly, the renormalized Hamiltonian $\tilde{\mathcal{H}}_{\rm Im}$ again corresponds to a pure imaginary hopping problem, but with two fewer sites; in particular, the matrix $\tilde{\mathcal{H}}_{\rm Im}$ has no diagonal terms, $\tilde{t}_{ii} \equiv 0$.

Some remarks on the proposed RG approach are in order here. Note that our RG rule Eq. (2.7) is an *exact* transformation for the zero-energy wave function, and as such provides information on the zero-energy localization properties. From a numerical point of view, it can be viewed as a construction of the zero-energy wave function in an *a priori* stable manner. Moreover, this transformation can also be viewed as an approximate but accurate scheme for evaluating the "Sturm sequence," i.e., the integrated density at very low energies, with the approximations involved being well-controlled when the low-energy effective couplings are broadly distributed. Lastly, note that in the limit of strong disorder and in the absence of strong correlations between different couplings, the right hand-side of Eq. (2.7) can be replaced with the "max" (in absolute value) of the three terms.

So far, we have ignored the restrictions that would be imposed on the couplings of the ImRH problem in a spinful (i.e., when both spin species need to be considered) T-invariant situation. In this case, it is more natural to work with the block-sites and block-couplings defined earlier [Fig. 2.1(b)]. To begin with, note that the eigenstates now occur in doubly degenerate pairs with energies $\pm\epsilon$. Thinking in terms of blocks automatically incorporates this degeneracy, since the eigenstates of a two–block-site problem $\mathcal{H}_\tau[\mathbf{1},\mathbf{2}]$ come in such doubly degenerate pairs with energies $\pm r_{\mathbf{12}} = \pm\sqrt{a_{\mathbf{12}}^2 + b_{\mathbf{12}}^2}$. Our RG approach now eliminates four states at each step, two at the top and two at the bottom of the band with energies $\pm\Omega$, where $\Omega \equiv \max\{r_{\mathbf{ij}}\}$. The resulting effective block-couplings among the remaining block-sites are again given by Eq. (2.7), but now each $\hat{t}_{\mathbf{ij}}$ is a $2{\times}2$ matrix of the form (2.5). The effective problem is again an ImRH problem in the same block-form, and no block-diagonal terms are generated. For the RG rule Eq. (2.7), the flows of bond energies r and bond angles θ do not separate. However, for strong disorder and in the absence of strong correlations (i.e., roughly, when the "max" RG rule applies) the energy variables r flow exactly as in the ImRH representation of a spinless superconductor without T invariance, while the angle variables simply randomize. Thus, we expect essentially identical results for this spinful problem with T invariance and the corresponding spinless problem without T invariance whenever both flow to strong disorder sufficiently rapidly.

2.5 Critical points and Griffiths effects in 1D: Transfer matrix analysis

Before we go on to our more detailed RG analysis of the low-energy properties, it is useful to have a picture of the phase diagram in each case. We use an elementary transfer matrix analysis to develop such a picture in terms of the zero-energy localization properties of the system. The goal here is to show by direct means that generically all our models are localized, and to demonstrate that there are critical points representing transitions between distinct localized phases; of course, these critical points can only be accessed by fine-tuning the disorder distributions.

In general terms, we are looking at the zero-energy localization properties of M-leg ladder systems governed by a Schrödinger equation

$$\epsilon\vec{\psi}_n = \hat{t}_n\vec{\psi}_{n+1} + \hat{t}^\dagger_{n-1}\vec{\psi}_{n-1} + \hat{u}_n\vec{\psi}_n \ , \tag{2.8}$$

where $\hat{t}_n$ and $\hat{u}_n$ are $M\times M$ matrices, and the wave function $\vec{\psi}_n$ is an M-dimensional vector defined at each rung n. We find it convenient to work with the following transfer matrix formulation:

$$\begin{pmatrix} \vec{\psi}_{n+1} \\ \hat{t}^\dagger_n\vec{\psi}_n \end{pmatrix} = \begin{pmatrix} \hat{t}_n^{-1}(\epsilon - \hat{u}_n) & -\hat{t}_n^{-1} \\ \hat{t}^\dagger_n & 0 \end{pmatrix} \begin{pmatrix} \vec{\psi}_n \\ \hat{t}^\dagger_{n-1}\vec{\psi}_{n-1} \end{pmatrix} ; \tag{2.9}$$

this defines elementary transfer matrix $\hat{\mathrm{T}}_n$.

The bipartite ladder problems

To begin with, consider the bipartite problem mentioned above, in which one has M coupled chains with no rung couplings, $\hat{u}_n \equiv 0$. This system was studied by Brouwer *et al.* [38, 39] who found that for both real or complex hopping amplitudes there are $M+1$ localized phases separated by M dimerization driven delocalized critical points; each critical point exhibits a strong Dyson singularity in the density of states $\rho(\epsilon) \sim 1/\epsilon|\ln^3\epsilon|$. Here, we rederive by completely elementary means the existence of M delocalized critical points, and also characterize the $M+1$ distinct localized phases; the ideas introduced in the process will generalize naturally to our superconductor systems.

Being bipartite, the two sublattices decouple at $\epsilon = 0$:

$$\hat{\mathrm{T}}_{n+1}\hat{\mathrm{T}}_n = \begin{pmatrix} -\hat{t}^{-1}_{n+1}\hat{t}^\dagger_n & 0 \\ 0 & -\hat{t}^\dagger_{n+1}\hat{t}^{-1}_n \end{pmatrix} \ . \tag{2.10}$$

We are thus led to study the Lyapunov spectra of the random matrix products $\hat{t}^{-1}_{2k}\hat{t}^\dagger_{2k-1}\ldots\hat{t}^{-1}_2\hat{t}^\dagger_1$ and $\hat{t}^\dagger_{2k}\hat{t}^{-1}_{2k-1}\ldots\hat{t}^\dagger_2\hat{t}^{-1}_1$. At zero dimerization ($\hat{t}_{2k}$ and $\hat{t}_{2k+1}$ distributed identically) the Lyapunov spectra of both products (consisting of M distinct Lyapunov exponents in the general case) are identical and symmetric around zero, and the full Lyapunov spectrum (of the full transfer matrix product) is doubly degenerate. Thus, for even M the smallest (in absolute value) Lyapunov exponent is nonzero and the zero-energy modes are localized, while for odd M there is always a zero Lyapunov exponent. (The actual values of these exponents are not of much concern here, only the fact that they are all distinct.) Now, consider adding dimerization by simply multiplying every odd bond $\hat{t}_{2k+1}$ by a scale factor e^{δ} and every even bond $\hat{t}_{2k}$ by a factor $e^{-\delta}$. Clearly, the whole Lyapunov spectrum for one reduced sublattice problem is shifted rigidly by δ (and by the exactly opposite amount for the other sublattice). Thus, as we scan δ from $-\infty$ to $+\infty$, there will be exactly M points where two of these exponents of the full transfer matrix cross zero. For the given sublattice, if we label each noncritical region by $(k, M-k)$ with k growing modes and $M-k$ decaying modes, these critical points represent consecutive "delocalization" transitions $(k, M-k) \to (k+1, M-k-1)$. Of course, this can also be restated in terms of the number of zero-energy states localized at each end in a finite odd-length chain with free boundary conditions, and provides a "topological" distinction between the different localized phases; each transition corresponds to a single zero-energy state becoming delocalized and migrating from one end of the chain to the other.

In a bulk system, at any of these critical points, one has two $E=0$ delocalized *Lyapunov modes* (linear combinations of which can roughly be interpreted as a "left-moving" and a "right-moving" slow modes). Since any description of the low-energy properties of the critical system in terms of such "slow" modes has to respect the bipartite nature of the original problem, it is natural to expect that such a low-energy effective theory is in the same universality class as the bipartite single chain RH problem. [21, 40] This provides a clear rationale for the critical low-energy density of states to be of the Dyson form. Similarly, we expect that the localized phases in the vicinity of any critical point look, at low energies, similar to the dimerized Griffiths phases obtained by introducing a small amount of dimerization in the single chain problem—in particular, we expect Griffiths singularities in the density of states consistent with the results of Refs. [38, 39].

Single-channel spinless superconductor without T invariance

Returning to the dirty superconductor problems, consider first the spinless fermion system with no T invariance in the ImRH language. In this case, the rung coupling is of the form $\hat{u}_n = \mu_n \sigma_y$ with some real μ_n (σ_y acts on the copy label K), while the hopping term is a general pure imaginary 2×2 matrix $\hat{t}_n$. Because of the identity $\sigma_y \hat{a}^{-1} \sigma_y = \hat{a}^T / \det \hat{a}$ valid for any 2×2 matrix $\hat{a}$, the zero-energy transfer matrices "decouple"

$$\hat{\mathrm{T}}_n = -\begin{pmatrix} 1 & 0 \\ 0 & \sigma_y \end{pmatrix} \begin{pmatrix} \mu_n \hat{t}_n^{-1} \sigma_y & \hat{t}_n^{-1} \sigma_y \\ \tau_n \hat{t}_n^{-1} \sigma_y & 0 \end{pmatrix} \begin{pmatrix} 1 & 0 \\ 0 & \sigma_y \end{pmatrix} , \tag{2.11}$$

where $\tau_n = \det \hat{t}_n$. Thus, Lyapunov exponents of the product of $\hat{\mathrm{T}}_n$ are given by a "superposition" of the Lyapunov exponents of the product of $\sqrt{|\tau_n|}\, \hat{t}_n^{-1}\sigma_y$ and of the product of $\begin{pmatrix} \mu_n/\sqrt{|\tau_n|} & 1/\sqrt{|\tau_n|} \\ \mathrm{sgn}\,(\tau_n)\sqrt{|\tau_n|} & 0 \end{pmatrix}$. The former product is very similar to the product $\Pi_k \hat{t}_{2k}^{-1}\hat{t}_{2k-1}^{\dagger}$ studied earlier (note, however, the particular "normalization" used here); the Lyapunov spectrum consists of two exponents $\pm\gamma_t$, with γ_t of order one. The latter product is essentially the transfer matrix product at $\epsilon = 0$ for a 1D Anderson problem with random energies $\pm\mu_n$ (depending on the sign of τ_n) and random hopping amplitudes $\sqrt{|\tau_n|}$; the two corresponding exponents are $\pm\gamma_\mu$. The full Lyapunov spectrum thus consists of the four exponents $\pm\gamma_t \pm \gamma_\mu$. As we increase the strength of the rung couplings μ_n (e.g., by increasing the root mean square strength $R \equiv R_\mu \equiv \sqrt{\overline{\mu^2}}$ with $\overline{\mu} = 0$ kept fixed) from 0 to ∞, γ_μ also increases from 0 to ∞. Thus, at some critical strength $R = R_c$ of the rung couplings, γ_μ will equal γ_t, and two Lyapunov exponents will be zero corresponding to an isolated delocalized critical point along the R axis.

Now, in the superconductor problem, there are no eigenstates at precisely zero energy in any system—this is due to the presence of the rung couplings. Nevertheless, there may be states with exponentially small (in system size) energy, and the localized phases on either side of the critical point can again be characterized in terms of such almost–zero-energy end states. Consider again an open odd-length chain. When $\mu_n \equiv 0$ (and $\delta \equiv 0$), there are two zero-energy states, one at each end of the chain. Turning on the rung couplings enables the two to mix, but since they are separated by the entire length of the chain, the splitting is exponentially small in the length of the chain—as long as $R < R_c$. Thus, in this phase, there will be two such (essentially) zero-energy end-states. In terms of the quasiparticle spectrum of the original superconductor $\hat{H}_{\mathrm{SC}}$, there is a single quasiparticle state with an exponentially small energy and a wave function with weight only at the two ends of the chain. On the other hand, in the phase with $R > R_c$, there are no such end states with nearly zero energy, as may be argued by starting with the limit of large μ_n. Thus, we have two different localized phases distinguished by this topological property; if we think in terms of a more general "dimerization-rung coupling" (δ-R) parameter plane, we have a phase diagram shown schematically in Fig. 2.2. Moreover, we again expect the low-energy properties in the vicinity of the transition between the phases to be in the universality class of the single chain bipartite RH problem in the vicinity of its zero-dimerization critical point. In particular, we again expect Griffiths singularities in the density of states of either localized phase

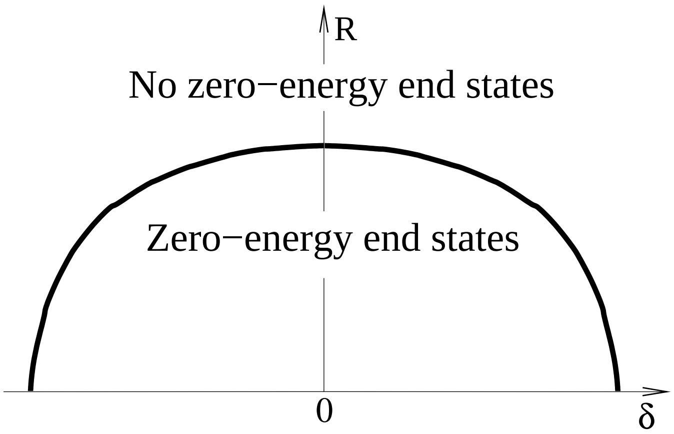

Figure 2.2: Schematic phase diagram in the δ-R plane for both the general spinless case without T invariance, and the spinful model with T invariance. We use R to denote some measure of the strength of the rung couplings which correspond to the random on-site terms of the original superconductor problem (e.g., for a symmetric distribution of random rung couplings, we can define R to be a root mean square of this distribution). The vicinity of the phase boundary is expected to exhibit strong Griffiths effects.

in the vicinity of the critical point—our expectations will be borne out by the more detailed RG analysis in the next section.

Single-channel spinful T-invariant superconductor

Consider now the spinful system with T invariance (but no SR invariance). In the bipartite representation, Eq. (2.6), the rung coupling is $\hat{u}_n = \begin{pmatrix} 0 & w_n \sigma_y \\ w_n^* \sigma_y & 0 \end{pmatrix}$ with some c-number w_n, while the hopping term has a form $\hat{t}_n = \begin{pmatrix} 0 & \hat{a}_n \\ \hat{b}_n & 0 \end{pmatrix}$ with $\hat{b}_n = -\hat{a}_n^*$ but otherwise general complex 2×2 matrix $\hat{a}_n$. From the transfer matrix, Eq. (2.9), the sublattice decoupling at zero energy is seen immediately; on one sublattice, we need only consider the product of

$$\hat{Q}_n = - \begin{pmatrix} \hat{a}_n^{-1} w_n \sigma_y & \hat{a}_n^{-1} \\ \hat{a}_n^T & 0 \end{pmatrix} . \tag{2.12}$$

Lyapunov exponents of this product together with their negatives (from the other sublattice) form the full Lyapunov spectrum of the system. But this product further "decouples" precisely as in Eq. (2.11) into the product of $\sqrt{|\alpha_n|}\hat{a}_n^{-1}\sigma_y$ and the product of $\begin{pmatrix} w_n/\sqrt{|\alpha_n|} & 1/\sqrt{|\alpha_n|} \\ \alpha_n/\sqrt{|\alpha_n|} & 0 \end{pmatrix}$; here $\alpha_n = \det \hat{a}_n$. Lyapunov exponents of the former product are $\pm\gamma_a$ with some γ_a of order one. However, the 1D Anderson localization problem corresponding to the latter product is non-Hermitian: while the hopping amplitudes can be chosen real and equal to $\sqrt{|\alpha_n|}$, the on-site energies $|w_n|e^{i\psi_n}$ are complex, with the phases ψ_n having contributions from the phases of both w and α. Nevertheless, the Lyapunov spectrum still consists of two exponents $\pm\gamma_w$. The spectrum of the product of the $\hat{\mathrm{Q}}_n$ is thus $\pm\gamma_a \pm \gamma_w$, and the other sublattice merely duplicates this to make the full Lyapunov spectrum doubly degenerate. Now, all we need to know is that for small values of rung couplings the corresponding γ_w is also small, while for large values of rung couplings γ_w is large. Then, as in the spinless case, there is an isolated delocalized critical point along the $R \equiv R_w \equiv \sqrt{\overline{w^2}}$ axis for some critical strength R_c of the rung coupling terms (at which $\gamma_w = \gamma_a$). Note that at this critical point, a total of four Lyapunov exponents will simultaneously cross zero; the corresponding two pairs of critical modes are related to each other by T invariance. Again, the phase with $R < R_c$ is characterized by the presence of end states with exponentially small energies. The only difference from the spinless case is that there are now four of them—this corresponds, in terms of $\hat{H}_{\mathrm{SC}}$, to two T-symmetry related quasiparticle states, each with an exponentially small energy and a wave function having weight only at the two ends of the chain. The phase with $R > R_c$ again has no such nearly zero energy end states. In the full δ-R plane, we thus have the schematic phase diagram shown in Fig 2.2. Again, the critical point and the phases in its vicinity are expected to look, at low energies, similar to those in the single chain RH problem, with the additional degeneracy introduced by T invariance. A direct numerical check of the Dyson form for the critical density of states in this spinful T-invariant case is shown in Fig. 2.3, while the RG results of the next section confirm the underlying physical picture in detail.

Parenthetically, we also note that these Lyapunov exponent crossing arguments imply that in all cases considered so far, the inverse of the smallest Lyapunov exponent diverges as $|g - g_c|^{-1}$, where g is some tuning parameter that drives the system through the critical point at g_c. This implies that the exponent ν for the typical localization length is $\nu = 1$ at all these transitions.

Single-channel spinful superconductor without T invariance

Finally, we turn to the spinful case with neither T invariance nor SR invariance—again, with only a single transverse channel. (Note that a quasi-1D spinless fermion superconductor with two transverse channels would also be modeled by the same

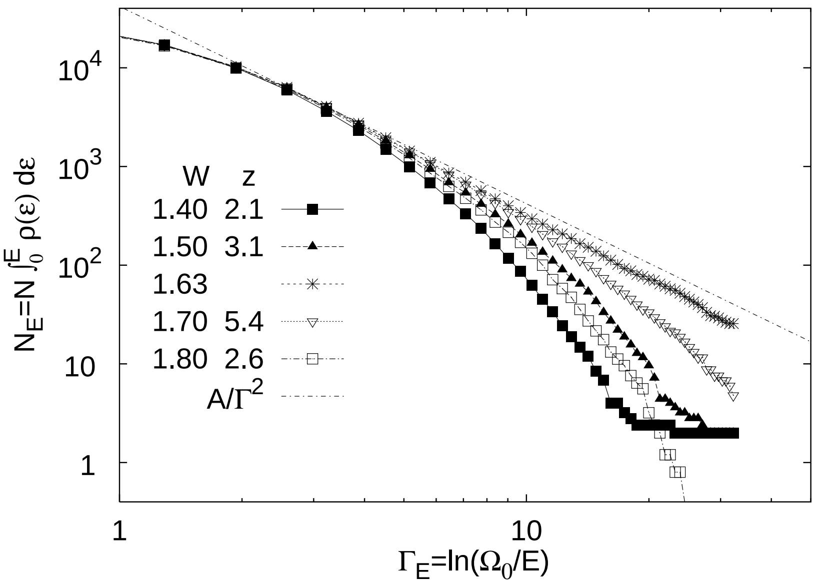

Figure 2.3: Numerical check of the Dyson singularity in the spinful T-invariant case. Number of states with energies between 0 and E for an open chain of length $L = 10^5$, averaged over 5 disorder realizations, is plotted vs the log-energy scale $\Gamma_E = \ln(1/E)$. Independent intersite couplings (real and imaginary parts, of independent hopping and pairing amplitudes) are chosen from a uniform distribution over $[-1, 1]$, while independent on-site couplings (real chemical potential and real singlet pairing amplitude) are chosen from a uniform distribution over $[-W, W]$. Critical $W_c = 1.630 \pm 0.001$ was found accurately from numerical transfer matrix analysis. At this point, we clearly have $N_\Gamma \sim 1/\Gamma^2$ (which is shown displaced from the data for clarity). We also show several off-critical points and give rough estimates of the corresponding dynamical exponents z from the Griffiths fits $N_E \sim E^{d/z}$ over $4 < N_E < 1000$.

BdG problem, with a somewhat different interpretation for the various couplings. Thus, analysis of this case is of value in demonstrating that our basic conclusions are not special to the single-channel case in any of the problems we consider.)

In this case, we have been unable to come up with any simple decoupling scheme that would map the corresponding transfer matrix to that of some problem with sublattice symmetry—the exact mapping we have used earlier is thus special to the two single-channel cases considered above. However, when the rung couplings are all zero, we do know that the corresponding bipartite four-leg ladder has five phases as we scan the dimerization parameter δ—these are labeled $(k, 4-k)$ with $k = 0, 1, 2, 3, 4$ corresponding to $4 - k$ zero-energy states localized at one end and k states localized at the other end for a finite ladder with an odd number of rungs and free boundary conditions. In particular, in the vicinity of $\delta = 0$ one has two such states at each end. Now, turning on some weak rung couplings allows these two states (at each end) to mix amongst themselves, and there will thus be no states with exponentially small energies in this regime. On the other hand, the same is clearly true for very large values of the rung couplings. Thus, the phases obtained in either case in the vicinity of $\delta = 0$ are expected to "look" the same (this is made more precise later using our RG approach).

The question then arises: Is there a single intervening phase (at $\delta = 0$) which is topologically different? This would result in *two* phase transitions as we scan the magnitude of the rung couplings. Another simple possibility is that there is no transition at all as a function of increasing rung coupling. Of course, there can also be other more complicated scenarios (some possibilities for the full phase diagram are sketched in Fig. 2.4). Moreover, since there are several independent rung couplings corresponding to each physical lattice site, there are many different ways of "increasing the rung coupling" and the possible phases and transitions encountered along the way will most likely depend on how we scan.

To get a more detailed picture, we performed an extensive numerical transfer matrix analysis (to obtain accurate results, we used the technique of Ref. [41]; see also our Appendix 2.A), as well as exact diagonalization studies, for particular choices of scan. In one choice of scan, we include all possible interrung couplings, but allow only those (intra)rung couplings that correspond to random on-site chemical potentials in the original superconductor problem. In this case, we can clearly delineate the phase boundaries to conclude that we have a phase diagram of the type shown in Fig. 2.4(A), with no transition along the R axis at $\delta = 0$ (with R now a measure of the

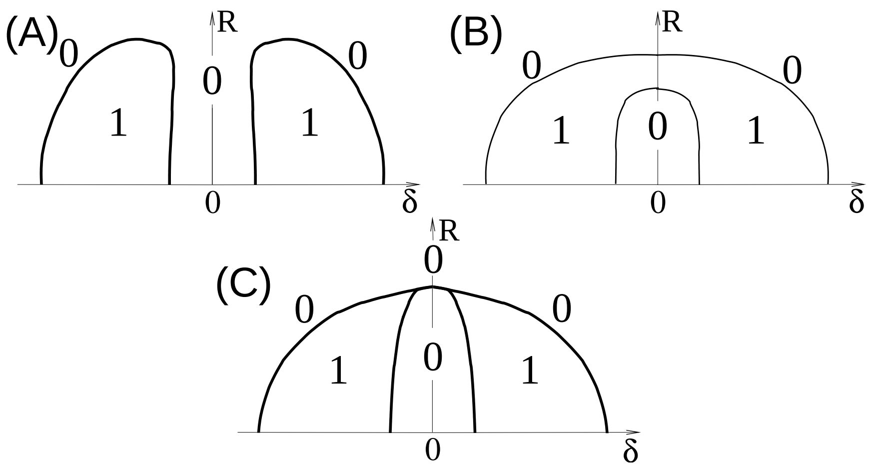

Figure 2.4: Possible phase diagrams in the δ-R plane for the spinful case without T symmetry. We use R to represent some measure of the strength of the rung-couplings. On the diagrams, we denote the phases with zero-energy end-states by `1` and the phases with no such states by `0`. (`A`) and (`B`) represent two simple possibilities, while a more complicated case with a multicritical point is shown in (`C`). Our numerical transfer matrix studies tentatively suggest that in the most "random" such superconductor (i.e., with all couplings present and independent) the phase diagram is very nearly that of the panel (`C`). In many other cases (e.g., when we allow only on-site chemical potentials in the original superconductor problem, but completely general intersite couplings), we observe the phase diagram (`A`). We have not found realizations that would clearly exhibit the phase diagram (`B`); however, we do not have arguments that would rule out this possibility.

strength of the on-site potentials). If we scan across the phase boundary at a fixed nonzero value of dimerization (so that we start in the phase with zero-energy end states and leave it by increasing the mean-square strength of the random potentials), we find that the typical localization length defined by the inverse Lyapunov exponent again diverges with $\nu = 1$, and the critical density of states is again of the Dyson form.

In another scan, we take the most random such system (i.e., with all allowed couplings present and independent) and boost the strength of all the (independent) rung couplings by the same amount on average, while keeping distribution of the interrung couplings fixed. As we increase the typical magnitudes of the rung couplings from zero in this manner, we again see strong Griffiths singularities in the density of states developing, and, possibly, critical behavior. However, near such a tentative critical point the two Lyapunov exponents that come close to zero seem to have a mutual "level repulsion" and the Lyapunov spectrum seems to exhibit the analog of an "avoided level crossing;" this results in huge localization lengths and strong near-critical behavior in large regions around the tentative critical point. A more detailed investigation away from $\delta = 0$ yields a phase diagram of the type shown in Fig. 2.4(`C`). Thus, to within our numerical accuracy, there seems to be a multicritical point in the δ-R phase diagram at $\delta = 0$. However, we can not exclude the possibility that we are seeing a case with no transition along the R axis (but phase boundaries coming very close to this axis) or an almost-degenerate case with two very closely spaced transitions. Crossing the phase boundaries away from the putative multicritical point again gives a localization length exponent of $\nu = 1$. However, we are unable to make any reliable statements in the vicinity of the multicritical point.

We have scanned along several other directions in the parameter space (corresponding to different interpretations of the rung-coupling parameter R), but have not clearly seen two distinct transitions as in Fig. 2.4(`B`); however, behavior of the type shown in Fig. 2.4(`A`) is the most common. (Note that the weak-disorder analysis of Ref. [30] did find critical behavior in the conductance at $\delta = 0$ when the interrung and intrarung couplings are taken from the same Gaussian distribution. Moreover, their result is consistent with our predictions for critical behavior at "ordinary" critical points, as opposed to multicritical points.)

These numerical results thus confirm our suspicion that the structure of the full phase diagram in this general spinful case (or in multichannel versions of all the cases) is quite complicated. The specific phase diagram obtained by tuning the parameters of a particular physical system (in which some subset of the allowed couplings may be identically zero) can thus be very different from case to case (a similar observation in related 2D models has been made in Refs. [41] and [42]). However, it is clear that there can be, in general, two kinds of localized phases. Moreover, whenever both phases are present in the phase diagram of a particular system, we again expect (analogous to the single-channel cases considered above) the system in the vicinity of the phase boundary to "look" at low-energies similar to the single-chain RH problem with weak dimerization (note that the numerical estimate $\nu = 1$ that we obtain away from any special "multicritical" points supports this picture, and our RG results provide further confirmation of the same).

This is as far as we can go with an elementary transfer matrix analysis. For a more detailed characterization of the low-energy properties, we now turn to the strong disorder RG analysis.

2.6 Critical points and Griffiths effects in 1D: RG analysis

To test the above picture in detail, we have implemented the RG numerically in all three single-channel cases. Since the single-channel spinful problem without T invariance is essentially identical to the corresponding two-channel spinless problem, this last example also serves to establish that our conclusions do not depend on any special properties of the single-channel case. In the single-channel spinless case without T-symmetry, and the similar spinful case with T invariance, we focus mainly on the vicinity of the rung-coupling driven phase transition with $\delta = 0$ (see Fig. 2.2). In the spinful case without T invariance, we consider the two different realizations described in the previous section—these have phase diagrams of the types shown in Fig. 2.4(A) (in which we scan across the phase boundary at nonzero dimerization so that we leave the phase having end-states by increasing the strength of the onsite potentials) and in Fig. 2.4(C) (in this case, we focus on the immediate vicinity of the putative multicritical point). (For completeness, we have also studied the transitions as a function of dimerization in the bipartite ladder problems.)

For the $\delta = 0$ spinless case (and the spinful T-invariant case) we consider systems with lengths as large as $L = 2 \times 10^5$. The initial conditions used have random (interrung) hoppings chosen from a uniform distribution over $[-1, 1]$, and random (intra)rung couplings u chosen from a symmetric (with either sign equally probable) power-law distribution $P(u) = \frac{1}{2g}|u|^{-1+1/g}$, $|u| \leq 1$. Note that the RG transformation (2.7) can be formulated entirely in terms of the imaginary parts of the couplings, and this is the language that we use here. For the spinful case without T symmetry, we are restricted to $L \leq 5 \times 10^4$. When we scan at finite dimerization, we enforce this dimerization by choosing the even and odd interrung couplings from the symmetric power-law distribution, but with different fixed values $g_{\text{even}} \neq g_{\text{odd}}$ for the power-law exponents. The strength of the rung couplings is again tuned by varying the corresponding power-law exponent g_{rung}.

Apart from the immediate vicinity of the putative multicritical point of Fig. 2.4(C) (which we comment upon separately), our results are equally reliable and essentially identical in all the cases studied. In the interests of brevity, we present in detail only the results obtained in the spinless case at $\delta = 0$ (see Fig. 2.2).

We search for the critical point by looking at the fraction of "isolated" sites among the remaining sites in the system: If there are N sites left, we find all the sites that are "covered" by the $N/2$ strongest remaining bonds. Roughly speaking, the fate of these covered sites is clear—they will be frozen dynamically at about this log-energy scale. The rest of the sites are still dynamically free at this scale, and we call them "isolated." In a localized phase, this fraction quickly approaches zero. On the other hand, at a critical point, we expect that new couplings which contribute, upon their subsequent decimation at a lower energy, to the density of states at that lower scale, are formed continually over all energy scales in a scale-invariant way. The fraction of isolated sites at criticality is therefore expected to saturate to some constant at low energies. In the case of the single critical RH chain, a quarter of the remaining sites is notionally isolated at each stage of the RG: each site has a bond to the right and to the left, and the bond strengths are uncorrelated; since each bond has a 50% chance of being "weak," the site is "isolated" with probability 1/4. This gives us a very direct test for the location and nature of the critical point.

Results of such a search for our spinless case are shown on Fig. 2.5. We clearly identify a critical $g_c \approx 0.95$, and note that the fraction of isolated sites at this critical point remains essentially 0.25, which is evidence that the low-energy behavior is that of a single one-dimensional "backbone" that goes critical. Note that it is also possible to further probe the geometry associated with the low-energy theory, as is done, e.g., below in our "order-parameter" studies, and even more exhaustively by looking in detail at probability distributions of the various couplings (which we have not pursued fully—the RG results shown here already confirm our basic picture of

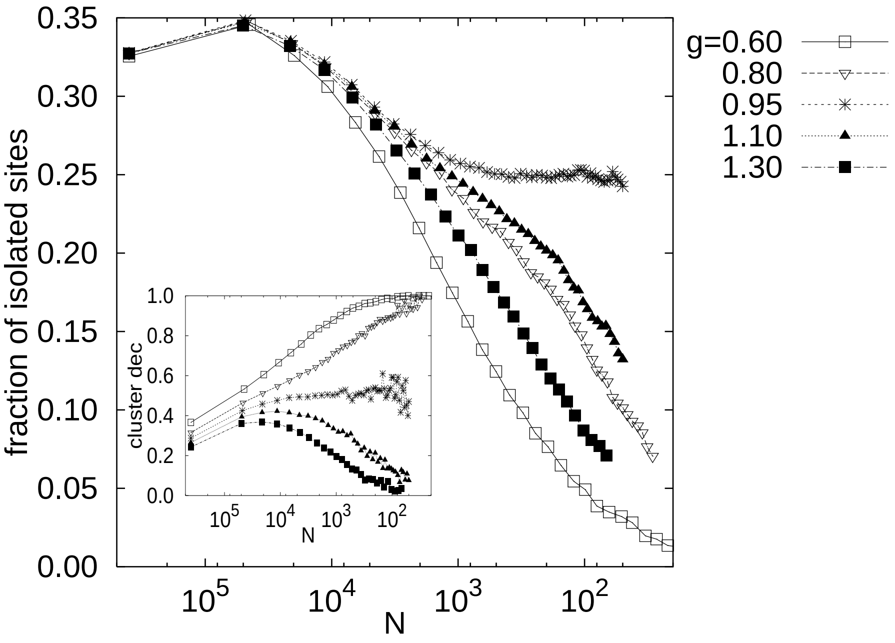

Figure 2.5: Fraction of isolated sites among the remaining sites for the two-leg ImRH ladder representing spinless fermion superconducting wire. Critical $g_c \approx 0.95$ is clearly identified. Inset shows the fraction of cluster decimations (see text for details).

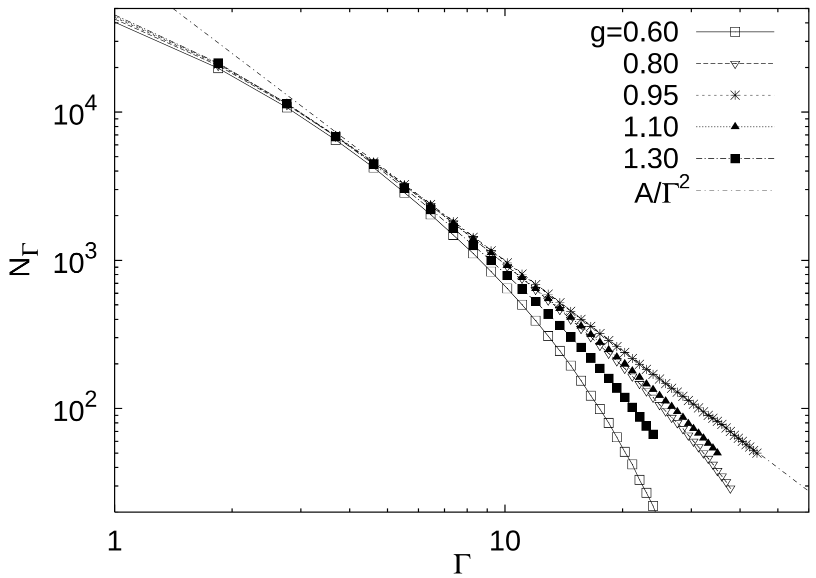

Figure 2.6: Number of remaining sites N vs log-energy scale Γ. Also shown is the fit of the critical N_Γ to the form A/Γ^2.

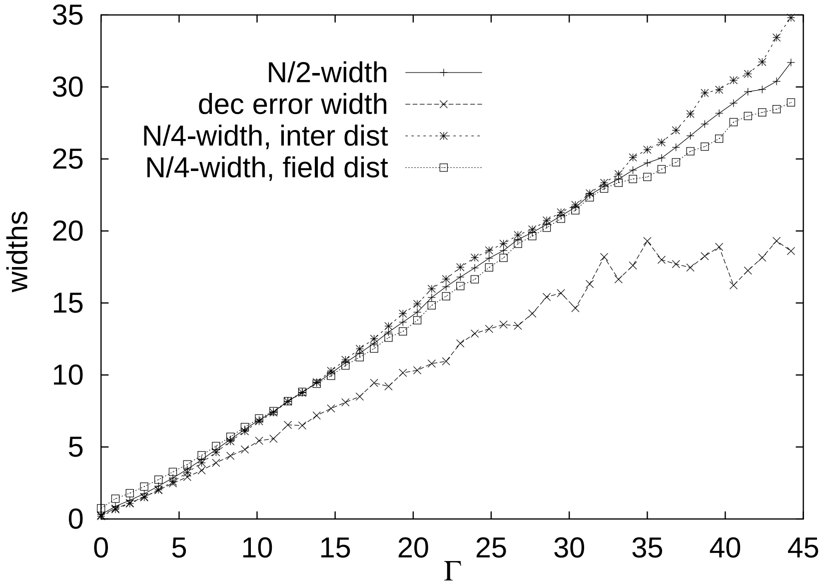

Figure 2.7: At the critical point (determined from Fig. 2.5) different measures of the widths of the log-coupling distributions all scale linearly with Γ. We plotted the $N/2$-width of the distribution of all bonds, the "decimation error" width (defined as the average logarithm of the ratio of the decimated bond to the strongest nearby bond), and also the $N/4$-widths of the interaction and field distributions with respect to the vertical reference cover (see text for details).

the low-energy physics).

At the critical point, the number of sites remaining at the log-energy scale $\Gamma \equiv \ln(\Omega_0/\Omega)$ is $N_\Gamma \sim 1/\Gamma^2$, as can be readily seen from Fig. 2.6. Since N_Γ is essentially the integrated density of states, this is consistent with the Dyson $\rho(\epsilon) \sim 1/\epsilon|\ln^3\epsilon|$. Moreover, at $g = g_c$, the distributions of all couplings become broader and broader on the *logarithmic* scale, with the characteristic widths growing linearly with Γ. This is shown on Fig. 2.7. In conjunction with our result for the fraction of isolated sites at low energies at criticality, this indicates that the critical point is in the same universality class as the single chain RH problem. Note that since the system effectively reduces to a single RH chain "backbone" in the low-energy limit, we expect [21, 40] the critical average thermal conductance $\kappa_c(L)$ of the original superconductor to scale as $k_B T/\sqrt{L}$, where L is the length of the wire—this is consistent with the weak disorder result of Ref. [30]. As mentioned earlier, this leads us to believe that their analysis was performed only at such a critical point and does not represent the generic behavior of the system.

Consider now the two different localized Griffiths phases. As expected, we find

$N_\Gamma \sim e^{-\Gamma/z}$ with a continuously varying dynamical exponent z which diverges as $z \sim |g-g_c|^{-1}$ as we tune across the critical point. Within our strong-disorder approach, the two Griffiths phases are distinguished by the character of the corresponding RG-generated dimer patterns. To discuss this intuitive distinction more precisely, we compare such RG-generated dimer covers against some fixed reference dimer cover. A natural choice of the reference cover for the spinless problem at hand is a "vertical" cover with reference dimers covering the rungs of the ladder, i.e., joining the two copies of each of the original fermions of $\hat{H}_{\rm SC}$. We use this specific reference cover in our numerical studies presented below; the following discussion, however, is fairly general. (We use the same "vertical" reference cover in the other two superconductor problems we study with the RG.)

We call two sites connected by such a reference bond a *cluster*, and the corresponding coupling between the two sites a *field* on the cluster. Couplings that connect sites in different clusters are called *interactions* between the clusters. This terminology is borrowed from the 1D random transverse field Ising model (RTFIM), but we emphasize that the correspondence is *not* exact although we do expect that the *critical* behavior, characterized with respect to a well-chosen cover, is essentially that of the RTFIM (we expect this to be true because a similar analysis for the dimerized single chain RH problem using the natural reference cover consisting of alternate bonds gives an exact mapping to the 1D RTFIM). When a coupling connecting two sites in the same cluster is decimated (field decimation), the corresponding cluster is *killed*. When a coupling connecting two sites in different clusters is decimated (interaction decimation), the two clusters are *joined* into one new cluster, which is now specified by the two other (remaining) end points of the two original clusters. The number of original sites that belong to a cluster defines its "magnetic moment," and it then makes sense to talk of the magnetization density m for the system. Pictorially, the reference dimer cover specifies some connectivity rules for the RG-formed dimers, with natural notions of clusters and percolation with respect to such connectivity rules, while the RG rules prescribe the dynamics (as a function of increasing Γ) obeyed by the clusters. Such connectivity properties can be used to distinguish between different RG-generated dimer covers and, thus, to characterize the different phases. [43] Within the strong-disorder RG, this is the distinction that captures the different "topological" character of the two Griffiths phases.

Going back to our numerical RG studies, we find that, with respect to the vertical reference cover, in the phase which obtains for strong rung couplings (small values of

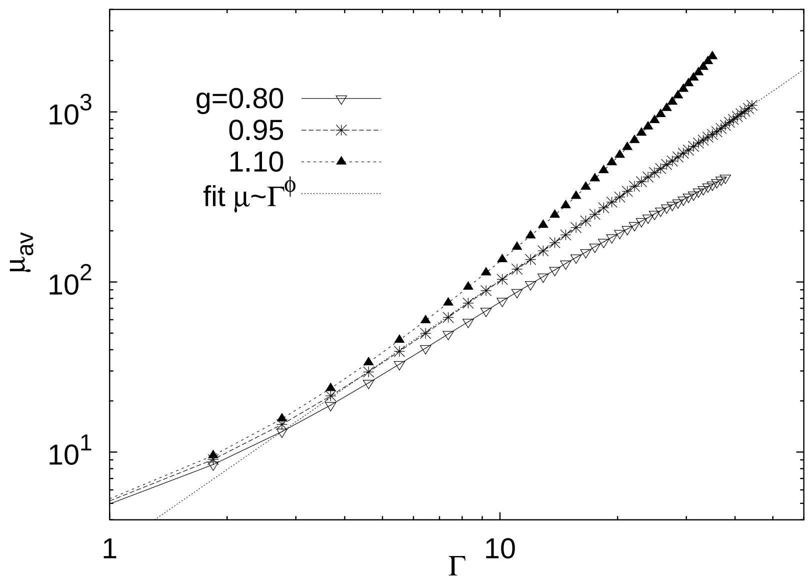

Figure 2.8: Average moment of the remaining clusters with respect to the vertical reference cover. Also shown is the fit at the critical point for the exponent ϕ. From this fit we obtain $\phi \approx 1.59$, which can be compared with the corresponding exponent for the quantum Ising model $\phi_{\mathrm{RTFIM}} = (1+\sqrt{5})/2 \approx 1.62$.

g) there are only small clusters and no connectedness across the whole system, while for weak rung couplings (large values of g) there is an infinite percolating cluster that forms in the limit of large Γ. This development of topological order for $g > g_c$ is characterized by an exponent β defined by the scaling of the average magnetization density $m(\Gamma \to \infty) \sim (g - g_c)^{\beta}$. At criticality, the average moment of the surviving clusters scales as $\mu \sim \Gamma^{\phi}$, which defines the exponent ϕ; in complete analogy to the RTFIM, [18] the exponent β for the topological order parameter ("magnetization") can be obtained from ϕ via the scaling relation $\beta = 2 - \phi$. Figure 2.8 shows our numerical result for the Γ dependence of the average moment of the surviving clusters at the critical point. The numerical value obtained for the exponent ϕ is very close to that of the 1D RTFIM. The value $\beta \approx 0.41$ we infer using the scaling relation is then very close to the corresponding exact result for the single dimerized chain, which has a β exactly equal [44] to the magnetization exponent $(3-\sqrt{5})/2$ of the 1D RTFIM. [18] We also note that, similarly to the quantum Ising model, the critical point is the point of balance between the cluster fields and cluster interactions; this is shown in the inset of Fig. 2.5, and provides alternative means for identifying the critical point. This completes our RG description of the spinless case.

Essentially the same results are obtained for the corresponding spinful problem with T invariance consistent with our general argument in Sec. 2.4. We also repeated this analysis for the specific realization of the spinful problem without T-symmetry corresponding to Fig. 2.4(A). All the results obtained for this case in the vicinity of the transition as a function of increasing R at fixed finite dimerization are essentially identical to the results shown above for the spinless case. (Entirely analogous results are also obtained in all cases for the dimerization driven transitions of the bipartite ladder problems.) Thus, our general picture for the low-energy physics appears to be validated by the RG results so long as we are not in the vicinity of any special multicritical points.

Finally, a brief comment on the RG results in the vicinity of the putative multicritical point, Fig. 2.4(C). As we scan R at $\delta = 0$, strong Griffiths effects again show up clearly over a wide region in the vicinity of the putative multicritical point. Moreover, the phases at large and small R both look "paramagnetic" in terms of clusters defined with respect to the vertical reference cover (and also many other reference covers). This is consistent with our arguments in the previous section. However, our RG results are also inconclusive when it comes to pinning down the structure of the phase diagram near this apparent multicritical point—again the analysis is plagued by near-critical behavior over a wide region. The corresponding long crossovers do not allow us to make any definitive statements regarding either the presence or the universality class of such multicritical points. This remains the principal unresolved question in our entire analysis of the one-dimensional examples.

2.7 How are the low-energy states generated?

We now consider precisely how the states in the singular low-energy tail of the density of states are generated, and identify the corresponding Griffiths regions in the ImRH language. As is already implicit in the above discussion, such a pair of low-energy states is formed if there are two "isolated" sites separated by a region in which all the other sites are locked into short-ranged (dimer) pairs. Griffiths effects are a consequence of such isolated sites being generated sufficiently often. An example of a pair of such sites is shown in Fig. 2.9. The isolated sites are very weakly coupled to each other—the coupling is of order $\epsilon \sim e^{-cl}$, where l is the length of the region. In a disordered system, there is always a probability of order p^l, with some $p < 1$, of finding such a region—this gives a power-law contribution $\sim \epsilon^{|\ln p|/c}$

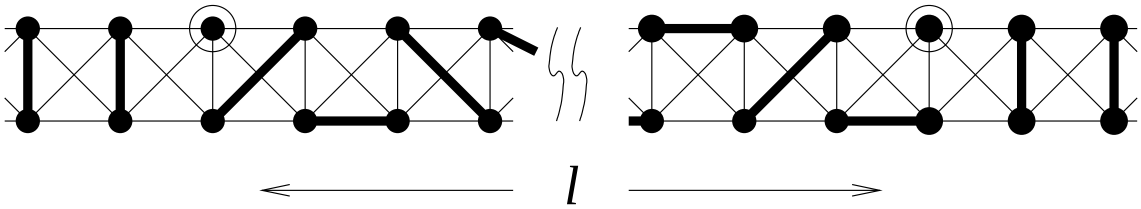

Figure 2.9: Griffiths generation of low-energy states.

to the integrated density of states from such regions. Thus, we *always* expect a variable power-law (Griffiths) density of states in such random hopping problems in which no on-site energies (i.e., diagonal terms) are allowed; we conclude that Griffiths phases are generic. The specific example shown in the figure is expected to be relevant to Griffiths effects in the phase in which the rung couplings dominate on average. The regions to the left and right of the pair are intended to be a caricature of the typical regions in this regime, while the region in the middle is comparatively rare. Decreasing the strength of the rung couplings would increase the probability of having such regions, corresponding to the observed increase in the dynamical exponent as one approaches the transition to the other phase. The critical point is then characterized by a proliferation of such Griffiths regions on all energy scales.

The picture that emerges is thus very similar to that in our toy model of Sec. 2.2 in which the low-energy states are closely associated with "domain walls" between the two different gapped phases of the pure system.

It is useful, at this point, to recast some of this in terms of the original superconductor Hamiltonian $\hat{H}_{\rm SC}$ (similar direct RG in the superconductor language was used by Levitov in Ref. [45]). This will give us a somewhat different perspective on the origin of these low-energy states. For simplicity, we restrict the discussion below to the spinless case. We first examine the basic RG rule Eq. (2.7). Consider a two-site problem

$$\hat{H}[\alpha,\beta] = \epsilon_\alpha c_\alpha^\dagger c_\alpha + \epsilon_\beta c_\beta^\dagger c_\beta + (t c_\alpha^\dagger c_\beta + \Delta c_\alpha^\dagger c_\beta^\dagger + \text{H.c.}).$$

This can be diagonalized by an appropriate Bogoliubov transformation to give

$$\hat{H}[\alpha,\beta] = \epsilon_+ \gamma_+^\dagger \gamma_+ + \epsilon_- \gamma_-^\dagger \gamma_- + \text{const},$$
$$\epsilon_\pm = \tfrac{1}{2}\left|\sqrt{(\epsilon_\alpha+\epsilon_\beta)^2 + 4|\Delta|^2} \pm \sqrt{(\epsilon_\alpha-\epsilon_\beta)^2 + 4|t|^2}\right|.$$

From this solution, it is clear that states at both α and β simultaneously contribute to either eigenstate only if either $|t| \gtrsim |\epsilon_\alpha - \epsilon_\beta|$ or $|\Delta| \gtrsim |\epsilon_\alpha + \epsilon_\beta|$. When this happens, we can no longer think of the two sites in isolation and need to account for the *resonance* between them. Now, if $|t|^2 - |\Delta|^2 \sim \epsilon_\alpha \epsilon_\beta$, ϵ_- for such a resonance can be very small. In order to obtain a good low-energy description in such a situation, we would eliminate the high-energy "+" state and keep only the "−" state by introducing a single *effective* site with site energy ϵ_-. In our ImRH RG language, this corresponds to a situation in which a single bond connecting sites on two different rungs is decimated, leaving behind one site on each rung; these two remaining sites are coupled by a weak bond precisely equal in magnitude to ϵ_-. On the other hand, if there is no mixing of the states at α and β, i.e., when one of the local potentials, say ϵ_α, dominates, we would eliminate the state α completely; in the ImRH RG this corresponds to decimating the corresponding rung. Thus, our RG procedure either eliminates a full fermion state because it is frozen out by a strong local potential, or eliminates "half of a fermion" from each of the two sites in resonance and recombines the remaining halves to create a new effective fermion with site energy equal to the new coupling introduced (our RG is thus really defined on the corresponding Majorana fermion states).

Now, consider for concreteness the Griffiths phase in which the on-site potentials dominate. At low enough energies, a description in terms of isolated effective sites (with negligible mixing between them) with some renormalized distribution of effective site energies is clearly appropriate. However, to arrive at such a description, one has to first account for all the resonances at higher energy scales that arise from any anomalous regions in which hopping and pairing amplitudes are large compared to local potentials. As a specific example of such anomalies, consider the central region of Fig. 2.9. In the original superconductor language, this region corresponds to both Δ and t being relatively large and comparable in magnitude, in addition to having a somewhat definite relationship between their phases throughout this region. Eliminating all the resonances between the sites in this region finally gives a low-energy description in terms of a single effective site with an exponentially small energy. This effective site in the original superconductor language clearly corresponds, in the ImRH language, to the pair of isolated sites shown in Fig. 2.9. The ImRH RG thus provides the natural language for capturing the important low-energy physics. Crudely speaking, the "effective site-energies" in the original superconductor language correspond to the "cluster field couplings" with respect to the natural vertical reference dimer cover in the ImRH RG language. Note also that an important ingredient of the physical picture that emerges is the spatial character of the quasiparticle states (in particular, note that wave function of a low-energy quasiparticle in the phase with zero-energy end states is split into two spatially separated pieces). Such spatial information is also kept most naturally in the ImRH RG; in particular, the development of the "topological order" is seen most naturally in this language.

Finally, we can now go back and ask what is the precise role played by the various symmetry restrictions. As discussed above, Griffiths effects in the ImRH RG language are associated with situations in which we repeatedly eliminate only a subset of the couplings connecting two rungs (for instance, only *one* of the couplings in the spinless example above), thus splitting the original fermion states. Now, if some symmetry restrictions require that some of the original couplings between rungs equal one another, then we would be forced to decimate several of them simultaneously—for example, we could be forced to eliminate only complete fermion states. Within the RG approach, this could then rule out the possibility of Griffiths effects. It is easy to see that the restrictions imposed by T invariance are not enough for this to happen. On the other hand, *in the SR-invariant case*, a simple analysis of the symmetry constraints for the corresponding ImRH problem shows that this is precisely what happens. (The same is true if we write the usual Anderson localization problem in the ImRH language—this is consistent with the expectation that disorder does not lead to any singular behavior of the density of states at the Fermi energy in a normal, noninteracting electron system.) In the strong disorder limit, this then is the true significance of the absence or presence of SR invariance for quasiparticles of a superconductor.

2.8 Discussion

Instead of conclusions, which have been stated clearly before, this discussion emphasizes the main questions that remain not answered as of now about such one-dimensional superconducting wires in which the quasiparticle spin is not a good quantum number.

Our explicit proofs that the system is generically localized for the single-channel spinless superconductor with no T invariance and the single-channel spinfull superconductor with T invariance relied crucially on the observed decompositions of the corresponding transfer matrices, which is very specific (coincidence) for these single-channel systems. For the more generic single-channel spinfull superconductor with no T invariance, no such decomposition exists, and we had to do numerical transfer matrix studies to verify that the behavior is generically localized except at some special fine-tuned critical points; we also checked this for the two-channel such system. Our feeling is that there must be a structural property of the corresponding random matrix products of $O(N, N)$ matrices that is responsible for the generic localized behavior (for some hints on the special character of such products see Appendix 2.A).

Related to the above is the question of the existence and the nature of the putative multicritical point of Fig. 2.4(C). Why is the near-critical region near this point so large? (Tentatively, the typical localization length diverges as $|R - R_c|^{-2}$ in this single-channel case; also, the near-critical region is even larger in the two-channel case.) What is the density of states at this multicritical point? (It is fairly hard to decide from our numerics whether it is Dyson or some other infinite-z form.) What are the different crossovers in the multi-channel wires? All these questions need further study.

Finally, do such Griffiths effects exist in two or more dimensions? This last question is answered in affirmative in the next chapter, but many details have not been addressed yet (see in particular the corresponding Discussion Sec. 3.6).

2.A Chalker's method for $O(N,N)$ matrices

In this Appendix, we describe in some detail the numerical method used in our transfer matrix studies of the ImRH problem. This method is due to Chalker *et al.* [41] and applies to random matrix products of $2N \times 2N$ matrices $\mathtt{M}$ that satisfy $\mathtt{M}^\dagger \Sigma_3 \mathtt{M} = \Sigma_3$, where $\Sigma_3 = \begin{pmatrix} \hat{1}_N & 0 \\ 0 & -\hat{1}_N \end{pmatrix}$. Such matrices appear naturally[46] in localization problems—they are transfer matrices for the corresponding plane wave amplitudes, while the $U(N,N)$ [$O(N,N)$ for real matrices] defining property simply reflects the particle flux conservation. Transfer matrices in ImRH problem, which is the case studied here, can be written as real $O(N,N)$ matrices (see below). Ref. [41] has only a brief description of the method, and does not mention an important subtlety when applying the method to such real matrices. Our detailed analysis of this subtlety, in fact, reveals important structure of the ImRH localization problem, pertinent to the appearance of two distinct localized phases. (See also very recent Ref. [47].)

Computation of Lyapunov exponents: general case

To set up our notation, consider first the case of a general random matrix product $\mathtt{P}_L = \mathtt{X}_L \mathtt{X}_{L-1} \ldots \mathtt{X}_1$, where $\mathtt{X}_i$ are $K \times K$ random matrices.[48] Behavior of $\mathtt{P}_L$ is characterized by the multiplicative ergodic theorem, which states that the limiting matrix $\lim_{L\to\infty} [\mathtt{P}_L^\dagger \mathtt{P}_L]^{1/(2L)}$ has nonrandom positive spectrum $\exp[\lambda_i]$. The growth exponents $\lambda_1 \geq \lambda_2 \geq \ldots \geq \lambda_K$ are called Lyapunov exponents of the random matrix product. (Here and in the following, "growth" and other dynamical notions refer to the implied "evolution" of various objects $\mathcal{O}(L) = \mathtt{P}_L \mathcal{O}_0$ with "time" L). The largest Lyapunov exponent λ_1 determines the growth rate of the length of any vector $\mathbf{v}$:

$$\lambda_1 = \lim_{L\to\infty} \frac{1}{L} \ln \left(\frac{||\mathtt{P}_L \mathbf{v}||}{||\mathbf{v}||} \right) . \tag{2.A.1}$$

Similarly, the p largest Lyapunov exponents determine the growth rate of the volume of any p-dimensional parallelepiped $[\mathbf{v}_1, \ldots, \mathbf{v}_p]$:

$$\lambda_1 + \ldots + \lambda_p = \lim_{L\to\infty} \frac{1}{L} \ln \left(\frac{\mathrm{Vol}_p[\mathtt{P}_L \mathbf{v}_1, \ldots, \mathtt{P}_L \mathbf{v}_p]}{\mathrm{Vol}_p[\mathbf{v}_1, \ldots, \mathbf{v}_p]} \right) . \tag{2.A.2}$$

This is all that would be needed to calculate the Lyapunov spectrum on a machine with infinite precision. Note, however, that according to Eq. (2.A.1) each vector $\mathbf{v}_i$ grows with the largest Lyapunov exponent λ_1 and is essentially projected onto the same limiting vector—the fastest growing mode; the slower modes determine the remaining degree of "nonparallelity" and thus the volume spanned by the p vectors. If we applied Eq. (2.A.2) using finite-precision arithmetic, the fastest growing mode would drown the slower modes, and we would not be able to determine the corresponding Lyapunov exponents. This can be avoided by an elegant orthonormalization procedure: Instead of keeping the vectors $[\mathbf{v}_1(L), \ldots, \mathbf{v}_p(L)]$ that define the parallelepiped we keep the orthonormal basis $[\mathbf{g}_1(L), \ldots, \mathbf{g}_p(L)]$ spanning the same p-plane and accumulate the volume growth factors on the fly. More precisely, unit time step consists of first evolving the vectors, $\mathbf{h}_1 = \mathtt{X}_L \mathbf{g}_1, \ldots, \mathbf{h}_k = \mathtt{X}_L \mathbf{g}_k$, and then Gramm-Schmidt–orthonormalizing

$$\begin{aligned} \tilde{H}_1 &= \|\mathbf{h}_1\| \ , & \tilde{\mathbf{g}}_1 &= \mathbf{h}_1 / \tilde{H}_1 \ ; \\ \tilde{H}_p &= \|\mathbf{h}_p - \textstyle\sum_{i<p} \langle \tilde{\mathbf{g}}_i | \mathbf{h}_p \rangle \tilde{\mathbf{g}}_i \| \ , & \tilde{\mathbf{g}}_k &= \Big(\mathbf{h}_p - \textstyle\sum_{i<p} \langle \tilde{\mathbf{g}}_i | \mathbf{h}_p \rangle \tilde{\mathbf{g}}_i \Big) / \tilde{H}_p \ . \end{aligned}$$

This process is then repeated starting with new $\mathbf{g}_i(L+1) \equiv \tilde{\mathbf{g}}_i$, while the Lyapunov exponents are determined from the corresponding accumulated growth factors $\lambda_i = \lim_{L\to\infty} L^{-1} \ln \Big(\prod_{t=1}^{L} \tilde{H}_i(t) \Big)$. (In practice, the orthonormalization, which is the costliest part of the procedure, needs to be repeated only so often, say, every ten steps.)

Computation of Lyapunov exponents: flux-conserving matrices

Consider now quasi-1D single-particle localization problems with N transverse channels. The $2N \times 2N$ transfer matrices satisfy $\mathtt{M}^\dagger \Sigma_3 \mathtt{M} = \Sigma_3$. The matrix product $\mathtt{M}\mathtt{M}^\dagger$ and its inverse $(\mathtt{M}\mathtt{M}^\dagger)^{-1} = \Sigma_3 \mathtt{M}\mathtt{M}^\dagger \Sigma_3$ have the same set of eigenvalues, or in other words, the eigenvalues of $\mathtt{M}\mathtt{M}^\dagger$ come in inverse pairs $\exp(\pm\Lambda_i)$. Thus, we need only the positive half $\lambda_1 \geq \lambda_2 \geq \ldots \geq \lambda_N \geq 0$ of the Lyapunov spectrum.

To calculate the Lyapunov exponents, we can apply the above orthormalization procedure to the product or transfer matrices, and this is what is usually done.[49] Note that this procedure does not enforce explicitly the flux conservation property. Still, it works reasonably well in the case of the usual Anderson localization (when matrices $\mathtt{M}$ are complex). However, in the ImRH problem (with real matrices $\mathtt{M}$) we find empirically (together with Ref. [41]) that roundoff errors produce a systematic positive error in the smallest Lyapunov exponent λ_N inhibiting the study near the delocalization transitions. This is presumably because the flux conservation property is lost (Ref.[47] has a nice illustration of how this happens). However, the idea of Chalker *et al.*, which we now describe, allows us to enforce the flux conservation at every stage of the computation.

Each transfered vector $\mathbf{v}_i$ is a $2N$-vector, which we write as $\mathbf{v}_i = \begin{pmatrix} \mathbf{a}_i \\ \mathbf{b}_i \end{pmatrix}$ with two N-vectors $\mathbf{a}_i$ and $\mathbf{b}_i$. We are transfering N vectors $[\mathbf{v}_1, \ldots, \mathbf{v}_N]$, which we write as a $2N \times N$ matrix $\mathtt{V} = \begin{pmatrix} \mathtt{A} \\ \mathtt{B} \end{pmatrix}$. Flux conservation implies that the difference $\mathtt{A}^\dagger \mathtt{A} - \mathtt{B}^\dagger \mathtt{B}$ of the Gramm matrices of the two vector sets $[\mathbf{a}_1, \ldots, \mathbf{a}_N]$ and $[\mathbf{b}_1, \ldots, \mathbf{b}_N]$ remains unchanged under the transfer, and the Chalker's method enforces this property by orthonormalizing the two blocks $\mathtt{A}$ and $\mathtt{B}$ separately. More precisely, instead of starting with N orthonormal but otherwise arbitrary $2N$-vectors $[\mathbf{v}_1, \ldots, \mathbf{v}_N]$, we start with two separately orthonormal N-sets of N-vectors $[\mathbf{a}_1, \ldots, \mathbf{a}_N]$ and $[\mathbf{b}_1, \ldots, \mathbf{b}_N]$. Since the Gramm matrices of the two remain equal to each other after the transfer, the orthonormalization procedure on $\mathtt{V}$ can indeed be performed separately on the two blocks $\mathtt{A}$ and $\mathtt{B}$.

Transfer matrix analysis of ImRH problems

Consider the transfer matrix Eq. (2.9) at $E = 0$ in ImRH. We have $\hat{t}_n = i\hat{\tau}_n$ with real but otherwise general matrix $\hat{\tau}_n$, and $\hat{u}_n = i\hat{w}_n$ with real antisymmetric matrix $\hat{w}_n$, $\hat{w}_n^T = -\hat{w}_n$. By writing

$$\hat{\mathrm{T}}_n = U^{-1} \mathtt{M}_n U, \tag{2.A.3}$$

with $U = \frac{1}{\sqrt{2}} \begin{pmatrix} -i & 1 \\ -i & -1 \end{pmatrix}$, the real matrices $\mathtt{M}$ satisfy the flux conservation $\mathtt{M}^T \Sigma_3 \mathtt{M} = \Sigma_3$. (The above essentially amounts to writing the transfer matrices in terms of plane waves with Fermi wave vector $k_F = \pi/2$ at half filling. Note again that matrices $\mathtt{M}$ are *real* in the ImRH problem, whereas we would obtain complex matrices in the usual Anderson localization.)

The main point of this Appendix is the following observation about the Chalker's method for products of real $O(N,N)$ matrices: If we apply the method starting with orthogonal matrices $\mathtt{A}$ and $\mathtt{B}$, the first $N-1$ extracted growth exponents give the $N-1$ largest Lyapunov exponents $\lambda_1, \ldots, \lambda_{N-1}$ of the random matrix product, but the N-th extracted growth exponent will either give $+\lambda_N$ or $-\lambda_N$ depending on the relative orientation of the two initial sets of orthonormal vectors $\mathtt{A}$ and $\mathtt{B}$. Indeed, let us consider the transfer of $[\mathbf{v}_1, \ldots, \mathbf{v}_N]$ together with a transfer with a different initial N-th vector $\mathbf{v}'_N = \begin{pmatrix} \mathbf{a}_N \\ -\mathbf{b}_N \end{pmatrix}$. Writing the transfers explicitly, we define $\begin{pmatrix} \mathbf{c}_i \\ \mathbf{d}_i \end{pmatrix} = \mathtt{M} \begin{pmatrix} \mathbf{a}_i \\ \mathbf{b}_i \end{pmatrix}$ for $i = 1, \ldots, N$, and $\begin{pmatrix} \mathbf{c}'_N \\ \mathbf{d}'_N \end{pmatrix} = \mathtt{M} \begin{pmatrix} \mathbf{a}_N \\ -\mathbf{b}_N \end{pmatrix}$. Flux conservation implies

$$\begin{aligned}
\mathbf{c}_i^T \mathbf{c}_j - \mathbf{d}_i^T \mathbf{d}_j &= \mathbf{a}_i^T \mathbf{a}_j - \mathbf{b}_i^T \mathbf{b}_j = 0\ , \quad i,j = 1,\ldots,N && (2.A.4)\\
\mathbf{c}_i^T \mathbf{c}'_N - \mathbf{d}_i^T \mathbf{d}'_N &= 0\ , \quad i = 1,\ldots,N-1 && (2.A.5)\\
\mathbf{c}_N^T \mathbf{c}'_N - \mathbf{d}_N^T \mathbf{d}'_N &= 2\ . && (2.A.6)
\end{aligned}$$

The N-th growth factor H_N is given by the component of $\mathbf{c}_N$ (or $\mathbf{d}_N$) perpendicular to the span of $[\mathbf{c}_1,\ldots,\mathbf{c}_{N-1}]$ (correspondingly, $[\mathbf{d}_1,\ldots,\mathbf{d}_{N-1}]$), $H_N = \|\mathbf{c}_N^\perp\| = \|\mathbf{d}_N^\perp\|$, and similarly for the N-th growth factor $H'_N = \|\mathbf{c}'^\perp_N\| = \|\mathbf{d}'^\perp_N\|$ for the other N-th vector $\mathbf{v}'_N$. Equations (2.A.6) imply that

$$(\mathbf{c}_N^\perp)^T \mathbf{c}'^\perp_N - (\mathbf{d}_N^\perp)^T \mathbf{d}'^\perp_N = 2 \quad \Longrightarrow \quad \tilde{\mathbf{a}}_N^T \tilde{\mathbf{a}}'_N - \tilde{\mathbf{b}}_N^T \tilde{\mathbf{b}}'_N = \frac{2}{H_N H'_N}\ , \tag{2.A.7}$$

where the last equation is for the normalized $\tilde{\mathbf{a}}_N \equiv \mathbf{c}_N^\perp / H_N$, etc. But the two unit vectors $\tilde{\mathbf{a}}_N$ and $\tilde{\mathbf{a}}'_N$ are either parallel or antiparallel, since they are both perpendicular to the $(N-1)$-dimensional plane spanned by $[\mathbf{c}_1,\ldots,\mathbf{c}_{N-1}]$, and similarly for $\tilde{\mathbf{b}}_N$ and $\tilde{\mathbf{b}}'_N$. We immediately conclude that $\tilde{\mathbf{a}}'_N = \tilde{\mathbf{a}}_N$, $\tilde{\mathbf{b}}'_N = -\tilde{\mathbf{b}}_N$, and $H'_N = H_N^{-1}$, which is what we have set out to show.

To see what is happening in more general terms, consider the polar decomposition of our $O(N,N)$ matrix $\mathtt{M}$

$$\mathtt{M} = \begin{pmatrix} \mathtt{Q}' & 0 \\ 0 & \mathtt{R}' \end{pmatrix} \begin{pmatrix} \cosh\hat{\Lambda} & \sinh\hat{\Lambda} \\ \sinh\hat{\Lambda} & \cosh\hat{\Lambda} \end{pmatrix} \begin{pmatrix} \mathtt{Q} & 0 \\ 0 & \mathtt{R} \end{pmatrix}\ , \tag{2.A.8}$$

where $\mathtt{Q}$, $\mathtt{R}$, $\mathtt{Q}'$, and $\mathtt{R}'$, are $N \times N$ orthogonal matrices, and $\hat{\Lambda}$ is a diagonal matrix consisting of the positive growth exponents. At first sight, it seems unlikely that "growing" the N vectors $\mathtt{V} = \begin{pmatrix} \mathtt{A} \\ \mathtt{B} \end{pmatrix}$ we could pick up anything but the N largest Lyapunox eponents. But let us consider the volume of

$$\tilde{\mathtt{A}} = (\cosh\hat{\Lambda})\mathtt{QA} + (\sinh\hat{\Lambda})\mathtt{RB} = \frac{1}{2}e^{\hat{\Lambda}}(\tilde{\mathtt{Q}} + \tilde{\mathtt{R}}) + \frac{1}{2}e^{-\hat{\Lambda}}(\tilde{\mathtt{Q}} - \tilde{\mathtt{R}})\ , \tag{2.A.9}$$

where $\tilde{\mathtt{Q}} = \mathtt{QA}$ and $\tilde{\mathtt{R}} = \mathtt{RB}$. The first $N-1$ columns of the matrix $\tilde{\mathtt{Q}} + \tilde{\mathtt{R}}$ will in general be linearly independent, and we will therefore extract the $N-1$ largest Lyapunov exponents. However, when the two orthogonal matrices $\tilde{\mathtt{Q}}$ and $\tilde{\mathtt{R}}$ have the opposite orientation, $\det\tilde{\mathtt{Q}} = -\det\tilde{\mathtt{R}}$, the matrix $\tilde{\mathtt{Q}} + \tilde{\mathtt{R}}$ is degenerate [since the orthogonal matrix $\tilde{\mathtt{Q}}^T\tilde{\mathtt{R}}$ has a (-1) eigenvalue], so the N-th column of $\tilde{\mathtt{Q}} + \tilde{\mathtt{R}}$ is a linear combination of the first $N-1$ columns. In this case, the volume of $\tilde{\mathtt{A}}$ will pick up the largest "mode" of $e^{-\hat{\Lambda}}(\tilde{\mathtt{Q}} - \tilde{\mathtt{R}})$, i.e., the exponent $(-\lambda_N)$. Thus, depending on the relative orientation of the matrices $\mathtt{QA}$ and $\mathtt{RB}$, the extracted N-th exponent is either $+\lambda_N$ or $-\lambda_N$.

In our numerical studies, we start with $\mathtt{A}$ and $\mathtt{B}$ having the same orientation; the change of the sign of the N-th extracted exponent as we scan the parameters of the system then signals the change of the relative orientations of the matrices $\mathtt{Q}$ and $\mathtt{R}$ in the polar decomposition, and we interpret this as indicating a transition between phases with no zero-energy edge states and with edge states (see below). This is how we determined the phase diagram boundaries in Figs. 2.2 and 2.4, and concluded that everywhere on these boundaries the localization length exponent is $\nu = 1$. For the special scan along the rung-coupling axis of Fig. 2.4($\mathtt{C}$), the N-th extracted exponent does not seem to be changing sign anywhere but instead approaches the zero in a parabolic fashion $\nu_N \sim (R - R_c)^2$ near the putative multicritical point R_c.

We now show the connection between the relative orientation of $\mathtt{Q}$ and $\mathtt{R}$ in the polar decomposition Eq. (2.A.8) of the limiting transfer matrix and the existence of the zero-energy edge states. Let us go back to our transfer matrix formulation Eq. (2.9), and consider a semi-infinite sample with rung label $j \geq 1$. If there is a zero-energy edge state, then there must exist $\vec{\psi}_1$ such that transfering via $\hat{\mathrm{T}}_j$ with initial $\begin{pmatrix} \vec{\psi}_1 \\ \vec{\psi}_0 \end{pmatrix} = \begin{pmatrix} \vec{\psi}_1 \\ \vec{0} \end{pmatrix}$, which amounts to solving the $E = 0$ eigen-equation with free boundary conditions, produces an exponentially decaying (and therefore normalizable) wave function $\vec{\psi}_j$. Recalling the transformation Eq. (2.A.3), $\hat{\mathrm{T}} \to \mathtt{M}$, which brings our transfer matrices to the $O(N,N)$ form, the initial vector acted upon by $\mathtt{M}$ is essentially $\begin{pmatrix} \mathbf{a} \\ \mathbf{b} \end{pmatrix} = \begin{pmatrix} \vec{\psi}_1 \\ \vec{\psi}_1 \end{pmatrix}$, and we obtain similarly to Eq. (2.A.9)

$$\mathtt{M} \begin{pmatrix} \vec{\psi}_1 \\ \vec{\psi}_1 \end{pmatrix} = \frac{1}{2} \begin{pmatrix} \mathtt{Q}' \Big[e^{\hat{\Lambda}} (\mathtt{Q} + \mathtt{R}) + e^{-\hat{\Lambda}} (\mathtt{Q} - \mathtt{R}) \Big] \vec{\psi}_1 \\ \mathtt{R}' \Big[e^{\hat{\Lambda}} (\mathtt{Q} + \mathtt{R}) - e^{-\hat{\Lambda}} (\mathtt{Q} - \mathtt{R}) \Big] \vec{\psi}_1 \end{pmatrix} . \tag{2.A.10}$$

As is clear from the above discussion, if and only if $\mathtt{Q}$ and $\mathtt{R}$ have opposite orientations will there be a decaying mode—the zero-energy edge state, with the inverse localization length given precisely by λ_N.

Chapter 3

Two-dimensional bipartite random hopping

3.1 Introduction

Random hopping on a two-dimensional bipartite lattice has been a subject of considerable recent interest—particularly in the context of studies of the plateau transitions in the integer quantum Hall effect—as an example of a localization problem that exhibits delocalized states only at a special energy. It has been noticed some time ago that,[50] because of the special particle-hole symmetry ($E \to -E$), this problem has unusual properties near the band center $E = 0$, very different from the properties of the usual Anderson localization problems. Thus, Soukoulis *et al.* [51] and Evangelou[52] found that localization length diverges at the band center, and Inui *et al.* [53] observed unusual localization characteristics of the zero-energy wavefunction, while Evangelou[52] also found a power-law diverging density of states near the band center.

More recently, Gade and Wegner[7, 8] proposed a critical field theory for such sublattice localization problems predicting a strongly divergent density of states

$$\rho(E) \sim \frac{1}{E}\, e^{-c\sqrt{|\ln E|}}, \tag{3.1}$$

stronger than any power law $\sim E^{-1+d/z}$ with a finite dynamical exponent z. If we define an energy-dependent length scale $L(E)$ from the density of states so that the integrated density $N(E) \equiv \int_0^E dE' \rho(E') \equiv L^{-2}(E)$, then the Gade form of the density of states corresponds to a kind of an infinite-z scaling

$$|\ln E| \sim (\ln L)^2 \tag{3.2}$$

between the energy scale and the corresponding length scale. These predictions were confirmed very recently[54] from a somewhat different perspective, and it has also been pointed out that there is a direct connection with a well-studied vortex glass problem.[55, 56, 57]

However, such a strong divergence in the low-energy density of states (DOS) has never been observed in the many numerical studies: Rather, one typically observes effectively power-law diverging or even vanishing density of states with nonuniversal (disorder-dependent) power-law exponents (for an illustration, see Sec. 3.5.1 below).

Here, we propose some resolution to this discrepancy. We note that the asymptotic form Eq. (3.1) is predicted to be valid at low energies below a crossover energy scale

$$E_{\text{cross}} \sim \Omega_0 e^{-16\pi^2 y^2 \overline{\sigma}^2}, \tag{3.3}$$

where Ω_0 is some bare energy, $\overline{\sigma}$ is the dimensionless "conductivity" of the 2D system, and y is some other dimensionless parameter that is greater than one. At intermediate energies $E_{\text{cross}} < E < \Omega_0$, on the other hand, the density of states is well approximated by an effective power-law, with a finite effective exponent z_{eff} that depends weakly on energy. We can estimate the conductivity $\overline{\sigma}$ using transfer-matrix analysis (Sec. 3.5.3), and for the systems typically studied we find it to be fairly large $\overline{\sigma} \sim 1$, which can lead to the crossover energies beyond the scales accessible to numerical studies. When we make the bipartite system less "delocalized" (smaller $\overline{\sigma}$, larger E_{cross}), we indeed observe significant deviations of the DOS from the power-law form, as is shown in Sec. 3.5.4 below.

At the same time, we also propose that the asymptotic scaling between the energy and length scales has a somewhat different infinite-z form, namely,

$$|\ln E| \sim (\ln L)^{3/2}, \tag{3.4}$$

with the corresponding asymptotic density of states

$$\rho(E) \sim \frac{1}{E}\, e^{-c|\ln E|^{2/3}}. \tag{3.5}$$

The proposed divergence is weaker than the original Gade form (this may be another reason why it has proved difficult to observe the Gade DOS). While it is almost impossible to distinguish the two forms (3.1) and (3.5) in the numerical DOS studies (but see Sec. 3.5), we propose a compelling physical picture in favor of the modified-Gade expression (3.5).

We briefly sketch our basic argument; for details and some relevant definitions see Secs. 3.2, 3.3. First of all, note that irrespective of the actual form of the divergence, it is indisputably true that disorder is generating very many low-energy states in this bipartite problem—states that are not present in the original pure system. Relevant physical question is how this happens, i.e., what is the mechanism of this generation. Strong candidate for such a mechanism is suggested by considering a particular particle-hole symmetric model—massless Dirac fermions in a random vector potential—first studied by Ludwig *et al.*[5]. The model is specified by a random Gaussian field $\Phi(\mathbf{r})$ with the strength of disorder g [see defining Eqs. (3.16) and (3.17)]. At strong randomness $g \gg 1$, the low-energy states "live" near the extrema of the surface $\Phi(\mathbf{r})$, with their log-energies roughly determined by the corresponding relative surface heights. Such extremal properties of the two-dimensional Gaussian surfaces are well-characterized (see Appendix 3.A); in particular, in a sample of size L, the energy of the lowest state is

$$|\ln E| \sim \Phi_{\max}(L) - \Phi_{\min}(L) \sim \sqrt{g} \ln L \ , \tag{3.6}$$

implying power-law dynamical scaling with the corresponding exponent at strong randomness

$$z \sim \sqrt{g} \ . \tag{3.7}$$

Ref. [5] indeed predicts power-law density of states in this model, but with the dynamical exponent

$$z = 1 + \frac{g}{\pi} \ ; \tag{3.8}$$

this result is believed to be perturbatively exact to all orders in g. The above "surface argument" shows, however, that Eq. (3.8) cannot hold for strong disorder, since the smallest energy in the problem cannot fall beyond the limits fixed by the extrema of the surface. In Sec. 3.4.1, we indeed argue that there is a dynamical transition at $g = g_c \equiv 2\pi$, such that the exponent z changes its behavior from the weak-disorder form (3.8) to the strong-disorder (3.7) [see also Eq. (3.34)]. This dynamical transition is a counterpart of a static transition[58, 59] known to occur when the wave function $e^{-[\Phi(\mathbf{r})-\Phi_{\min}]}$ (the zero-energy "pseudo-eigenstate" defined so that its peak value is 1) remains normalizable in the limit $L \to \infty$.

Consider now the general case. From the above discussion, we expect some power-law density of states to be produced as long as there is some "vector potential" randomness. Moreover, RG analysis[55, 56, 57, 54] shows that any amount of a more general "random mass" disorder (see Sec. 3.2 below) generates additional vector potential randomness, driving the latter to stronger disorder

$$g(L) \sim \ln L \ . \tag{3.9}$$

The low-energy states are again associated with the extrema of some effective surface (the logarithm of the magnitude of the lowest-energy wave function), but the height extrema of this surface, and correspondingly the log-energies, now scale with L as

$$|\ln E| \sim z(L) \ln L \sim \sqrt{g(L)}\, \ln L \sim (\ln L)^{3/2} \ , \tag{3.10}$$

which is the proposed modified-Gade form. The original Gade form itself would obtain from

$$|\ln E| \sim z(L) \ln L \overset{!?!}{\sim} g(L) \ln L \sim (\ln L)^2 \ , \tag{3.11}$$

i.e., if the weak-disorder form Eq. (3.8) were used; however, since g is eventually driven to strong disorder, this form cannot be used for the asymptotic behavior. In Sec. 3.4.2, we give a more precise argument from a different perspective using results of Ref. [60] for the vortex glass problem.

So far, we have mentioned only critical ("delocalized") bipartite systems. However, it is possible to drive such a system into a localized state preserving at the same time the sublattice symmetry: This can be achieved, for example, by making some prescribed bonds that produce a complete dimer cover of the lattice stronger on average, thus introducing some preferred "dimerization" pattern. If this dimerization is weak, the system may remain critical, but strong dimerization eventually drives it into a localized state. We propose an interesting mechanism for disorder to generate power-law contributions to the low-energy DOS in such bipartite insulating phases: The low-energy states are associated with the end-points of "strings" along which the background dimer pattern is broken as in Fig. 3.1. Simple probability counting argument shows that this mechanism is actually operative in any dimension, and also in localized phases of related pure imaginary random hopping problems that describe quasiparticle localization in disordered superconductors with broken spin-rotation invariance (in the latter case, particular dimerization patterns appear quite naturally, coming from different kinds of couplings in such dirty superconductors). In our bipartite systems, this mechanism can produce power-law diverging DOS and then dominates over all other mechanisms of filling the band gap.

This Chapter is organized as follows: Sec. 3.2 defines our models and reviews the connection with the vortex-glass problem. Sec. 3.3 introduces a strong-randomness picture of the low-energy physics, motivating the more precise bounds of Sec. 3.4 on the dynamical scaling in the system. Sec. 3.5 summarizes our numerical evidence for the preceding discussion. We conclude in Sec. 3.6 with a discussion of some remaining questions and further prospects.

3.2 Models and definitions; connection with dimers

Bipartite random hopping problem is specified by a single-particle Hamiltonian

$$\hat{H} = \sum_{\langle\alpha\beta\rangle} \Big(t_{\alpha\beta} |\alpha\rangle\langle\beta| + \mathrm{H.c.} \Big) \equiv \begin{pmatrix} 0 & \hat{t}_{AB} \\ \hat{t}^{\dagger}_{AB} & 0 \end{pmatrix} , \qquad (3.12)$$

where α belongs to sublattice A and β belongs to sublattice B of some bipartite lattice. We only consider real hopping problems and in two dimensions, having the following specific models in mind: π-*flux* model, *honeycomb* lattice model, and *general* bipartite lattice model. We define each model as a nearest-neighbor hopping problem on an appropriate lattice, with some additional constraints on the allowed signs of the couplings:

The π-flux model[61] is defined on a square lattice with a requirement that there is one half of a magnetic flux quanta per square plaquette. A particular convenient gauge is

$$t_{\mathbf{j},\mathbf{j}+\hat{\mathbf{x}}} = (-1)^{j_y} t_x(\mathbf{j}) \ , \qquad t_{\mathbf{j},\mathbf{j}+\hat{\mathbf{y}}} = t_y(\mathbf{j}) \ , \qquad (3.13)$$

where $\mathbf{j} = \{j_x, j_y\}$ labels sites of the square lattice, $\hat{\mathbf{x}}$ and $\hat{\mathbf{y}}$ are unit lattice vectors, and $t_x(\mathbf{j})$ and $t_y(\mathbf{j})$ are (random) nonnegative hopping amplitudes. The honeycomb (brickwall) lattice model[62] is defined on a honeycomb lattice with nonnegative hopping amplitudes. The general lattice model is defined, e.g., on a square or honeycomb lattice with no constraint on the allowed signs of the hopping amplitudes.

Pure-system spectra in the above models can be quite different: thus, the pure π-flux, honeycomb, or weakly staggered square lattice models have Dirac points and a linearly vanishing density of states at $E = 0$, while the pure rectangular lattice model has a Fermi surface and a constant density of states in the general anisotropic case and van Hove singularity in the isotropic square lattice case. With randomness, all these models are believed to have similar low-energy long-wavelength localization physics. In our studies, it is often convenient to think in terms of a particular model when using a particular approach, and we switch among the models at will.

Continuum description

The pure π-flux model has two Dirac points. The corresponding weakly-disordered model is described by a continuum Dirac Hamiltonian[61] $\hat{h}_4 = \begin{pmatrix} 0 & \hat{h}_2 \\ \hat{h}_2^{\dagger} & 0 \end{pmatrix}$, with

$$\hat{h}_2 = \sigma_x(-iv_x\partial_x + iA_x) + \sigma_y(-iv_y\partial_y + iA_y) - iV\mathbf{1}_2 + M\sigma_z \ . \qquad (3.14)$$

In a particular representation, we have $v_x = 2t_x^{(0)}$, $v_y = 2t_y^{(0)}$, $A_x = -2\delta t_x(\mathbf{j})(-1)^{j_x+j_y}$, $A_y = -2\delta t_y(\mathbf{j})(-1)^{j_x+j_y}$, $V = -2\delta t_x(\mathbf{j})(-1)^{j_x}$, and $M = -2\delta t_y(\mathbf{j})(-1)^{j_y}$. Here, the lattice constant has been set to unity, and notation $a(\mathbf{j}) = \delta t(\mathbf{j})e^{i\,\mathbf{q}\cdot\mathbf{j}}$ means that $\delta t(\mathbf{j}) = a(\mathbf{j})e^{-i\,\mathbf{q}\cdot\mathbf{j}} + \ldots$ with slowly varying $a(\mathbf{j})$. Similar continuum Hamiltonians obtain for the honeycomb and weakly staggered square lattice models.

Dirac Hamiltonian $\hat{h}_2$ is non-hermitian and contains a real random mass M, a random imaginary potential $-iV$, and a random imaginary gauge field. The $\{M, V\}$ terms form a "complex random mass" part, which we refer to simply as random mass part. In its absence, $M \equiv V \equiv 0$, the full Hermitian Hamiltonian $\hat{h}_4$ decomposes into two blocks, with the "1-4" block having a form

$$\hat{h}_{\mathcal{A}} = \sigma_x(-i\partial_x + \mathcal{A}_1) + \sigma_y(-i\partial_y + \mathcal{A}_2) \ , \tag{3.15}$$

identical to the (real) random vector potential model of Ref. [5] [here $\{\mathcal{A}_1, \mathcal{A}_2\} \equiv \{A_y, -A_x\}$], and similarly for the "2-3" block. In the following, we refer to the $\{A_x, A_y\}$ part of $\hat{h}_4$ as simply random vector potential part.

The random vector potential model on a lattice

Consider a "random-surface" BPRH defined by "adding" a surface $\Phi(\mathbf{r})$ "on top of" a pure system $\hat{t}_{AB}^{(0)}$ as follows:

$$t_{\alpha\beta} = e^{\Phi(\alpha)}\ t_{\alpha\beta}^{(0)}\ e^{-\Phi(\beta)}. \tag{3.16}$$

One can easily see that if $\vec{\Psi}_A^{(0)}$ is a zero-energy eigenstate of the pure problem, then $\vec{\Psi}_A$ with $\Psi_A(\alpha) = e^{-\Phi(\alpha)}\Psi_A^{(0)}(\alpha)$ is a zero-energy eigenstate of the random-surface problem with $\Phi(\mathbf{r})$.

This provides a particular lattice realization of the random vector potential model. Indeed, in the continuum limit Eq. (3.14) of the π-flux model with weakly-disordered $\Phi(\mathbf{r})$ we obtain $M \equiv V \equiv 0$, $A_x = v_x\partial_x\Phi(\mathbf{r})$, and $A_y = v_y\partial_y\Phi(\mathbf{r})$, so that $\hat{h}_{\mathcal{A}}$ of Eq. (3.15) becomes $\hat{h}_{\mathcal{A}} = \sigma_x(-i\partial_x + \partial_y\Phi) + \sigma_y(-i\partial_y - \partial_x\Phi)$. Field $\Phi(\mathbf{r})$ thus represents the physical (non-gauge) degrees of freedom of the random vector potential.

We consider (continuum or lattice) Gaussian $\Phi(\mathbf{r})$

$$\mathrm{Prob}[\Phi] \propto \exp\left[-\frac{1}{2g}\int d\mathbf{r}\,(\nabla\Phi)^2\right] \ , \tag{3.17}$$

with dimensionless disorder strength g; relevant properties of such surfaces in two dimensions are summarized in Appendix 3.A.

A remark is in order here. In the continuum limit of a general problem, we can separate the random vector potential and random mass parts. However, on a lattice, such separation is not clear to us, but we do know if a problem has only vector potential randomness when we see one Eq. (3.16). Renormalizing on a lattice in Sec. 3.3, we will still speak of the flows of the two parts, implicitly assuming some coarse-grained description and relying on the corresponding results for the continuum model. A more precise lattice alternative to this is a domain wall energetics picture of Ref. [60].

Connection with random dimer problems

There is a direct connection between the π-flux random hopping problem and a random dimer model on the same square lattice. The dimer model consists of all complete coverings (matchings) $\{\mathcal{M}\}$ of the (bipartite) lattice by nearest-neighbor dimers; the energy of a given covering $\mathcal{M}$ is

$$\mathcal{E}_d[\mathcal{M}] \equiv \sum_{\langle\alpha\beta\rangle\in\mathcal{M}} \epsilon_{\alpha\beta}, \tag{3.18}$$

where the sum is over all dimers in this covering, and $\epsilon_{\alpha\beta}$'s are the random bond energies. The fermion-dimer connection is stated most easily for open boundary conditions. In this case, the partition function of the dimer model $Z_d \equiv \sum_{\mathcal{M}} \exp(-\mathcal{E}_d[\mathcal{M}]/T_d)$ at a given dimer temperature T_d can be written as a determinant of an appropriate connection matrix $\hat{t}_{AB}$, $Z_d[A,B] = \det \hat{t}_{AB}$, where

$$t_{\alpha\beta} = \pm e^{-\epsilon_{\alpha\beta}/T_d} \ , \tag{3.19}$$

and the signs of the π-flux model are exactly right [63, 64] to make all the terms in the determinant expansion positive. The honeycomb lattice model with nonnegative bonds has similar dimer connection (our definitions of the π-flux and honeycomb models were made precisely with this in mind), but a more general lattice model has no such direct connection.

Localized bipartite hopping systems

The typically studied bipartite hopping models (e.g., all of the above models with some generic distributions of random hopping amplitudes) are found to be *critical*, by which we mean that the behavior at $E = 0$ is neither truly delocalized nor truly (exponentially) localized. Abusing the language, we will often refer to a system in such a critical state as being in a "delocalized" or "metallic" phase, to distinguish from possible truly localized insulating phases that obtain, e.g., by introducing strong dimerization in the couplings. Pure-system counterparts of these localized phases are gapped band insulators. In our studies, we will specifically consider only one such localized phase most simply described as a strongly-staggered square lattice, with the honeycomb lattice variant shown in Fig. 3.5(a).

3.3 A kind of strong randomness. On the origin of low-energy states

Gade-like dynamical scaling

$$|\ln E| \sim (\ln L)^x \tag{3.20}$$

with $x > 1$ suggests a kind of infinite randomness (the dynamical exponent $z = \infty$), albeit a weak one. This motivates us to try a strong-randomness RG description.[3, 4]

3.3.1 Real-space RG

Consider the bipartite hopping Hamiltonian (3.12). The eigenstates of $\hat{H}$ occur in pairs with energies $\pm E$, and strong-randomness RG proceeds by eliminating, at each step, such a pair of states with energies near the top and the bottom of the band: One finds the largest (in absolute value) coupling in the system, say $t_{1,2}$ connecting sites $1 \in A$ and $2 \in B$; this defines the bandwidth of the problem $2\Omega = 2\max\{|t_{\alpha,\beta}|\}$. If the distribution of the couplings is broad, the eigenfunctions of the two-site problem $\hat{H}[1,2]$ will be good approximations to the eigenstates with energies $\pm\Omega$, since the couplings $t_{1,\beta}$ and $t_{2,\alpha}$ of the pair to the rest of the system will typically be much smaller. These couplings can then be treated perturbatively, and eliminating the high-energy states living on the sites 1 and 2 gives us the following effective couplings between the remaining sites:

$$t'_{\alpha,\beta} = t_{\alpha,\beta} - t_{\alpha,2}\; t_{1,2}^{-1}\; t_{1,\beta} \ . \tag{3.21}$$

The renormalized Hamiltonian is again a bipartite hopping problem, but with two fewer sites; in particular, no diagonal terms are generated. This procedure is now iterated to reach lower and lower energy.

Before proceeding with the discussion of the strong-randomness RG, we remark that we do not address in detail the question of its self-consistency (that is, in which regimes—if at all—the system flows to stronger disorder, with the RG becoming more and more accurate). Rather, we use this RG to give a physical picture behind the more precise arguments to follow. To test some ideas, we have also tried the RG numerically. In the localized phases, the RG indeed provides qualitatively and quantitatively accurate description of the low-energy physics, with the relative "decimation errors" diminishing quickly at low energies; in this case, the RG can be viewed as a consistent implementation of the "Griffiths" arguments given below. But in the delocalized phase, the observed flow to stronger disorder is very weak, and the consistency of the RG is less clear.

Note, however, that the RG actually contains some exact and useful information for any strength of the disorder: The rule Eq. (3.21) is actually an exact transformation for the zero-energy wave function, and as such provides information on the $E=0$ localization properties. Also, running this RG corresponds to running the Sturm sequence method for calculating the integrated density of states at $E=0$ and doing so in a particular order that is, without any a priori knowledge, numerically most reliable; the intermediate terms that appear in this process at a particular length scale give us a rough idea about the corresponding energy scale in the problem.

3.3.2 On the origin of states

The strong-randomness RG associates the low-energy states of the original Hamiltonian with the sites that "survive" down to the corresponding low energy scale. Such a "free" site—say, an A-site—is found if all the B-sites in its immediate neighborhood happen to be "locked" (by stronger bonds) into pairs with some other A-sites. Then, this free A-site can only couple to the next available B-sites, and the corresponding effective couplings are relatively weak since they are mediated through some distance of intervening pair-locked regions.

Anticipating the discussion to follow, note that it is at first difficult to see how such free sites with the associated low energies can be produced often enough in dimensions $d>1$: Naively, the energy scale associated with a pair $\{\alpha, \beta\}$ of "isolated" sites distance l apart is $\sim e^{-c_E l}$. Now, it may seem that to produce such a pair we need of order l^d specific events—for example, we can imagine having a particular pairing pattern for all the other sites in the neighborhood of the two unpaired sites α and β—and this has very low probability $Prob \sim e^{-c_p l^d}$ to happen in $d>1$.

In the dimerized band insulator phase, however, there is an insulating background to start with, and to produce such a pair one only needs to "break" the background

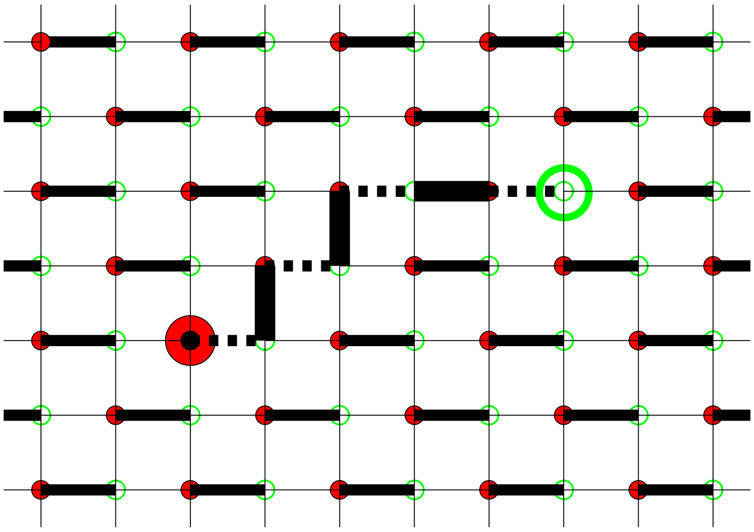

Figure 3.1: "String" mechanism for generating low-energy states in the band insulator phases. Filled and open circles represent A and B sites correspondingly. Medium thick bonds represent a particular background dimer pattern (i.e., bonds that are typically stronger), broken such bonds represent the ones that happened to be atypically weak in a given disorder realization, while the heavy thick bonds represent the couplings that happened to be atypically strong. There is a pair of low-energy states associated with the end-points of the resulting string.

dimer pattern along a string joining the two sites—i.e., of order l specific events (see Fig. 3.1), with the resulting occurrence rate $\sim e^{-c_p' l}$ high enough to give a power-law contribution to the low-energy density of states. Our numerical RG and exact diagonalization studies confirm that this is indeed what happens in such band insulator phases. Note that the above argument goes through for the localized phases in any dimension!

In the "delocalized" phase, on the other hand, we do not have such insulating background. However, the local properties of the "isolating" region need not be very "sharp", as was assumed in $Prob \sim e^{-c_p l^d}$. Rather, there might be some smooth "textures" of the random pairing ("dimer") pattern producing such isolated sites ("defects"), and these may occur with much higher probability.

To be more specific, consider the "random-surface" model Eq. (3.16) (i.e., the random vector potential model) in the limit of strong disorder $g \gg 1$. The RG, being the exact transformation for the zero-energy wave function, preserves the random-surface character of the problem keeping the same $\Phi(\mathbf{r})$: the randomness in the effective couplings that are generated by the RG rule Eq. (3.21) is of the same random-surface form Eq. (3.16) with the same $\Phi(\mathbf{r})$. Thus, at each stage of the RG, the magnitude of the coupling between any two remaining sites α and β is roughly $\sim e^{\Phi(\alpha)-\Phi(\beta)}$. Since the RG eliminates the stronger couplings first, an A-site $\alpha_{\min}$ that is a local minimum of $\Phi(\mathbf{r})$ cannot be decimated out until the "probing" log-energy scale is large enough to "see" the next even lower minima: Indeed, before this happens, the other A-sites in the neighborhood of $\alpha_{\min}$, having higher Φ, are more strongly coupled to any available B-sites in the same neighborhood. The same holds for any B-site $\beta_{\max}$ that is a local maximum of $\Phi(\mathbf{r})$. Thus, the low-energy states of the problem are associated with the local extrema of the surface $\Phi(\mathbf{r})$, while their effective log-energies are given by the corresponding surface height differences (see also Fig. 1.2). In particular, in a finite system, the smallest energy scale is associated with the global extrema of $\Phi(\mathbf{r})$. Our Introduction arguments Eqs. (3.6)–(3.7) now follow. Thus, we see that the random-surface model does generate enough such "isolated" sites to produce a power-law contribution to the density of states, with the dynamical exponent $z \sim \sqrt{g}$. Note that in the above, for the purposes of a rough argument, we ignored the effect of running the RG transformation on the pure model itself—this will change the actual value of the exponent z, but not the $\sim \sqrt{g}$ disorder contribution for $g \gg 1$. For more precise arguments, see Sec. 3.4.1.

In the general case, the Introduction arguments Eqs. (3.9)–(3.10) again follow. As we have already mentioned, within our strong-randomness RG on a lattice, we do not know how to separate the random vector potential and random mass parts in a clear-cut way, so we have to rely on the results of a different RG analysis[55, 57] when discussing how the two types of randomness flow and affect each other. A similar naive argument was used in Ref. [65] to obtain crossover scales in the vortex glass problem. Thus, we predict the modified-Gade forms Eq. (3.4) and (3.5).

We conclude this discussion on the origin of low-energy states with few interesting observations. Recall that the surface in the random vector potential case is also the logarithm of the pseudo-zero-energy-wave function $\Psi_A(\alpha) \sim e^{-\Phi(\alpha)}$. Also, our RG is an exact transformation for such a wave function in the general case. The above analysis then suggests that the $E \neq 0$ low-energy states in the problem are related to the extremal properties of this $E = 0$ wave function.

Note also predictions of this "surface" mechanism in other dimensions. In one dimension, any disorder is of purely "longitudinal" (random-surface) type, and the Gaussian surface is more rough, with

$$|\ln E| \sim \Phi_{\max}(L) - \Phi_{\min}(L) \sim \sqrt{L} \; ; \tag{3.22}$$

this is precisely the Dyson critical scaling for the 1D chain, as discussed in Introduction Chapter 1. For ladders and other bipartite systems that are finite in all but one direction,[38, 39] at the delocalization critical points such that the zero-energy wave function is not exponentially localized, the corresponding surface "looks," at long wavelengths, like the 1D Gaussian surface, and the Dyson DOS again results. On the other hand, in dimensions three and higher the Gaussian surface is basically flat, and this mechanism cannot generate power-law contributions to the density of states. Much of what has been said above for the two-dimensional problem is therefore very specific to 2D.

3.3.3 Detailed structure of the RG

We now establish a suggestive connection between the low-energy states in the bipartite hopping problem and the monomers (defects) in the corresponding random dimer problem. Consider running the above "zero-energy" RG in some specified order. At a given stage of the RG, if we have sites $\mathfrak{A} = \{a_1, \ldots, a_n\} \subset A$ and sites $\mathfrak{B} = \{b_1, \ldots, b_n\} \subset B$ decimated out, the effective coupling between any two remaining sites α and β is

$$t'_{\alpha,\beta} = t_{\alpha,\beta} - \hat{t}_{\alpha,\mathfrak{B}}\, \hat{t}^{-1}_{\mathfrak{A},\mathfrak{B}}\, \hat{t}_{\mathfrak{A},\beta} \ . \tag{3.23}$$

Here, $\hat{t}_{\mathfrak{C},\mathfrak{D}}$ is a matrix of the original bonds joining two subsets $\mathfrak{C} \subset A$ and $\mathfrak{D} \subset B$ (thus, $\hat{t}_{\alpha,\mathfrak{B}}$ is a row-vector, $\hat{t}_{\mathfrak{A},\beta}$ is a column-vector, and $\hat{t}_{\mathfrak{A},\mathfrak{B}}$ is an $n \times n$ matrix). Expression (3.23) follows readily if we note how the RG "solves" for the zero-energy wave function by eliminating any reference to the decimated sites, and this holds for any order of the decimations. One easily obtains

$$t'_{\alpha,\beta} = \frac{\det \hat{t}_{\alpha+\mathfrak{A},\,\beta+\mathfrak{B}}}{\det \hat{t}_{\mathfrak{A},\,\mathfrak{B}}} \ , \tag{3.24}$$

where $\alpha+\mathfrak{A} \equiv \alpha \cup \mathfrak{A} \equiv \{\alpha, a_1, \ldots, a_n\}$, and similarly for $\beta+\mathfrak{B}$.

Recall from Sec. 3.2 that for any two such sets $\mathfrak{C}$ and $\mathfrak{D}$ of equal cardinality

$$\det \hat{t}_{\mathfrak{C},\,\mathfrak{D}} = \sum_{\mathcal{M}} \mathrm{sgn}(\mathcal{M}) \prod_{\langle\alpha\beta\rangle\in\mathcal{M}} t_{\alpha\beta} \ , \tag{3.25}$$

where the sum is over all complete dimer coverings of $\mathfrak{C} \cup \mathfrak{D}$, and $\mathrm{sgn}(\mathcal{M})$ denotes the appropriate permutation sign for matching $\mathcal{M}$. Each term of the sum has a form $\pm \exp\left(-\,\mathcal{E}_d[\mathcal{M}]/T_d\right)$, with the dimer bond energies $\epsilon_{\alpha\beta}$ defined from $|t_{\alpha\beta}| = \Omega_0 e^{-\epsilon_{\alpha\beta}/T_d}$. In the limit of infinite randomness, or equivalently, zero temperature of the dimer system $T_d = 0$, one term—the ground state dimer covering—dominates the whole sum; obviously, the permutation signs never enter in this case.

Consider first this infinite-randomness limit. Specializing to the preceding discussion, the largest term in $\det \hat{t}_{\alpha+\mathfrak{A},\,\beta+\mathfrak{B}}$ corresponds to the optimal (ground state) dimer covering of $\{\alpha+\mathfrak{A}\} \cup \{\beta+\mathfrak{B}\}$, while the largest term in $\det \hat{t}_{\mathfrak{A},\,\mathfrak{B}}$ corresponds to the optimal covering of $\mathfrak{A} \cup \mathfrak{B}$. The two optimal coverings "differ" by a "string" connecting the "added" sites α and β, while the effective coupling $t'_{\alpha,\beta}$, Eq. (3.24), in this infinite-randomness limit, is determined precisely by "propagating" along this string $t'_{\alpha,\beta} = t_1 t_3 \dots t_{2k+1}/(t_2 \dots t_{2k})$, which is the optimal (i.e., producing the largest $|t'|$) such path from α to β utilizing the decimated out sites.

This suggests the following infinite-randomness "dimer RG" sequence: At the n-th stage of the dimer RG, we find the ground state configuration $\mathcal{M}_n^{(gs)}$ with n dimers, defining $\mathcal{E}_n^{(gs)} \equiv \mathcal{E}_d[\mathcal{M}_n^{(gs)}]$, and refer to the $2n$ covered sites as decimated out. The monotonicity property of such optimal partial coverings ensures that this definition of the decimated out sites is indeed sensible, since the optimal $(n+1)$-dimer covering differs from the optimal n-dimer covering by two added sites (and the connecting string). A natural hopping problem energy scale associated with the two sites decimated out going from stage n to $n+1$ is $|t'| = \Omega_0 \exp\left[-(\mathcal{E}_{n+1}^{(gs)} - \mathcal{E}_n^{(gs)})/T_d\right]$. The property $\mathcal{E}_{n+1}^{(gs)} - \mathcal{E}_n^{(gs)} \geq \mathcal{E}_n^{(gs)} - \mathcal{E}_{n-1}^{(gs)}$ ensures the expected monotonicity of the sequentially eliminated hopping energies in this dimer RG. Note, however, the subtle balancing in the "pairings" of the decimated out sites—these do not stay rigid but can change each time we decimate sites.

Of course, this can all be reformulated starting from the ground state complete dimer covering (with $N = L^2/2$ dimers) of the whole lattice and then adding monomers (defect pairs) into the system in the most optimal way. In particular, the lowest energy state in the hopping problem corresponds precisely to the first such pair, with the corresponding estimate

$$|t'|_{\min}^{(\text{dimerRG})} \equiv \Omega_0 \exp\left(\frac{\mathfrak{E}_{\text{opt.def.}}}{T_d}\right) ; \tag{3.26}$$

where $\mathfrak{E}_{\text{opt.def.}} \equiv \mathcal{E}_{N-1}^{(gs)} - \mathcal{E}_N^{(gs)}$ is the optimized (lowest energy) defect pair energy. This is all, of course, assuming the system has complete coverings to start with.

[We use this natural context to also characterize the situations when the random hopping problem has true $E=0$ eigenstates. There are two ways for such eigenstates to appear. First, the properties of the hopping lattice may force the existence of the zero-energy states for any values of couplings: the simplest such example has unequal numbers of A and B sites $N_A \neq N_B$, while in the $N_A = N_B$ case we may have some disconnected or "dangling" lattice parts. Second, there may be some cancellations occurring in the system making $\det \hat{t}_{\mathfrak{A},\,\mathfrak{B}} = 0$ for some relevant subsets $\mathfrak{A}$ and $\mathfrak{B}$. Of course, the zero-energy RG, by the very construction, will find all the $E = 0$ states in the system—these will appear as free sites that decouple completely from the rest of the system. Now, ignoring the accidental "cancellations" in the general case, the dimer RG will also find all the zero-energy states that appear for purely graph reasons. More precisely, one can easily show that the number of such "graph-zero-energy-eigenstates" is equal to the minimal number of free sites that are left uncovered by any partial cover of the system (also called "deficiency" number of the bipartite graph).]

Returning to the finite-randomness case, there are several issues that stand out when trying to relate the low-energy states of the hopping problem to the monomers in the corresponding finite-temperature random dimer system. The determinant $\det \hat{t}_{\mathfrak{A},\,\mathfrak{B}}$ and the dimer partition function $Z_d[\mathfrak{A}, \mathfrak{B}]$ still contain the same (in absolute value) terms, but now the dimer ground state by itself does not determine the corresponding full sums, so the permutation signs become important. But even if we use the dimer partition function only to bound the absolute value of the determinant, we are still faced with the dimer problem at finite temperature, which now has significant entropic contributions, since local moves from the ground state cost only finite energy. In this situation, to estimate $Z_d[\mathfrak{A}, \mathfrak{B}]$ we can no longer think solely in terms of the ground state pairing. However, we are primarily interested in the ratios of the determinants like $\det \hat{t}_{A,\,B}$ and $\det \hat{t}_{A-\alpha,\,B-\beta}$, i.e., the difference in the corresponding free energies of the dimer system without defects and with two defects. Since large parts of the entropic terms in the two systems come from the same local moves, the ground state energy difference of the two may still be a relevant object. More precisely, we have to consider *effective thermodynamics* of the defects themselves—i.e., taken relative to the defect-free system—and whether this effective thermodynamics is ground-state dominated. We postpone this discussion till a more specific setting of Sec. 3.4.2.

3.4 "Variational" bounds on the states near the band center

Motivated by the above observations, we now establish more rigorous bounds on the dynamical scaling in the system. Consider the bipartite Hamiltonian (3.12) in a finite sample and assume that there are no zero-energy states and no edge states; for concreteness, we can think of some regular lattice block with some nice boundary conditions, e.g., the π-flux model on an $L\times L$ square with free bc and even L. We can then calculate the smallest positive energy $E_{\rm min}\equiv E^{+}_{\rm min}$ of $\hat{H}$ from

$$E_{\rm min}=\frac{1}{||\hat{t}_{AB}^{-1}||}\ . \tag{3.27}$$

Here $||\hat{C}||$ is the matrix norm of the operator $\hat{C}$ and satisfies

$$\max_{i,j}|C_{ij}|\leq||\hat{C}||\leq\sqrt{\sum_{i,j}|C_{ij}|^2}\leq\sum_{i,j}|C_{ij}|\ . \tag{3.28}$$

Expressions (3.27) and (3.28) formalize the above association of the low-energy states with the optimized defects for the case of the smallest positive energy eigenstate. Indeed, we have

$$(\hat{t}_{AB}^{-1})_{\beta\alpha}=\pm\frac{\det\hat{t}_{A-\alpha,\,B-\beta}}{\det\hat{t}_{AB}}\ , \tag{3.29}$$

which is precisely the already encountered ratio of the determinants, and the above inequalities suggest that the two "defect" sites α and β should be chosen in some optimal way. We will use these inequalities to obtain, most importantly, *lower bounds* for the smallest positive energy. [Note in passing that the leftmost inequality in Eq. (3.28) implies that the zero-energy RG estimate Eq. (3.24) is always an upper bound for $E^{+}_{\rm min}$.]

3.4.1 The random vector potential model

Applying the above bounds to the "random-surface" model Eq. (3.16), we obtain, in particular,

$$||\hat{t}_{AB}^{-1}||^2\leq\sum_{\alpha,\beta}e^{2\Phi(\beta)-2\Phi(\alpha)}|G_0(\beta,\alpha)|^2, \tag{3.30}$$

where $G_0(\beta,\alpha)\equiv(\hat{t}_0^{-1})_{\beta\alpha}\equiv\langle\beta|\hat{H}_0^{-1}|\alpha\rangle$ is the $E=0$ Green's function (propagator) for the pure lattice problem. The propagator G_0 can be calculated explicitly for each particular pure system. In the following, we consider specifically the π-flux lattice model with free bc; the lattice propagator (Dirac fermions!) can be found, e.g., in Ref. [66], but here we need only to know that $G_0(\mathbf{r}_1, \mathbf{r}_2)$ is bounded and behaves as $|G_0(\mathbf{r}_1, \mathbf{r}_2)| \sim |\mathbf{r}_1 - \mathbf{r}_2|^{-1}$ for large $|\mathbf{r}_1 - \mathbf{r}_2| \gg 1$. A simple (completely rigorous) bound $\|\hat{t}_{AB}^{-1}\| \leq \text{const} \times \mathfrak{Z}(L)$ immediately follows from the boundedness of G_0, but we can do better. Here, $\mathfrak{Z}(L)$ is the partition function for a classical particle living in a potential $V(\mathbf{r}) = 2\Phi(\mathbf{r})$—see Appendix 3.A, where we also summarize other needed properties of such 2D Gaussian surfaces.

In the *strong-randomness* regime $g > g_c \equiv 2\pi$, we expect that the sum (3.30) is dominated by the β's near the maxima of $\Phi(\mathbf{r})$ and the α's near the minima of $\Phi(\mathbf{r})$—similarly to the sum Eq. (3.A.3) for $\mathfrak{Z}(L)$. We also expect that these extrema are separated by distances of order L (the precise statement would be that the distance between the global maximum and minimum of $\Phi(\mathbf{r})$ is L times a random number of order one). This suggests that

$$\|\hat{t}_{AB}^{-1}\| \leq \textit{(num.fact.)} \times \frac{e^{\Phi_{\max}(L) - \Phi_{\min}(L)}}{L} \sim \frac{\mathfrak{Z}(L)}{L} \; . \tag{3.31}$$

The expected uncertainty in the rhs of this expression from one disorder realization to another is simply a random $O(1)$ numerical factor *(num.fact.)*. [Note that even though the above estimate of the sum (3.30) does not constitute a rigorous proof, it is fairly robust, while a more formal proof is likely possible along the lines of Refs. [58, 59].] Since the sum in the norm estimate is essentially dominated by few terms, this also provides a lower bound for $\|\hat{t}_{AB}^{-1}\|$, that differs from the upper bound (3.31) by only an $O(1)$ numerical factor:

$$\|\hat{t}_{AB}^{-1}\| \geq \max_{\alpha,\beta} |(\hat{t}_{AB}^{-1})_{\beta\alpha}| = \text{const} \times \frac{e^{\Phi_{\max}(L) - \Phi_{\min}(L)}}{L} \; ; \tag{3.32}$$

the bound is rigorous (and completely general) since the distance between the global extrema cannot exceed the sample size. Thus, the smallest positive energy is expected to scale with the system size as

$$E_{\min} = \textit{(num.fact.)} \times \frac{L}{\mathfrak{Z}(L)} \sim \frac{(\ln L)^{\frac{3}{2}\sqrt{\frac{g}{g_c}}}}{L^{4\sqrt{\frac{g}{g_c}} - 1}} \; . \tag{3.33}$$

In particular, for the dynamical exponent we obtain

$$z = 4\sqrt{\frac{g}{g_c}} - 1 \; , \quad g > g_c \; . \tag{3.34}$$

In Eq. (3.33) we have also included the logarithmic correction from Ref. [59] to show that the minimal energy is somewhat larger than expected from the simple-z power-law; note, however, that the actual form of such log-corrections can in general depend on the boundary conditions used.[59]

In the *weak-randomness* regime $g < g_c$, the bound Eq. (3.30) is not as precise. Thus, in the pure-system $g = 0$ case we obtain

$$\sum_{\alpha,\beta} |G_0(\beta,\alpha)|^2 = \mathrm{Tr}\, \hat{H}_0^{-2} \sim L^2 \ln L \ , \tag{3.35}$$

i.e., $E_{\min} \geq L^{-1}(\ln L)^{-1/2}$, which gives the correct exponent $z = 1$, but is certainly an underestimate. Similarly, in the $g \neq 0$ case, we can prove that for any $\eta > 0$

$$\|\hat{t}_{AB}^{-1}\| \leq \mathrm{const} \times L^{1+2g/g_c+\eta} \tag{3.36}$$

with probability one in the limit $L \to \infty$. The proof (following the lines of Ref. [58]) applies the inequality $Prob\,(X \geq K) \leq \langle X \rangle / K$, valid for any nonnegative random variable X, to the special X equal to the rhs of Eq. (3.30). Thus, for the dynamical exponent we obtain quite generally

$$z \leq 1 + \frac{2g}{g_c} \ . \tag{3.37}$$

While this result is valid in the strong disorder regime as well, in this case an individual realization essentially never samples the tails of the distributions that determined the average $\langle X \rangle$, and our earlier treatment leading to Eq. (3.34) is more appropriate. For weak randomness $g < g_c$, we can also give a plausible argument for the opposite inequality $z \geq 1 + 2g/g_c$. It suffices to provide an upper bound for $E_{\min}$, and a good trial wave function for this seems to be

$$\vec{\psi}_B = \hat{t}_{AB}^{-1} e^{-\Phi(\vec{A})} \ , \tag{3.38}$$

with $E_{\min} \leq \|\hat{t}_{AB}\vec{\psi}_B\| / \|\vec{\psi}_B\|$ bounded by

$$E_{\min}^2 \leq \frac{\sum_\alpha e^{-2\Phi(\alpha)}}{\sum_\beta e^{2\Phi(\beta)} \Big(\sum_\alpha G_0(\beta,\alpha) e^{-2\Phi(\alpha)} \Big)^2} \ . \tag{3.39}$$

We first justify that we can reasonably estimate

$$\Big| \sum_\alpha G_0(\beta,\alpha) e^{-2\Phi(\alpha)} \Big| \sim \sum_\alpha |G_0(\beta,\alpha)| e^{-2\Phi(\alpha)} \ . \tag{3.40}$$

Indeed, $G_0(\mathbf{r}_1, \mathbf{r}_2)$ is some fixed function, while the sums involving $e^{-2\Phi(\alpha)}$ over macro-subregions (with $G_0 > 0$ and $G_0 < 0$) always have $O(1)$ random numerical factors (see, e.g., expressions for $\mathfrak{Z}(L)$ in Appendix). Now, using $|G_0| \geq L^{-1}$ we obtain $E_{\min} \leq$ *(num.fact.)* $\times L/\mathfrak{Z}(L)$, which gives the desired bound in the weak-disorder regime (and reproduces our earlier result in the strong-disorder regime).

Even though we cannot prove it rigorously, we expect that the expression

$$z = 1 + \frac{2g}{g_c} , \quad g < g_c , \tag{3.41}$$

is exact without any logarithmic corrections. This is also the original expression of Ref. [5] from their weak-disorder replica analysis, which is known to give exact results also for the static quantities of Appendix 3.A—but only in the regime $g < g_c$. Finally, note that the two expressions for $z(g)$, Eqs. (3.34) and (3.41), join continuously and smoothly at g_c [and we expect that $E_{\min} =$ *(num.fact.)* $\times L/\mathfrak{Z}(L)$ is valid for any disorder strength.]

The above results are formally valid only for the dynamical exponent z_1 that determines the scaling of the smallest gap in the system. Of course, having the upper bounds on $E_{\min}(L)$, we can always construct bulk density of states with the DOS dynamical exponent $z_{\rm DOS}$ at least as large. But quite generally, we expect that there is only one dynamical exponent in the system $z_{\rm DOS} \equiv z_1 \equiv z$. Some numerical checks for the bulk density of states are shown in Figs. 3.2 and 3.3, and these are in good agreement with the above expectations. (See also Ref. [67] studying essentially identical dynamical freezing phenomenon for random walks in random log-correlated potentials in one and two dimensions).

To conclude this subsection, we emphasize again our main result $z(g) \sim \sqrt{g}$ for the dynamical exponent at strong randomness; pictorially, the surface $\Phi(\mathbf{r})$ does not allow the low-energy states to fall beyond its extrema.

3.4.2 Scaling of the lowest energy in the general case

In general, we can always bound the numerator in Eq. (3.29) as $|\det \hat{t}_{A-\alpha,B-\beta}| \leq Z_d[A-\alpha, B-\beta]$ by the corresponding dimer partition function with two *fixed* monomers α and β. We now specialize to the π-flux model with free bc (or any other model with the direct dimer connection), so that for the lattice with no defects we have $|\det \hat{t}_{AB}| = Z_d[A, B] \equiv Z_N$, with $N = L^2/2$ the total number of dimers.

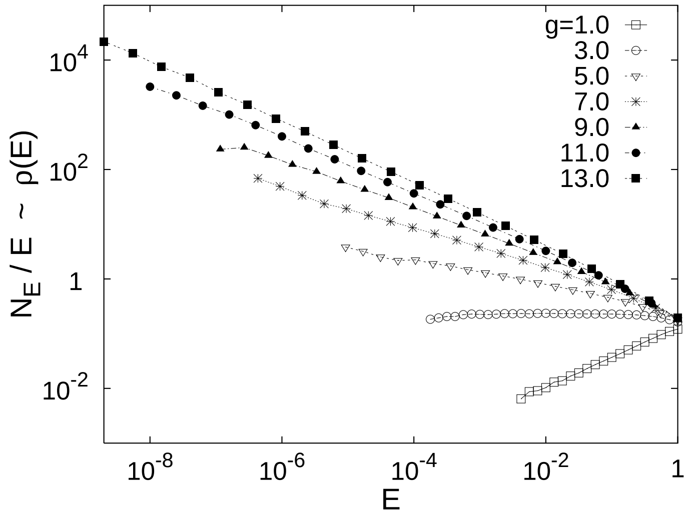

Figure 3.2: Density of states in the π-flux model with the "random-surface" disorder [see Eq. (3.16)] calculated for 192×192 system with open boundary conditions, for varying disorder strength g. The data is averaged over 10 disorder realizations. Note that the plots have some curvature for strong disorder—this is probably because of the logarithmic corrections to the power-laws in this regime.

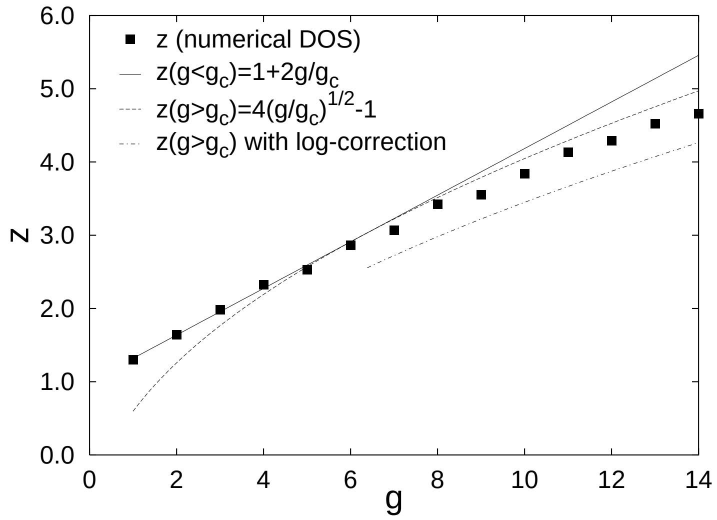

Figure 3.3: Dynamical exponent for the π-flux model with the random-surface disorder extracted from the data of Fig. 3.2. The additional lines show theoretical predictions in the two regimes (with $g_c = 2\pi$)), and also a rough estimate $z_{\rm eff}(L) = z(\infty) - (3/2)\sqrt{g/g_c}\,(\ln\ln L)/(\ln L)$ of the log-correction in the strong-disorder regime for the specific system size studied.

In this case, we don't have to worry about the denominator at all, obtaining, e.g.,

$$||\hat{t}^{-1}_{AB}|| \le \frac{\sum_{\alpha\beta} Z_d[A-\alpha, B-\beta]}{Z_d[A,B]} = \frac{Z_{N-1}}{Z_N} \ , \tag{3.42}$$

where Z_{N-1} is the partition function of the dimer problem with two *free* defects allowed to be anywhere on the lattice.

Analysis of Ref. [60] suggests that the effective finite-temperature thermodynamics of such a pair of defects (i.e., taken relative to the thermodynamics of the dimer system with no defects) can be obtained by treating the defects as classical charged particles (with opposite charges for A and B monomers) in a random "electrostatic" potential $\upsilon(\mathbf{r})$ with average correlations

$$\overline{[\upsilon(\mathbf{r}) - \upsilon(\mathbf{r}')]^2} \sim \ln^2|\mathbf{r} - \mathbf{r}'| \ . \tag{3.43}$$

The extremal properties of this random surface $\upsilon(\mathbf{r})$ are also characterized in Ref. [60]. In a finite box of linear size L, we have for the average and the standard deviation of the distribution of the global extrema

$$\overline{\upsilon_{\max}} \sim (\ln L)^{3/2}, \qquad \sigma(\upsilon_{\max}) \sim (\ln L)^{1/2} \ , \tag{3.44}$$

This immediately implies

$$\frac{Z_{N-1}}{Z_N} \le L^4 \exp\left[\frac{\upsilon_{\max} - \upsilon_{\min}}{T_d}\right] \le \exp\left[\text{const} \times (\ln L)^{3/2}\right] \ , \tag{3.45}$$

and correspondingly for the lower bound on the smallest positive energy

$$\ln E_{\min} \ge -\text{const} \times (\ln L)^{3/2} \ . \tag{3.46}$$

In the above, making the positive number "const" slightly larger takes care of any prefactors L^r and any uncertainty $o((\ln L)^{3/2})$ in $\upsilon_{\max}$. This is a simple manifestation of the ground state dominance[59] in our finite-temperature defect thermodynamics in the random potential $\upsilon(\mathbf{r})$ with correlations Eq. (3.43). The above crude estimates are good enough to reach the main conclusion Eq. (3.46) precisely because of this, even though the ground state dominance is a very weak one. Since it is effectively few defect positions that determine the above estimates, we expect that Eq. (3.46) provides not only the lower bound but the actual leading term in the logarithm of the smallest positive energy in the system, thus obtaining the modified-Gade scaling proposed in the Introduction.

To get some idea about the subleading terms and, in particular, the relationship between the actual lowest gap and the dimer RG "estimate" Eq. (3.26) from the optimized defect pair, it is instructive to consider the random vector potential model in the strong-randomness regime from this dimer perspective. In this case, for a given fixed configuration of monomers, any dimer covering has the same energy, and the partition function is essentially purely configurational (entropic). Thus, for two fixed defects α and β, we have

$$\frac{Z_\Phi[A-\alpha, B-\beta]}{Z_\Phi[A,B]} = \frac{Z_0[A-\alpha, B-\beta]}{Z_0[A,B]} \times e^{\Phi(\beta)-\Phi(\alpha)} \approx \frac{\text{const}}{|\mathbf{r}_\beta - \mathbf{r}_\alpha|^{1/2}} \times e^{\Phi(\beta)-\Phi(\alpha)} ,$$

since a relative number of configurations with defects decays as $|\mathbf{r}_\beta - \mathbf{r}_\alpha|^{-1/2}$ (Ref. [66]). Taking into account the ground state dominance, we obtain, instead of Eq. (3.45), $Z_{N-1}/Z_N \approx$ *(num.fact.)* $\times L^{-1/2} e^{\Phi_{\max}-\Phi_{\min}}$.

Consider now the step $|(\hat{t}_{AB}^{-1})_{\beta\alpha}| \le Z_d[A-\alpha, B-\beta]/Z_d[A,B]$ connecting the fermion and the dimer problems. The lhs is $\approx \text{const} \times |\mathbf{r}_\beta - \mathbf{r}_\alpha|^{-1} e^{\Phi(\beta)-\Phi(\alpha)}$, where we used the Dirac fermion propagator for $\hat{t}_0^{-1}$, and differs from the rhs precisely because of the permutation signs in the expansion of $\det \hat{t}_{A-\alpha,B-\beta}$. Finally, the defect pair energy for the optimized positions is $\mathfrak{E}_{\text{opt.def.}}/T_d = -(\Phi_{\max} - \Phi_{\min})$. Putting everything together, we obtain $E_{\min} \approx$ *(num.fact.)* $\times L^{-1} \exp(\mathfrak{E}_{\text{opt.def.}}/T_d)$, which of course coincides with our earlier result. Thus, the dimer RG expression (3.26) underestimates the smallest positive energy by a factor L^{-1} coming from the entropic and the fermionic sign terms.

Returning to the general case, we expect some similar underestimate L^{-r} factor, and in our numerical tests (see below) we indeed find that the dimer RG provides a strong lower bound for $E_{\min}$. However, we cannot be more precise here because of the following difficulty: Unlike the random vector potential case, we cannot separate the defect energetics from the dimer configurational combinatorics: Ref. [60] suggests that a fixed pair of defects will have an average energy $O(+\ln|\mathbf{r}_\alpha - \mathbf{r}_\beta|)$ because the system constrained by the presence of the defects cannot take as much advantage of the low energy bonds, and $\mathfrak{E}_{\text{opt.def.}}$ will have a similar $O(+\ln L)$ contribution, in addition to $O(-(\ln L)^{3/2})$ from $\upsilon_{\min} - \upsilon_{\max}$.

3.5 Numerical tests

We have performed extensive numerical tests using exact diagonalization and numerical RG. The results are consistent with the generalized-Gade scaling Eq. (3.20) in the delocalized phase and power-law scaling in the localized phase. Unfortunately, in the delocalized phase, direct diagonalization methods do not allow us to distinguish unambiguously the different exponents x in the generalized-Gade scaling. However, indirect methods indicate $x = 3/2$, different from the original Gade form. In the localized phase, on the other hand, all methods clearly point to power-law density of states (with nonuniversal dynamical exponent) generated by the "string" Griffiths mechanism discussed earlier.

3.5.1 Illustration

We first demonstrate some difficulties that plague direct diagonalization studies. Consider Fig. 3.4 where we show the calculated[68, 69, 70] density of states $\rho(E)$ for the honeycomb lattice with hopping amplitudes chosen uniformly from $[1-W, 1+W]$. For $W < 1$, on the length scales studied, the density of states is apparently power-law vanishing, with the observed effective exponent z_{eff} that depends on the strength of disorder W. It is simply impossible from the data to guess that there may be something else happening at still lower energy scales! For $W = 1.0$ the density of states is almost constant, with a slight hint on some weak divergence at still lower energies observed for the largest system studied. For $W > 1.0$ (i.e., now allowing both positive and negative couplings—the honeycomb lattice is still statistically isotropic, but the direct dimer connection is lost in this case), a power-law divergence is observed, and we also see some curvature in the log-log plot of $\rho(E)$ vs E suggestive of an even stronger divergence at still lower energy.

On the same figure, we also show some information about the "conducting" properties of the systems at $E = 0$, obtained from numerical transfer matrix analysis (see also Table 3.1). The displayed Lyapunov spectrum density $\mathcal{P}_{\text{Lyap},0}$ provides an estimate of the system's dimensionless conductivity $\overline{\sigma}$—see the following subsection for details. All we want to note here is that, for the typical systems studied, $\overline{\sigma}$ is of order one and can vary somewhat. Now, if we want to check the Gade prediction for the density of states, from the original Ref. [7] we realize that the asymptotic form Eq. (3.1) is expected to hold only below the crossover scale[71]

$$E_{\text{cross}} \sim \Omega_0 e^{-16\pi^2 y^2 \overline{\sigma}^2} \ . \tag{3.47}$$

Here, Ω_0 is some bare energy, and y is some dimensionless parameter of order one. We do not know how to estimate y precisely (but from Refs. [7, 54] we conclude $y \gtrsim 1$). In addition, we can estimate $\overline{\sigma}$ only up to some unknown numerical factor.

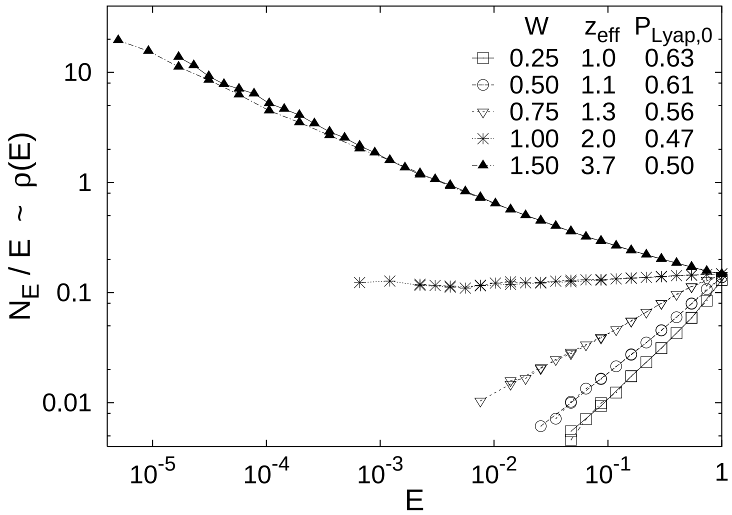

Figure 3.4: Illustration of the "apparently nonuniversal" behavior of the density states (normalized per lattice site). The system is a 192×192 honeycomb lattice with hopping elements chosen randomly from a uniform distribution in $[1-W, 1+W]$; free boundary conditions are used in one direction and periodic bc in the other [see Fig. 3.5(a)]. The data is averaged over 10 disorder realizations; the lowest energy shown in each case corresponds roughly to the second-lowest energy state in the finite sample. Similar data for a smaller 96×96 system is also shown; from such comparisons, we conclude that the density of states plotted is indeed the bulk density of states. The effective dynamical exponent $z_{\rm eff}$ is obtained by fitting the integrated density of states N_E to the form $N_E \sim E^{d/z}$ over the range $2 < L^2 N_E < 200$ in each case. Direction-averaged Lyapunov spectrum density $\overline{\mathcal{P}}_{\rm Lyap,0}$ is calculated from numerical transfer matrix studies and provides a rough idea on the conducting properties of the system (see text and Table 3.1 for details).

Table 3.1: Results of the transfer matrix studies for the same systems as in Fig. 3.4 [see also Fig. 3.5(a)]. We show the Lyapunov spectrum density $\mathcal{P}_{\rm Lyap,0}$ for transfer in both $\hat{\mathbf{x}}$ and $\hat{\mathbf{y}}$ directions (these densities are measured per lattice units of the square lattice underlying our brickwall lattice), as well as the geometric mean $\overline{\mathcal{P}}_{\rm Lyap,0} \equiv (\mathcal{P}^{xx}_{\rm Lyap,0}\, \mathcal{P}^{yy}_{\rm Lyap,0})^{1/2}$. We also show the ratio $\Lambda^{yy} \equiv (2\nu_N N)^{-1}$ for the transfer in the $\hat{\mathbf{y}}$ direction, which serves as an alternative measure of (de)localization in this direction.

W	$\mathcal{P}^{xx}_{\rm Lyap}$	$\mathcal{P}^{yy}_{\rm Lyap}$	$\overline{\mathcal{P}}_{\rm Lyap}$	Λ^{yy}
0.25	0.36	1.09	0.63	47
0.50	0.35	1.05	0.61	11
0.75	0.32	0.97	0.56	2.3
1.00	0.27	0.82	0.47	1.8
1.50	0.29	0.86	0.50	0.86

However, our goal here is not to get the precise crossover scales, but only some feeling of the numbers involved. To this end, we set $y = 1$ and check how this crossover energy changes as we vary $\overline{\sigma}$. For the three values $\overline{\sigma} = 1.0$, 0.5, and 0.2, we get $E_{\rm cross}/\Omega_0 = 10^{-69}$, 10^{-17}, and 10^{-3}, correspondingly! For energies above the crossover energy, Gade predicts effective power-law density of states, and this is probably all that has been observed in the previous numerical studies. Note also that the proposed modified-Gade form Eq. (3.5) is a weaker divergence than the original one, which is probably another reason why it has proved difficult to observe the Gade DOS. Of course, we expect more complicated crossovers in this case,[65] but some similar estimates will still hold. Being in two dimensions, one should therefore be very cautious when looking for the asymptotic behavior.

The above also suggests a way to bring the crossover energy up into the range accessible to direct numerical studies—we should make the system look less delocalized; this is what we do shortly.

3.5.2 The choice of the system

In the following, we present our numerical results only for one specific system—the brickwall (honeycomb) lattice of Fig. 3.5(a). Nearest-neighbor hopping amplitudes t_e are taken randomly and independently from uniform distribution $[0, J_e]$. When $J_e \equiv 1$ for all bonds of the lattice (i.e., all t_e's are taken from the same distribution and the underlying honeycomb lattice is statistically isotropic) the system is not exponentially localized at $E = 0$, as can be checked by direct transfer matrix analysis (see below). By allowing the horizontal bonds to be stronger on average, $J_e = e^{\delta}$ for the dark thick bonds in Fig. 3.5(a) (now obtaining anisotropic honeycomb lattice), we can drive the system into a localized state for strong enough $\delta > \delta_c$, but for small $\delta < \delta_c$ the system remains "delocalized." The phase diagram is shown in Fig. 3.5(b).

Our specific choice of the system is explained by the following reasoning: We want to perform all our numerics on the same system so that we can compare results of different approaches. We want a system that has the precise connection $\det \hat{t}_{AB} = Z_d[A, B]$ with the corresponding random dimer problem so that we can further check our arguments of Sec. 3.4.2 (therefore we allow only nonnegative random bonds for the honeycomb lattice). And finally, we want a system that in its isotropic form shows at least a hint of the low-energy singularity for the accessible system sizes [thus, the largest $z_{\rm eff}$ that we can observe for the π-flux lattice with order one bare randomness is $z_{\rm eff}(L{=}192) = 1.5$].

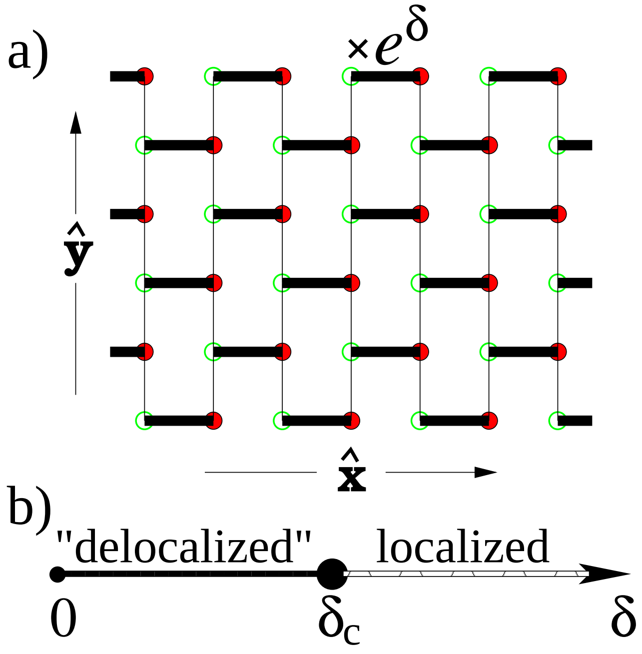

Figure 3.5: a) Brickwall lattice system that we study numerically. Different groups of hopping amplitudes are chosen from different uniform distributions $[0, J]$, with $J = 1$ for thin lines (regular bonds) and $J = e^{\delta}$ for dark thick lines (dimerized bonds). b) Phase diagram of this system from transfer matrix analysis; $\delta_c \approx 1.432$.

The fact that our lattice has the precise $E = 0$ dimer connection does not mean that the results presented below are non-generic. We also studied the honeycomb and square lattices with random bonds of any sign and obtained qualitatively similar results. In these systems with disorder strength of order one, we actually observe a stronger effective divergence in $\rho(E)$, which can be more readily checked for the precise functional form, but only through multi-parameter fits, which are not entirely convincing. Since we can also bring the crossover energy up into the numerically accessible range by increasing δ preserving at the same time the dimer connection, this is what we choose to do; the more precise "dimer" arguments are also more convincing. Note that the suggestive strong-randomness association of the low-energy states in the hopping problem with the optimized defects in the dimer problem is probably still valid in some effective sense even when the fermionic problem does not have the precise $E = 0$ dimer connection.

3.5.3 Transfer matrix analysis

We now summarize the transfer matrix analysis that gives us the phase diagram Fig. 3.5(b), and also explain our procedure for estimating the conductivity $\overline{\sigma}$. The general setting is as follows:[72, 49] Consider transferring the wave function along a strip of transverse size $N \equiv L_\perp$. The transfer matrix is a $2N \times 2N$ matrix, and we calculate the Lyapunov spectrum of the corresponding random matrix product. The $2N$ Lyapunov exponents ν_i come in $\pm$ pairs, and we focus on the positive half of the Lyapunov spectrum $\nu_1 \geq \nu_2 \geq \ldots \geq \nu_N \geq 0$. The largest localization length $\xi_{\rm max}$ in the quasi-1D strip is obtained as the inverse of the smallest in absolute value Lyapunov exponent, $\xi_{\rm max} \equiv 1/\nu_N$. If $\xi_{\rm max}(N)$ as a function of the transverse size N is found to increase linearly with N, the system is said to be delocalized (more precisely, the 2D system is not exponentially localized); the ratio $\Lambda \equiv \xi_{\rm max}/(2N) = (2\nu_N N)^{-1}$ then provides a rough measure of the delocalized character of the system. If, on the other hand, $\xi_{\rm max}(N \to \infty)$ saturates to a finite value, the 2D system is localized. Alternatively,[72] the system is delocalized if there is a finite density of Lyapunov exponents

$$\mathcal{P}_{\rm Lyap}(\nu) \equiv \lim_{N\to\infty} N^{-1} \sum_i \delta(\nu - \nu_i) \tag{3.48}$$

at $\nu = 0$; similarly, the system is localized if there is a gap in the Lyapunov spectrum around $\nu = 0$. In the delocalized state, the Lyapunov spectrum density $\mathcal{P}_{\rm Lyap,0} \equiv \mathcal{P}_{\rm Lyap}(\nu{=}0)$ at $\nu = 0$ is a measure of the conducting properties of the system. [We defined Λ so that the two measures Λ and $\mathcal{P}_{\rm Lyap,0}$ coincide when the Lyapunov spectrum exhibits a form of rigidity $\nu_N : \nu_{N-1} : \nu_{N-2} \ldots = 1 : 3 : 5 \ldots$ for the few smallest exponents.]

Specializing to our bipartite hopping problem at $E = 0$, we observe that the two sublattices decouple, and it is advantageous to transfer on one sublattice only (say, the A-sublattice), recovering the Lyapunov spectrum of the whole system from appropriate symmetries. Furthermore, for the brickwall lattice of Fig. 3.5(a), the sublattice transfer in the $\hat{\mathbf{x}}$ direction involves only one column of A-sites at a time, but now the individual sublattice Lyapunov spectrum is not symmetric around zero. (Note in passing that in such a system with a free left boundary, there will be edge states living on the A-sites of the boundary, and the number of such edge states is precisely the number of negative Lyapunov exponents for the transfer in this case.) We employ all these simplifications in our numerical calculations; however, for the final results, we always quote the $\mathcal{P}_{\rm Lyap,0}$ for the whole system including both sublattices.

For the brickwall lattice of Fig. 3.5(a), there are two inequivalent directions $\hat{\mathbf{x}}$ and $\hat{\mathbf{y}}$, and we check that from the transfer matrix point of view the system is either delocalized in both directions or is localized in both directions. Thus, even though the system is somewhat anisotropic, we expect it to exhibit true two-dimensional behavior in the delocalized phase not too close to the localization transition. Our numerical results are given in Table 3.1 for the systems of Fig. 3.4, and in Table 3.2 for the systems of Fig. 3.6. To estimate $\mathcal{P}_{\rm Lyap,0}$ we typically use several Lyapunov exponents that are closest in absolute value to zero. As an alternative localization measure in the $\hat{\mathbf{y}}$ direction, we also give the ratio Λ^{yy} [the two measures coincide for the systems with $W > 1.0$, while for $W \leq 1.0$ the smallest exponent ν_N is found relatively closer to zero than suggested by the rigidity ratios $1:3:5\ldots$]. The figures themselves quote only the direction-averaged $\overline{\mathcal{P}}_{\rm Lyap,0} \equiv \sqrt{\mathcal{P}^{xx}_{\rm Lyap,0}\,\mathcal{P}^{yy}_{\rm Lyap,0}}$: If the Lyapunov exponents are defined as growth exponents per unit length instead of per lattice unit, and if the corresponding density is also defined per transverse length, the lattice spacings a_x and a_y enter both $\mathcal{P}^{xx}_{\rm Lyap,0} \sim a_x/a_y$ and $\mathcal{P}^{yy}_{\rm Lyap,0} \sim a_y/a_x$, but not $\overline{\mathcal{P}}_{\rm Lyap,0}$.

We see that for $\delta = 0$ the system is indeed delocalized. The fact that it remains delocalized for some range of values $\delta > 0$ can be seen most clearly by considering the transfer on the A-sublattice in the $\hat{\mathbf{x}}$ direction. In this case, multiplying the horizontal bonds by e^{δ} simply shifts the whole Lyapunov spectrum rigidly down by δ, $\nu_i \to \nu_i - \delta$. Thus, there remains some finite Lyapunov spectrum density $\mathcal{P}_{\rm Lyap,0}$ for a range of δ, until the top of the spectrum reaches $\nu = 0$, and only then the system localizes. The critical δ_c can be estimated very accurately, since we need to know only the largest Lyapunov exponent in the $\delta = 0$ case; for the particular system studied, we find $\delta_c \approx 1.432$.

What "conducting" property of the system does the finite $\mathcal{P}_{\rm Lyap,0}$ correspond to? Chalker and Bernhard[72] suggest that $\mathcal{P}_{\rm Lyap,0}$ gives, up to some numerical factor, the conductivity of the 2D system in units of e^2/h:

$$\overline{\sigma} \sim \mathcal{P}_{\rm Lyap,0}. \tag{3.49}$$

However, we have to ask ourselves which conductivity is actually being "measured" by Eq. (3.49), particularly since we are dealing with systems that have singular density of states at the Fermi level. In this respect, note that the above transfer matrix approach can be equivalently formulated as a recursion procedure for calculating the

Green's function $(E-\hat{H})^{-1}$ between the first and the last slices of the long strip,[49] while the largest localization length from such transfer matrix analysis is obtained from the average modulus-squared of such "propagator" between the two slices. This transfer matrix estimate resembles most the definition of conductivity used in the sigma-model literature (see, e.g., Refs. [5] and [73]), which is precisely the conductivity that we need in Eq. (3.47). While we do not know whether the above connection is precise, we still expect the expression (3.49) to give us sensible estimates. To make such estimates more consistent, we fix the unknown numerical factor by comparing with the exactly known pure-system cases. Thus, an elementary calculation for the pure π-flux model gives $\mathcal{P}_{\rm Lyap,0} = 2/\pi$, which should be compared with $\overline{\sigma} = 2/\pi$ for the two Dirac points of the model's continuum limit (Ref. [5] showed that the free Dirac theory has $\overline{\sigma}_{\rm Dirac} = 1/\pi$). Similarly, consider the staggered square lattice system defined as $t_{\mathbf{j},\mathbf{j}+\hat{\mathbf{x}}} = t_x + (-1)^{j_x+j_y}\Delta_x$ and $t_{\mathbf{j},\mathbf{j}+\hat{\mathbf{y}}} = t_y$, which for $t_x < t_y$ has two Dirac points, with $v_x = 2a_x\Delta_x$ and $v_y = 2a_y\sqrt{t_y^2 - t_x^2}$ [brickwall lattice of Fig. 3.5(a) is a particular example with $\Delta_x \equiv t_x$]. For the transfer in the two direction we obtain $\mathcal{P}^{xx}_{\rm Lyap,0} = (v_x/v_y) \times 2/\pi$ and $\mathcal{P}^{yy}_{\rm Lyap,0} = (v_y/v_x) \times 2/\pi$, consistent with the anisotropic rescaling of the conductivity for Dirac fermions in 2D. From these considerations, we fix the proportionality factor in Eq. (3.49) to one, i.e., $\overline{\sigma} = \mathcal{P}_{\rm Lyap,0}$.

We comment briefly on the random vector potential model, for which Ref. [5] predicts $\overline{\sigma} = 2/\pi$ for *any* strength of the randomness. This result can be also obtained within the above transfer matrix approach, if we assume that we can indeed fix the unknown numerical factor in Eq. (3.47) to the appropriate constant value. When we add random surface $\Phi(\mathbf{r})$ on top of, say, the pure π-flux model [see Eq. (3.16)], the $E=0$ transfered wave functions need to be simply multiplied by the appropriate $e^{-\Phi(\alpha)}$ or $e^{\Phi(\beta)}$. But this cannot change the Lyapunov spectrum of the transfer along the quasi-1D strip for any finite transverse size of the strip, because $\Phi(\mathbf{r})$ in such geometry is effectively a one-dimensional Gaussian surface and cannot fluctuate stronger than $(\Phi(L_{||}) - \Phi(0))^2 \sim L_{||}$ along the strip. At this stage, it is not clear to us whether $\overline{\sigma}$ should have any signature of the "freezing" transition at g_c observed in the static and dynamic properties of this system (see Appendix 3.A and Sec. 3.4.1); the above argument seems to suggest that there is none, but we cannot rule out the possibility that taking the limit $L_{||} \to \infty$ while keeping $L_\perp$ fixed "loses" the information about the 2D system.

It is convenient at this point to comment somewhat more about the anisotropic dimer model on the brickwall lattice of Fig. 3.5(a). First of all, note that this lattice is special from the dimer system point of view, since in any given cover the number of horizontal dimers in each column of rungs is the same. Still, lattices with closed (periodic or spiral) boundary conditions in the $\hat{\mathbf{x}}$ direction allow this number to be anywhere between 1 and $L_y/2$, and there is a well-defined thermodynamic limit, with the dimer system exhibiting two-dimensional critical behavior in the high-temperature phase, and a fully locked low-temperature phase. [On the other hand, free bc in the $\hat{\mathbf{x}}$ direction force all dimers to point in the vertical direction, essentially disconnecting the rungs of the lattice! This "pathology" of the free boundary conditions is likely to be mitigated if we also allow monomers (free sites) into the system, breaking the winding number constraint; when we have a bulk density of such defects (which roughly corresponds to looking at the bulk density of the low-energy states in the RH problem) we expect sensible thermodynamic limit in this case as well.]

In the following, we always assume system with nice boundary conditions, say, "odd$\times$even" lattice with spiral bc in the $\hat{\mathbf{x}}$ direction and free bc in the $\hat{\mathbf{y}}$ direction.[74] The thermodynamic limit ($L_x \to \infty$, $L_y \to \infty$, $L_x/L_y = \text{const}$) can be also approached—via smooth finite size scaling forms—by the lattices of shape $L_x \times \infty$; however, the $\infty \times L_y$ lattices require more care.[75, 76] Here we note one aspect of the $\infty \times L_y$ systems—the energetics of domain walls, which are defined as transition cycles relative to the fully locked state. In the fully locked phase, $\delta > \delta_c$, there are no such domain walls, but these will appear one by one via first-order transitions as we lower δ. One can easily check that the number of domain walls at a given δ is precisely the number of positive Lyapunov exponents for the transfer in the corresponding hopping problem (this can be seen, for example, by calculating $Z_d[A,B] = \det \hat{t}_{AB}$ via successive block-diagonalizations, the matrices appearing in the diagonal blocks being precisely the transfer transfer matrices of the hopping problem); also, the free energy cost per unit length of adding or removing domain walls is precisely the spacing between the Lyapunov exponents near $\nu = 0$. Thus, we established the correspondence between the domain wall energetics of the dimer problem and the conducting properties of the hopping problem. We can now, for example, calculate the number density of domain walls near the locking transition: In the pure system, we easily obtain the Pokrovskii-Talapov $n \sim (\delta_c - \delta)^{1/2}$, since the Lyapunov band is quadratic near the top of the band, $\nu_k \sim \nu_0 - ck^2$ (k is the transverse wave vector used to diagonalize the transfer matrix of the pure system).

In the disordered system, on the other hand, we observe numerically $\nu_k \sim \nu_0 - c'k$ (here k is the ordinal number of the Lyapunov exponent, $\nu_1 \geq \nu_2 \geq \ldots$), so that $n \sim \delta_c - \delta$, in agreement with Ref. [77].

3.5.4 Exact diagonalization studies: density of states

Let us now see the behavior of the density of states when we increase dimerization from $\delta = 0$, eventually driving the system into a localized state for $\delta > \delta_c$. This is shown in Fig. 3.6, together with the appropriate information about the system's localization properties. Consistent with our discussion in Sec. 3.5.1, the divergence in the density of states becomes stronger as we approach the localization transition, with the effective exponent $z_{\text{eff}}(L=192)$ peaking at the transition. Deep in the localized phase, the log-log plot of $\rho(E)$ vs E is indeed a straight line, and the quoted values of z give the actual bulk dynamical exponents. In the delocalized phase, on the other hand, there is still some curvature at the lowest energy scale, and the extracted values z_{eff} can only serve as rough indicators of the strength of the divergence.

We now summarize further details of our analysis of the density of states. In the delocalized phase, we fit the integrated density of states $N_E \equiv \int_0^E \rho(E')dE'$—since this is what is calculated directly[68]—to the generalized-Gade form

$$N_E = a\Gamma_E^{1-1/x} e^{-c\Gamma_E^{1/x}}, \tag{3.50}$$

where $\Gamma_E \equiv \ln(\Omega_0/E)$. Specifically, we try two values for the exponent x—the original Gade $x = 2$ and the modified $x = 3/2$. The included prefactor $\Gamma_E^{1-1/x}$ is based on an assumption that there are no additional corrections to the asymptotic $E \to 0$ form $\rho(E) \sim E^{-1}\exp(-\Gamma_E^{1/x})$. This is something that we do not know—in fact, our lowest-gap analysis of Sec. 3.4.2 seems to suggest that there may be corrections stronger than any such Γ^r prefactor. In this situation, we treat the above fit function only as some baseline. To be consistent, we should also allow for the uncertainty $\Gamma_E \to \Gamma_E + \Gamma_0$ in the bare energy scale relative to which the log-scale Γ is defined. As one might suspect, for a fixed fit range, we can approximate any DOS curve with the three parameters a, c, and Γ_0, so we cannot be conclusive here. What we can do is to look for the overall consistency of such fits: We can ask, for example, how the fit parameters change as we change the fit region, or how sensible the obtained parameters are (thus, the parameter a should be of order one since the density of states is normalized per site). Generally, the $x = 3/2$ form fares somewhat

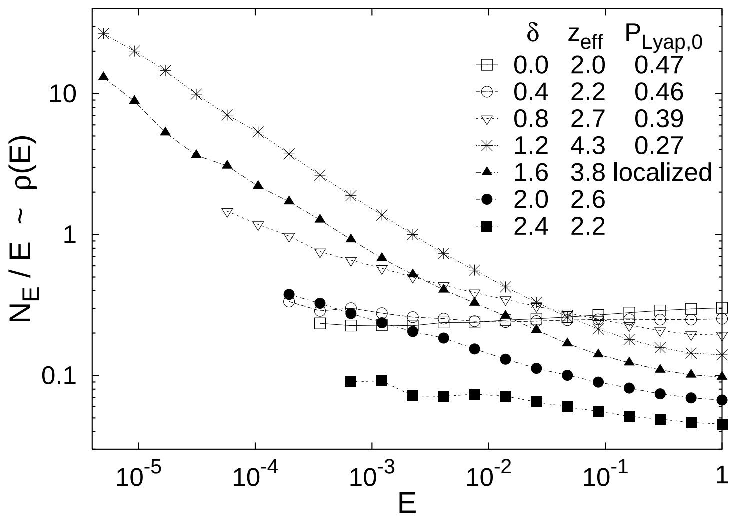

Figure 3.6: Density states for the anisotropic brickwall lattice of Fig. 3.5 calculated for 192×192 system with open bc in the $\hat{\mathbf{y}}$ direction and periodic bc in the $\hat{\mathbf{x}}$ direction. The regular (vertical) hopping amplitudes are chosen randomly from a uniform distribution in $[0, 1]$, while the dimerized (horizontal) hopping amplitudes are chosen from $[0, e^{\delta}]$. The more detailed characterization of the data is similar to that of Fig. 3.4.

Table 3.2: Results of the transfer matrix studies for the systems of Fig. 3.6. See text and Table 3.1 for the description of the table data.

δ	$\mathcal{P}^{xx}_{\rm Lyap}$	$\mathcal{P}^{yy}_{\rm Lyap}$	$\overline{\mathcal{P}}_{\rm Lyap}$	Λ^{yy}
0.0	0.27	0.82	0.47	1.8
0.4	0.38	0.56	0.46	1.15
0.8	0.48	0.32	0.39	0.52
1.2	0.60	0.12	0.27	0.12
> 1.432	localized			

better in such analysis; also, the extracted numerical value of the parameter c from such fits compares favorably with the lowest-gap results of the next subsection. But this is as far as our direct DOS studies can take us in the delocalized phase.

In the localized phase, we have also tried fitting the density of states using a power-law times a logarithmic correction $N_E \sim E^{d/z} (\Gamma_E)^r$. We typically find that such log-corrections fit to $r \cong 0$, suggesting that the density of states is a simple power-law form in the localized phase. This is also our conclusion from the lowest-gap studies to be presented below.

3.5.5 The lowest energy state: exact diagonalization and dimer optimized defects studies

We can extend our numerical tests further by considering distribution of the smallest positive energy in finite samples, paying particular attention to scaling with the sample size. Such direct diagonalization study can be performed for a factor of two larger systems than in our DOS studies, while indirect dimer methods can take us another factor of four in system size. This well-controlled and rather sensitive numerical approach is also a direct counterpart of our analytical arguments in Sec. 3.4.2.

We take the same brickwall lattice problem as in the previous subsections. However, we now consider $(2M_x + 1) \times 2M_y$ "odd $\times$ even" samples with spiral boundary conditions in the $\hat{\mathbf{x}}$ direction and free bc in the $\hat{\mathbf{y}}$ direction [see Fig. 3.5(a)]. The specific choice of the boundary conditions is such that $\det \hat{t}_{AB} = Z_d[A, B]$ holds precisely for this system,[74] which allows us to compare the lowest-energy state of the hopping problem with the optimized defects in the corresponding dimer problem exactly paralleling the discussion of Sec. 3.4.2 without any unnecessary distraction. To this end, we also calculate[78, 79] the dimer RG "estimate" Eq. (3.26) for the lowest gap, which is the quantity used in the bounds of Sec. 3.4.2. (We have also performed direct diagonalization studies of "even $\times$ even" samples with periodic bc in the $\hat{\mathbf{x}}$ direction and free bc in the $\hat{\mathbf{y}}$ direction[74] obtaining quantitatively similar results for the scaling behavior.)

For the purposes of illustration, we show our results for two values of δ, one in the delocalized phase ($\delta = 0.8$) and one in the localized phase ($\delta = 2.0$), both chosen well away from the transition point ($\delta_c = 1.432$).

Delocalized phase, $\delta = 0.8$

Fig. 3.7 shows distributions of the logarithm of the smallest positive energy in our samples in the delocalized phase. The exact diagonalization results for $\Gamma_{\rm opt} = \ln(1/E^{+}_{\rm min})$ are shown with open symbols and extend up to system sizes $L = 384$, while the corresponding dimer RG estimates $-\mathfrak{E}_{\rm opt.def.}$ [cf. Eq. (3.26)] are shown with filled symbols and extend up to $L = 1536$. We see that the distributions move out strongly to larger absolute log-energies (i.e., smaller energies) with increasing L and broaden somewhat at the same time. We also see that the dimer RG estimates for the lowest gap are consistently smaller and indeed provide strong lower bounds, at least for the larger systems. This is in agreement with our discussion in Sec. 3.4.2.

In Fig. 3.8, we analyze the behavior of the distributions $P(\Gamma_{\rm opt}; L)$ of Fig. 3.7, plotting their mean $\overline{\Gamma_{\rm opt}}(L)$ and the standard deviation $\sigma(\Gamma_{\rm opt}; L)$. On a plot with linear scales for both $\ln L$ and $\Gamma_{\rm opt}$ (not shown), we observe a visible curvature $\overline{\Gamma_{\rm opt}} \sim (\ln L)^x$ with $x > 1$ indicative of a stronger than any finite-z behavior. To get a rough idea about the exponent x, in Fig. 3.8 we use logarithmic scales for both $\ln L$ and $\Gamma_{\rm opt}$. The exact diagonalization results are seen to fall between the $x = 1$ and $x = 3/2$ lines, well away from the Gade $x = 2$; at the same time, the dimer optimized defects results, which extend to larger system sizes, clearly approach the $x = 3/2$ line, as has been already checked in Ref. [60] for a related model. We also note a much weaker $\sim(\ln L)^{1/2}$ dependence of the width of the distributions on the system size, consistent with the results of Ref. [60] summarized in Sec. 3.4.2.

A more detailed analysis in the spirit of Ref. [60] now follows. More specifically, we perform linear fits for $[\overline{\Gamma_{\rm opt}}]^{2/3}$ and $[\sigma(\Gamma_{\rm opt})]^2$ as functions of $\ln L$. For the exact diagonalization data, we obtain $[\overline{\Gamma_{\rm opt}}]^{2/3} \cong 0.60 + 0.87 \ln L$ and $[\sigma(\Gamma_{\rm opt})]^2 \cong 0.22 + 0.18 \ln L$, which translate to the asymptotic scaling $\overline{\Gamma_{\rm opt}} \approx 0.81\,(\ln L)^{3/2}$ and $\sigma \approx 0.42\,(\ln L)^{1/2}$. We can compare this with the result from the DOS studies: performing the generalized-Gade fit Eq. (3.50) of the data of Fig. 3.6, we extract the parameter $c \cong 2.2$, which translates to a fairly close asymptotic scaling prediction $\overline{\Gamma_{\rm opt}} \approx 0.87\,(\ln L)^{3/2}$. Similarly, the dimer RG data yields $\overline{\Gamma_{\rm opt}} \approx 1.30\,(\ln L)^{3/2}$, not unreasonably far from the above exact diagonalization predictions [as discussed in Sec. 3.4.2, we expect stronger subleading $O(\ln L)$ terms for the exact lowest gap $\Gamma_{\rm opt}$ than for the dimer $-\mathfrak{E}_{\rm opt.def.}$]. Finally, Ref. [80] calculated bulk defect density in a related vortex glass model as a function of the defect core energy (which corresponds to $\Gamma_{\rm opt}$ in the random hopping problem), obtaining $N_\Gamma \sim \exp\left(-c\Gamma^{0.74}\right)$, fairly close to the expected $1/x = 2/3$ scaling form.

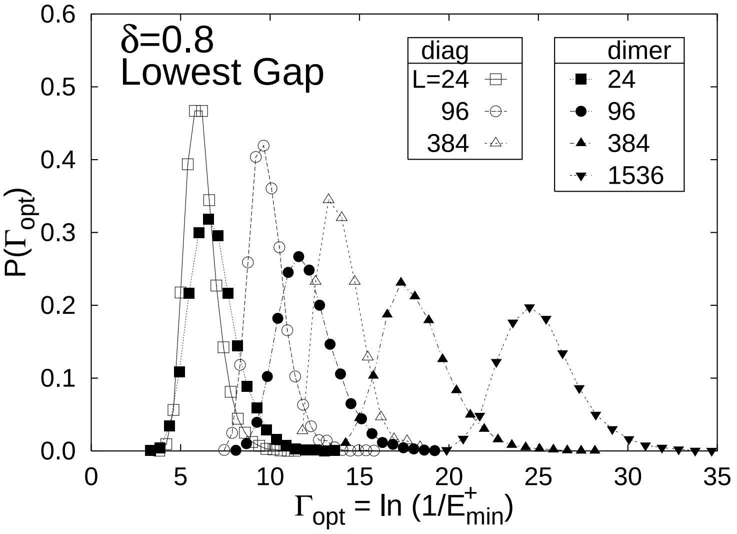

Figure 3.7: "Lowest-gap" analysis in the delocalized phase ($\delta = 0.8$) of the system of Fig. 3.5. We consider $(L + 1) \times L$ finite samples with spiral bc in the $\hat{\mathbf{x}}$ direction and free bc in the $\hat{\mathbf{y}}$ direction. Open symbols show distributions of the smallest positive energy calculated by exact diagonalization methods, while filled symbols show distributions of the corresponding dimer RG "estimate" Eq. (3.26).

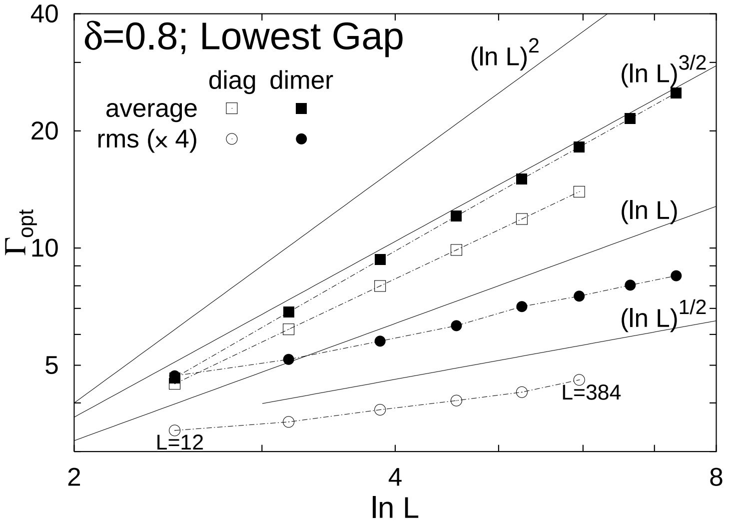

Figure 3.8: Detailed analysis of the distributions of Fig. 3.7. The mean $\overline{\Gamma_{\rm opt}}(L)$ and the standard deviation $\sigma(\Gamma_{\rm opt}; L)$ are plotted with open and filled symbols for the exact diagonalization and dimer RG results correspondingly. Note the logarithmic scale for both the $\ln L$ and $\Gamma_{\rm opt}$ axes. To gauge the L-dependence of $\overline{\Gamma_{\rm opt}}$ and $\sigma(\Gamma_{\rm opt})$, we also plot different powers $(\ln L)^x$ with $x = 2$, 3/2, 1, and 1/2.

Localized phase, $\delta = 2.0$

The lowest-gap analysis is simpler in the localized phase and is shown in Figs. 3.9-3.10. In this case also, the distributions move out to larger Γ_{opt} with increasing L, but now do so at a slower pace. We clearly observe a simple scaling $\overline{\Gamma_{\text{opt}}} = \text{const} + z \ln L$, with $z = 2.56$, which compares well with the estimate $z = 2.64$ from the DOS studies. Also, the widths of the distributions essentially do not change with the system size. Note that the effects discussed in Sec. 3.4.2 produce a much smaller difference between the exact diagonalization results and the dimer RG estimates in the localized phase, since the distance between the optimal defects is expected to scale very weakly $\sim \ln L$ with the sample size. Thus, this deep in the localized phase and for the sizes studied, the dimer RG gives numerically accurate results for the lowest gap and the two peaks of the corresponding wave function in each sample.

3.6 Discussion

Our main results have been already summarized in the Introduction, and we use this discussion to point some remaining questions about the two-dimensional bipartite random hopping problems, and also reflect on the closely related pure imaginary hopping problems. Some of this is still an ongoing work.

Our first remark concerns the zero-energy wave function in the "delocalized" critical phase of the general bipartite problem. The multifractal properties of this wave function, because of the flow to strong disorder $g \to \infty$, are expected to be trivial $\tau(q) \equiv 0$ (Ref. [58]). Equivalently, since the logarithm of the wave function magnitude is essentially the potential $\upsilon(\mathbf{r})$ seen by the defects of the corresponding dimer problem [see Eq. (3.43)], all participation ratios do not depend on the system size because of the ground state dominance in this random potential. In this respect, the critical wave function looks fairly localized. The typical correlations like $C_{\text{typ}}(r) = \overline{\log|\Psi(\mathbf{r})\Psi(\mathbf{0})|}$ are directly related to the correlations of $\upsilon(\mathbf{r})$. On the other hand, average correlations like $C_{\text{av}}(r) = \overline{|\Psi(\mathbf{r})\Psi(\mathbf{0})|}$ require better understanding of the statistics of such random surfaces; a particular question is whether $C_{\text{av}}(r)$ is dominated by near-returns of the surface to its global extrema, as is the case in the one-dimensional chain, and what is the probability of finding such quasi-degenerate minima at fixed distance r?

Another feature of the delocalized phase that we have not discussed is the suggested[57, 77] universal susceptibility variations in the vortex glass problem.

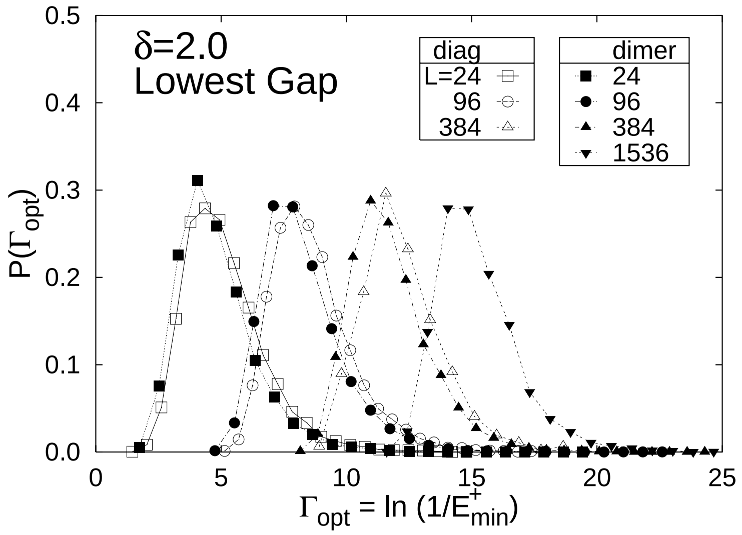

Figure 3.9: Lowest-gap analysis in the localized phase, $\delta = 2.0$, similar to that of Fig. 3.7.

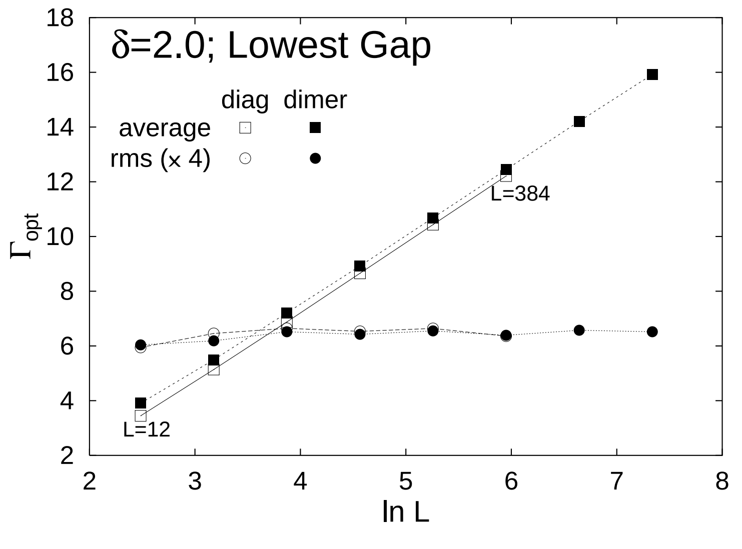

Figure 3.10: Analysis of the distributions of Fig. 3.9.

Naively, these correspond to a kind of polarizability fluctuations in the random hopping problem: In the geometry of Fig. 3.5(a) with the magnetic flux lines running in the $\hat{\mathbf{x}}$ direction, the number density of such lines (which are precisely the domain walls of Sec. 3.5.3) is essentially the surface density of the edges states in the hopping problem; also, the magnetic field driving the flux lines is the staggered dimerization of Fig. 3.5(a) acting like a polarizing electric field separating the A and B "charges". It would be interesting to study this in more detail.

Going from the delocalized phase to the localized phase, the character of the transition is a completely separate issue that we ignored altogether. One feature of this transition is that the conductivity $\overline{\sigma}_{xx}$ remains finite (because the Lyapunov spectrum density is finite at the top of the Lyapunov band), while $\overline{\sigma}_{yy}$ vanishes. It is not clear how this extreme anisotropy affects the properties of the transition and whether anything interesting remains.

In the localized phase, we have not discussed in detail the structure of our low-energy "string" excitations. Presumably, they look similar to the domain walls (flux lines) in the corresponding random dimer (vortex glass) problem. Note that in the particular localized phase that we studied, the strings are forced to run in the $\hat{\mathbf{x}}$ direction. In a more general localized phase, obtained by introducing some other dimerization pattern, the situation is more complicated, but it still seems that it will be some kind of directed strings that will contribute most to the low-energy density of states: The strings need to be stretched so that the end-to-end distance (setting the tunneling frequency $\sim\epsilon$) is of order the string length (determining the occurrence probability) for our counting arguments of Sec. 3.3.2 to work. An interesting system to study in this respect is a two-dimensional spinless superconductor with time-reversal invariance, which maps onto a bilayer bipartite real hopping problem. When the "p_x-wave" superconducting pairing amplitude $\Delta_{\mathbf{j},\mathbf{j}+\mathbf{x}}$ is zero, the system is just a doubled Anderson localization problem. Increasing Δ from zero, we have a bipartite localized phase that contains the standard Anderson insulator as a point. Note also the richness of the full phase diagram in this system: a simple Lyapunov spectrum shift argument shows that increasing Δ further drives the system from this localized phase first into a critical delocalized phase, and then again into a localized phase similar to our staggered band insulator.

The next group of comments refers to the pure imaginary hopping problems (ImRH). As is clear from the preceding discussion, we expect similar Griffiths effects in the localized phases of such systems. A relevant question is, of course, whether this Griffiths mechanism can compete with other mechanisms of "filling the gap" (which can, for example, produce a constant contribution to the density of states at the band center as in Ref. [12]). In particular, are there situations with a power-law diverging Griffiths density of states? While we haven't studied these questions in detail, there are situations where this indeed seems to happen. Thus, in the fermionic ImRH representation[81] of the two-dimensional random bond Ising model, our preliminary results suggest that the density of states is power-law vanishing to the left (the less disordered side) of the Nishimori line and power-law diverging to the right (this particular example was suggested to us by Nick Read and proved for the one-dimensional case in Ref. [82]).

Two-dimensional ImRH systems are believed to also have true metallic phases,[12] and it would be interesting to consider these from the perspectives of our work. In particular, can one use an analogous dimer connection to gain further insight into their properties?

Finally, is there anything to learn from our approach that could be useful in the study of the plateau transitions in the integer quantum Hall effect?

3.A 2D Gaussian surface

The following facts are used in the main text to obtain bounds for the dynamical scaling in the random vector potential model; these are transcribed directly from Ref. [59] for the two-dimensional Gaussian surface $\Phi(\mathbf{r})$, Eq. (3.17), in an $L \times L$ box (stipulating $\int d\mathbf{r}\, \Phi(\mathbf{r}) = 0$).

Extremal properties of the surface $\Phi(\mathbf{r})$ are sharply defined: e.g., the maximum scales as

$$\Phi_{\max}(L) = 2\sqrt{\frac{g}{2\pi}} \ln L - \frac{3}{2}\sqrt{\frac{g}{8\pi}} \ln\ln L + \delta\Phi_{\max}, \tag{3.A.1}$$

with the sample-to-sample dependence entering only through an $O(1) \times \sqrt{g}$ random variable $\delta\Phi_{\max}$.

The following "partition function"

$$\mathfrak{Z} = \sum_{\mathbf{r}} e^{-2\Phi(\mathbf{r})} \tag{3.A.2}$$

has a sharply defined logarithm:

$$\begin{aligned}
\ln \mathfrak{Z}_g(L) &= 2(1 + \frac{g}{g_c}) \ln L + \Delta_g \ , && g < g_c \equiv 2\pi \ ; \\
\ln \mathfrak{Z}_g(L) &= 4 \ln L - \frac{1}{2} \ln\ln L + \Delta_g \ , && g = g_c \ ; \\
\ln \mathfrak{Z}_g(L) &= \sqrt{\frac{g}{g_c}}(4 \ln L - \frac{3}{2} \ln\ln L) + \Delta_g \ , && g > g_c \ ;
\end{aligned}$$

where Δ_g is an $O(1)$ random number (different in each case). Note that for strong disorder $g > g_c$, $\mathfrak{Z}(L)$ is dominated by the global minimum:

$$\mathfrak{Z}_g(L) = e^{-2\Phi_{\min}(L)} \sum_{\mathbf{r}} e^{-2[\Phi(\mathbf{r}) - \Phi_{\min}(L)]}, \tag{3.A.3}$$

where the sum contributes no L-dependence because $e^{-2[\Phi(\mathbf{r}) - \Phi_{\min}]}$ remains normalizable in the limit $L \to \infty$.

Bibliography

[1] O. Motrunich, S.-C. Mau, D. A. Huse, and D. S. Fisher, "Infinite-randomness quantum Ising critical fixed points," Phys. Rev. B **61**, 1160 (2000).

[2] K. Damle, O. I. Motrunich, and D. A. Huse, "Dynamics and Transport in Random Antiferromagnetic Spin Chains," Phys. Rev. Lett. **84**, 3434 (2000).

[3] O. I. Motrunich, K. Damle, and D. A. Huse, "Dynamics and transport in random quantum systems governed by strong-randomness fixed points," Phys. Rev. B **63**, 134424 (2001).

[4] O. I. Motrunich, K. Damle, and D. A. Huse, "Griffiths effects and quantum critical points in dirty superconductors without spin-rotation invariance: One-dimensional examples," Phys. Rev. B **63**, 224204 (2001).

[5] A. W. W. Ludwig, M. P. A. Fisher, R. Shankar, and G. Grinstein, "Integer quantum Hall transition: An alternative approach and exact results," Phys. Rev. B **50**, 7526 (1994).

[6] D. Bernard, "(Perturbed) Conformal field theory applied to 2D disordered systems: An introduction," hep-th/9509137 (unpublished).

[7] R. Gade, "Anderson localization for sublattice models," Nucl. Phys. B **398**, 499 (1993).

[8] R. Gade and F. Wegner, "The $N = 0$ replica limit of $U(N)$ and $U(N)/SO(N)$ models," Nucl. Phys. B **360**, 213 (1991).

[9] S. Hikami, M. Shirai, and F. Wegner, "Anderson localization in the lowest Landau-level for a 2-subband model," Nucl. Phys. B **408**, 415 (1993).

[10] A. Altland and M. R. Zirnbauer, "Nonstandard symmetry classes in mesoscopic normal-superconducting hybrid structures," Phys. Rev. B **55**, 1142 (1997).

[11] I. M. Lifshits, S. A. Gredeskul, and L. A. Pastur, *Introduction to the theory of disordered systems* (Wiley, New York, 1988).

[12] T. Senthil and M. P. A. Fisher, "Quasiparticle localization in superconductors with spin-orbit scattering," Phys. Rev. B **61**, 9690 (2000).

[13] R. B. Griffiths, "Nonanalytic behavior above the critical point in a random Ising ferromagnet," Phys. Rev. Lett. **23**, 17 (1969).

[14] B. M. McCoy and T. T. Wu, "Theory of a two-dimensional Ising model with random impurities. I. Thermodynamics," Phys. Rev. **176**, 631 (1968).

[15] B. M. McCoy and T. T. Wu, "Theory of a two-dimensional Ising model with random impurities. II. Spin correlation functions," Phys. Rev. **188**, 982 (1969).

[16] B. M. McCoy, "Theory of a two-dimensional Ising model with random impurities. III. Boundary effects," Phys. Rev. **188**, 1014 (1969).

[17] B. I. Shklovskii and A. L. Efros, *Electronic properties of doped semiconductors* (Springer-Verlag, Berlin, 1984).

[18] D. S. Fisher, "Critical-behavior of random transverse-field Ising spin chains," Phys. Rev. B **51**, 6411 (1995).

[19] N. Read, S. Sachdev, and J. Ye, "Landau theory of quantum spin-glasses of rotors and Ising spins," Phys. Rev. B **52**, 384 (1995).

[20] T. P. Eggarter and R. Riedinger, "Singular behavior of tight-binding chains with off-diagonal disorder," Phys. Rev. B **18**, 569 (1978).

[21] L. Balents and M. P. A. Fisher, "Delocalization transition via supersymmetry in one dimension," Phys. Rev. B **56**, 12970 (1997).

[22] T. Senthil, M. P. A. Fisher, L. Balents, and C. Nayak, "Quasiparticle transport and localization in high-T_c superconductors," Phys. Rev. Lett. **81**, 4704 (1998).

[23] T. Senthil and M. P. A. Fisher, "Quasiparticle density of states in dirty high-T_c superconductors," Phys. Rev. B **60**, 6893 (1999).

[24] S. Vishveshwara, T. Senthil, and M. P. A. Fisher, "Superconducting "metals" and "insulators"," Phys. Rev. B **61**, 6966 (2000).

[25] R. Bundschuh, C. Cassanello, D. Serban, and M. R. Zirnbauer, "Weak localization of disordered quasiparticles in the mixed superconducting state," Phys. Rev. B **59**, 4382 (1999).

[26] R. Bundschuh, C. Cassanello, D. Serban, and M. R. Zirnbauer, "Localization of quasiparticles in a disordered vortex," Nucl. Phys. B **532**, 689 (1998).

[27] C. Pépin and P. A. Lee, "Density of states of a d-wave superconductor in the presence of strong impurity scatterers: A nonperturbative result," Phys. Rev. B **63**, 054502 (2001).

[28] W. A. Atkinson, P. J. Hirschfeld, A. H. MacDonald, and K. Ziegler, "Details of disorder matter in 2D d-wave superconductors," Phys. Rev. Lett. **85**, 3926 (2000).

[29] F. J. Dyson, "The dynamics of a disordered linear chain," Phys. Rev. **92**, 1331 (1953).

[30] P. W. Brouwer, A. Furusaki, I. A. Gruzberg, and C. Mudry, "Localization and delocalization in dirty superconducting wires," Phys. Rev. Lett. **85**, 1064 (2000).

[31] M. Titov, P. W. Brouwer, A. Furusaki, and C. Mudry, "Fokker-Planck equations and density of states in disordered quantum wires," cond-mat/0011146 (unpublished).

[32] The generic localized behavior predicted by us can also be studied using the supersymmetry method for the special case of a 1D single-channel spinless superconductor without T invariance (I. Gruzberg *et al.*, private communication).

[33] N. Read and D. Green, "Paired states of fermions in two dimensions with breaking of parity and time-reversal symmetries and the fractional quantum Hall effect," Phys. Rev. B **61**, 10267 (2000).

[34] This distinction between the two phases of the pure system can also be stated in topological terms as in Ref. [33].

[35] For examples of such self-consistent calculations, see A. Ghosal, M. Randeria, and N. Trivedi, Phys. Rev. B **63**, 020505 (2000); Phys. Rev. Lett. **81**, 3940 (1998); see also K. Sengupta *et al.*, cond-mat/0010206 (unpublished) for a one-dimensional self-consistent calculation closely related to our toy model.

[36] A. A. Abrikosov, "Superconductivity in a quasi-one-dimensional metal with impurities," J. Low Temp. Phys. **53**, 359 (1983).

[37] H. J. Schulz and C. Bourbonnais, "Quantum fluctuations in quasi-one-dimensional superconductors," Phys. Rev. B **27**, 5856 (1983).

[38] P. W. Brouwer, C. Mudry, B. D. Simons, and A. Altland, "Delocalization in coupled one-dimensional chains," Phys. Rev. Lett. **81**, 862 (1998).

[39] P. W. Brouwer, C. Mudry, and A. Furusaki, "Density of states in coupled chains with off-diagonal disorder," Phys. Rev. Lett. **84**, 2913 (2000).

[40] H. Mathur, "Feynman's propagator applied to network models of localization," Phys. Rev. B **56**, 15794 (1997).

[41] J. T. Chalker, N. Read, V. Kagalovsky, B. Horovitz, Y. Avishai, and A. W. W. Ludwig, "Thermal metal in network models of a disordered two-dimensional superconductor," cond-mat/0009463 (unpublished).

[42] N. Read and A. W. W. Ludwig, "Absence of a metallic phase in random-bond Ising models in two dimensions: Applications to disordered superconductors and paired quantum Hall states," Phys. Rev. B **63**, 024404 (2001).

[43] Connectivity with respect to a given cover measures the following string correlator

$$C(i,j) = \frac{\langle \mathrm{G}|(2\hat{n}_i - 1)(2\hat{n}_j - 1)\Pi_{p\in\mathrm{ref}}(f^\dagger_{p,1}f_{p,2} - f^\dagger_{p,2}f_{p,1})|\mathrm{G}\rangle}{\langle \mathrm{G}|\Pi_{p\in\mathrm{ref}}(f^\dagger_{p,1}f_{p,2} - f^\dagger_{p,2}f_{p,1})|\mathrm{G}\rangle},$$

where $\Pi_{p\in\mathrm{ref}}$ denotes the product over *all* dimers p of the reference cover, and $|\mathrm{G}\rangle$ is the ground-state Slater determinant obtained from the strong-disorder

RG. One can easily show that $C(i,j)=1$ if and only if the two sites belong to the same cluster, and $C(i,j)=0$ otherwise. A similar "cluster description" for a topological order parameter was used in the study of random antiferromagnetic spin-1 chains in C. Monthus, O. Golinelli, and Th. Jolicoeur, Phys. Rev. Lett. **79**, 3254 (1997).

[44] Note that the value of the exponent β for the string order parameter of a single dimerized chain used by us here for the purposes of comparison is taken from footnote 17 of R. A. Hyman and K. Yang, Phys. Rev. Lett. **78**, 1783 (1997), instead of the original article R. A. Hyman, K. Yang, R. N. Bhatt, and S. M. Girvin, *ibid.* **76**, 839 (1996).

[45] L. S. Levitov, "Critical Hamiltonians with long range hopping," Ann. Phys. (Berlin) **8**, 697 (1999).

[46] C. W. J. Beenakker, "Random-matrix theory of quantum transport," Rev. Mod. Phys. **69**, 731 (1997).

[47] F. Merz and J. T. Chalker, "The two-dimensional random-bond Ising model, free fermions and the network model," cond-mat/0106023 (unpublished).

[48] A. Crisanti, G. Paladin, and A. Vulpiani, *Products of random matrices in statistical physics* (Springer-Verlag, Berlin, 1993).

[49] A. MacKinnon and B. Kramer, "The scaling theory of electrons in disordered solids: additional numerical results," Z. Phys. B **53**, 1 (1983).

[50] R. Oppermann and F. Wegner, "Disordered system with N-orbitals per site—$1/N$ expansion," Z. Phys. B **34**, 327 (1979).

[51] C. M. Soukoulis, I. Webman, G. S. Grest, and E. N. Economou, "Study of electronic states with off-diagonal disorder in two dimensions," Phys. Rev. B **26**, 1838 (1982).

[52] S. N. Evangelou, "Spectral singularities and localization in one-dimensional and quasi-one-dimensional systems with off-diagonal disorder," J. Phys. C **19**, 4291 (1986).

[53] M. Inui, S. A. Trugman, and E. Abrahams, "Unusual properties of midband states in systems with off-diagonal disorder," Phys. Rev. B **49**, 3190 (1994).

[54] S. Guruswamy, A. LeClair, and A. W. W. Ludwig, "$gl(N|N)$ super-current algebras for disordered Dirac fermions in two dimensions," Nucl. Phys. B **583**, 475 (2000).

[55] J. L. Cardy and S. Ostlund, "Random symmetry-breaking fields and the XY model," Phys. Rev. B **25**, 6899 (1982).

[56] J. Toner and D. P. DiVincenzo, "Super-roughening: A new phase transition on the surfaces of crystals with quenched bulk disorder," Phys. Rev. B **41**, 632 (1990).

[57] T. Hwa and D. S. Fisher, “Vortex glass phase and universal susceptibility variations in planar arrays of flux lines,” Phys. Rev. Lett. **72**, 2466 (1994).

[58] H. E. Castillo, C. de C. Chamon, E. Fradkin, P. M. Goldbart, and C. Mudry, “Exact calculation of multifractal exponents of the critical wave function of Dirac fermions in a random magnetic field,” Phys. Rev. B **56**, 10668 (1997).

[59] D. Carpentier and P. Le Doussal, “Glass transition of a particle in a random potential, front selection in nonlinear renormalization group, and entropic phenomena in Liouville and sinh-Gordon models,” Phys. Rev. E **63**, 026110 (2001).

[60] C. Zeng, P. L. Leath, and D. S. Fisher, “Absence of two-dimensional Bragg glasses,” Phys. Rev. Lett. **82**, 1935 (1999).

[61] Y. Hatsugai, X.-G. Wen, and M. Kohmoto, “Disordered critical wave functions in random-bond models in two dimensions: Random-lattice fermions at $E = 0$ without doubling,” Phys. Rev. B **56**, 1061 (1997).

[62] F. D. M. Haldane, “Model for a quantum Hall effect without Landau levels: Condensed-matter realization of the “parity anomaly”,” Phys. Rev. Lett. **61**, 2015 (1988).

[63] P. W. Kasteleyn, “Graph theory and crystal physics,” in *Graph theory and theoretical physics*, edited by F. Harary (Academic Press, New York, 1967), pp. 44–110.

[64] E. W. Montroll, “Lattice statistics,” in *Applied combinatorial mathematics*, edited by E. F. Beckenbach (Wiley, New York, 1964), pp. 96–143.

[65] P. Le Doussal and T. Giamarchi, “Dislocations and Bragg glasses in two dimensions,” Physica C **331**, 233 (2000).

[66] M. E. Fisher and J. Stephenson, “Statistical mechanics of dimers on a plane lattice. II. Dimer correlations and monomers,” Phys. Rev. **132**, 1411 (1963).

[67] H. E. Castillo and P. Le Doussal, “Freezing of dynamical exponents in low dimensional random media,” cond-mat/0006373 (unpublished).

[68] We compute the integrated DOS on a specified grid of energy values using Sturm theorem, which gives the number of eigenvalues of a real symmetric matrix B that are greater than λ as the number of agreements in sign between consecutive leading principal minors of a matrix $B-\lambda$. The principal minors are evaluated by reducing $B-\lambda$ to triangular form using standard Gaussian elimination. Banded matrices with relatively narrow bands, of which our RH problems are specific examples, are particularly well suited for this approach, since the band form of the matrix is preserved over the entire course of the Gaussian elimination. This method was applied to the square lattice RH problem in Ref. [52]. Ref. [69] provides a direct algorithmic and numerically more stable realization, and our routine is based on the routine `bandet2` of this handbook. In this Sturm method, we do not need to store the full matrix at any time but only the current (in the Gaussian elimination process) part of it with the number of elements kept of

the order the bandwidth squared; thus the procedure is very memory efficient, and the main limiting factors for our computations are floating point arithmetics and computational time. The "lattice growing" character of the method and the essential bandedness require the use of free bc in the "growth" direction, while boundary conditions in the transverse direction can be either free or periodic. We find it computationally advantageous to apply the method to the matrix $\hat{H}^2$ instead of the matrix $\hat{H}$ itself: in the $\hat{H}^2$ the two sublattices are decoupled thus reducing the size of the full matrix that needs to be considered, and also the procedure is found to be numerically more stable in this case.

[69] R. S. Martin and J. H. Wilkinson, "Solution of symmetric and unsymmetric band equations and the calculation of eigenvectors of band matrices," in *Linear Algebra*, edited by J. H. Wilkinson and C. Reinsch (Springer-Verlag, New York, 1971), vol. II of *Handbook for automatic computation*, chap. I.6, pp. 70–92.

[70] The brickwall hopping problem of Fig. 3.5(a) with free bc in the $\hat{\mathbf{x}}$ direction has of order L_y edge states living on the free A- and B-sites of the correspondingly left and right boundaries, with the energies of these states exponentially small in L_x. Pure isotropic system has precisely $L_y/3$ such edge states on each vertical boundary,[62] while the anisotropic system in the limit of strong dimerization has $L_y/2$ edge states on each boundary, one per each free site. When studying the bulk DOS, one then has to separate the almost-zero-energy edge states (their number scaling as L) and the bulk (order L^2) low-energy states in the total DOS, and we have indeed verified that this can be done by varying the size L of the system studied. However, the bulk density of states can also be obtained more easily by studying the system with no free boundaries in the $\hat{\mathbf{x}}$ direction, and this is what we do throughout. Note that our numerical methods[68] for both the density of states and the lowest gap crucially employ the bandedness of the corresponding matrix diagonalization problems and therefore require free bc in one direction, which we choose to be the $\hat{\mathbf{y}}$ direction.

[71] Formula (3.47) is taken verbatim from Ref. [7], correcting for a minor inconsistency between Eqs. (6.6) and (6.12) there.

[72] J. T. Chalker and M. Bernhardt, "Scattering theory, transfer matrices, and Anderson localization," Phys. Rev. Lett. **70**, 982 (1993).

[73] A. J. McKane and M. Stone, "Localization as an alternative to Goldstone theorem," Ann. Phys. (NY) **131**, 36 (1981).

[74] $Z_d[A, B] = \det \hat{t}_{AB}$ for "odd $\times$ even" brickwall lattice with spiral bc in the $\hat{\mathbf{x}}$ direction and free bc in the $\hat{\mathbf{y}}$ direction because any transition cycle relative to the natural (horizontal) reference dimer cover winds precisely once along the $\hat{\mathbf{x}}$ direction and therefore has odd length (Refs.[63, 64]).

[75] S. M. Bhattacharjee and J. F. Nagle, "Finite-size effect for the critical point of an anisotropic dimer model of domain walls," Phys. Rev. A **31**, 3199 (1985).

[76] J. F. Nagle, C. S. O. Yokoi, and S. M. Bhattacharjee, "Dimer models on anisotropic lattices," in *Phase transitions and critical phenomena*, edited by

C. Domb and J. L. Lebowitz (Academic Press, San Diego, 1989), vol. 13, pp. 236–297.

[77] C. Zeng, P. L. Leath, and T. Hwa, "Thermodynamics of mesoscopic vortex systems in $1+1$ dimensions," Phys. Rev. Lett. **83**, 4860 (1999).

[78] A. A. Middleton, "Disorder-induced topological defects in a $d = 2$ elastic medium at zero temperature," Phys. Rev. B **61**, 14787 (2000).

[79] To find the optimized defects, we use a variant of the "maximum-weight bipartite matching—shortest path" combination of Ref. [78].

[80] C. Zeng and P. L. Leath, "Application of polynomial algorithms to a random elastic medium," Comput. Phys. Commun. **122**, 531 (1999).

[81] J. A. Blackman and J. Poulter, "Gauge-invariant method for the $\pm J$ spin-glass model," Phys. Rev. B **44**, 4374 (1991).

[82] I. A. Gruzberg, N. Read, and A. W. W. Ludwig, "Random-bond Ising model in two dimensions: The Nishimori line and supersymmetry," Phys. Rev. B **63**, 104422 (2001).